CORRECTING DENSITY FUNCTIONAL THEORY METHODS FOR DISPERSION INTERACTIONS USING PSEUDOPOTENTIALS

by

Ozan Karalti

B.S. Chemistry, Bilkent University, 2002

Submitted to the Graduate Faculty of

the Kenneth P. Dietrich School of Arts and Sciences in partial fulfillment

of the requirements for the degree of

Doctor of Philosophy

University of Pittsburgh

2014

UNIVERSITY OF PITTSBURGH

KENNETH P. DIETRICH SCHOOL OF ARTS AND SCIENCES

This dissertation was presented

by

Ozan Karalti

It was defended on

July 30, 2014

and approved by

Kenneth D. Jordan, Richard King Mellon Professor of Chemistry

Geoffrey Hutchison, Associate Professor of Chemistry

Sean Garrett–Roe, Assistant Professor of Chemistry

J. Karl Johnson, William Kepler Whiteford Professor of Chemical and Petroleum Engineering

Committee Chair: Kenneth D. Jordan, Richard King Mellon Professor of Chemistry

CORRECTING DENSITY FUNCTIONAL THEORY METHODS FOR DISPERSION INTERACTIONS USING PSEUDOPOTENTIALS

Ozan Karalti, PhD

University of Pittsburgh, 2014

The development of practical density functional theory (DFT) methods has provided the science community with a very important tool for modeling variety of systems such as materials, molecular and bio–molecular systems. Nonetheless, most practitioners of the method did not give enough attention to the deficiencies in modeling the dispersion interactions with the commonly used density functionals until a few years ago. Since then there have been many methods proposed to solve this problem and it is still a very active research area. I have tested a number of these dispersion–corrected DFT schemes for various systems that are of interest to our research group such as a water molecule interacting with a series of acenes and isomers of the water hexamer to see which of these methods give accurate results. Based on the tests, DFT–D3 of Grimme *et al.* and dispersion–corrected atom–centered pseudopotentials (DCACPs) attracted on our attention. DCACP procedure provided accurate interaction energies for the test cases, but the interaction energies fall too quickly as the distance between the molecules increases. I further investigated the effects of DCACPs on the employed density functionals with a detailed study of the interaction energies of isomers of the water hexamers and determined that with the original implementation it corrects for limitations of the BLYP functional in describing exchange-repulsion interaction as well as for dispersion interactions. We propose two different methods, namely DCACP+D and DCACP2, for improving the problems associated with the DCACP approach. These methods both provide improvements in the accuracy of the original DCACPs and also correct the quick fall-off

problem of the interaction energies at long–range.

TABLE OF CONTENTS

1.0 INTRODUCTION 1

1.1 THEORY OVERVIEW 1

1.1.1 DFT+D 2

1.1.2 Dispersion–Corrected–Atom–Centered–Pseudopotentials (DCACP's) 8

1.1.3 van der Waals density functional (vdW–DF) 10

1.1.4 Random phase approximation (RPA) 11

2.0 BENCHMARK CALCULATIONS OF WATER-ACENE INTERACTIONS 13

2.1 INTRODUCTION 13

2.2 THEORETICAL METHODS 16

2.3 RESULTS 19

2.3.1 DFT–SAPT calculations 19

2.3.2 Dispersion-corrected DFT calculations 25

2.3.3 Extrapolation to the DFT–SAPT results to water–graphene 27

2.4 CONCLUSIONS 28

2.5 ACKNOWLEDGEMENTS 29

3.0 LINEAR ACENES WITH WATER 30

3.1 INTRODUCTION 30

3.2 THEORETICAL METHODS 32

3.2.1 Geometries 32

3.2.2 Wavefunction-based methods 34

3.2.3 DF–DFT–SAPT . . . 37
3.2.4 DFT-based methods . . . 38
3.2.5 RPA-based methods . . . 40
3.3 RESULTS AND DISCUSSION . . . 40
3.3.1 DF–DFT–SAPT Results . . . 41
3.3.2 Basis set sensitivity of the interaction energies . . . 45
3.3.3 Wavefunction-based results . . . 47
3.3.4 DFT-based results . . . 50
3.3.5 RPA-based results . . . 52
3.3.6 Long-range interactions . . . 54
3.4 CONCLUSIONS . . . 55
3.5 ACKNOWLEDGEMENT . . . 56
4.0 WATER HEXAMER ISOMERS WITH DCACP . . . 57
4.1 INTRODUCTION . . . 57
4.2 DISCUSSION . . . 59
4.3 CONCLUSIONS . . . 65
5.0 DCACP+D . . . 66
5.1 INTRODUCTION . . . 66
5.2 METHOD . . . 67
5.3 TESTS . . . 68
5.4 CONCLUSIONS . . . 76
6.0 DCACP2 . . . 77
6.1 INTRODUCTION . . . 77
6.2 METHOD . . . 79
6.3 RESULTS . . . 80
6.4 CONCLUSIONS . . . 89
6.5 ACKNOWLEDGMENTS . . . 89
7.0 CONCLUSIONS . . . 90

APPENDIX A. COMMONLY USED ABBREVIATIONS 92
APPENDIX B. SUPPORTING INFORMATION FOR CHAPTER 6 94
APPENDIX C. ADSORPTION OF A WATER MOLECULE ON THE MGO(100) . . . 102
C.1 INTRODUCTION 102
C.2 COMPUTATIONAL DETAILS 103
C.3 RESULTS 105
C.3.1 $2X2$ Cluster model 105
C.3.2 $4X4$ Cluster models 108
C.3.3 $6X6$ Cluster model 110
C.3.4 GDMA calculations 113
C.4 CONCLUSIONS 119
C.5 ACKNOWLEDGEMENTS 119
BIBLIOGRAPHY 120

LIST OF TABLES

2.1 Methods and programs used in Chapter 3 17

2.2 Contributions to the DF–DFT–SAPT water–acene interaction energies 20

2.3 Interaction energies and R_{OX} values for water–coronene 21

2.4 Multipole moments for benzene, coronene, HBC and DBC 22

2.5 Electrostatic interaction energies for water-acenes 23

2.6 Net interaction energies for water–acene systems 24

3.1 Summary of methods and programs used in the current study. 35

3.2 Contributions to the DF–DFT–SAPT interaction energies (kcal/mol). 42

3.3 Electrostatic interaction energies of water–linear acenes 43

3.4 Influence of the basis set on the water–acene interaction energies (kcal/mol). 46

3.5 Net interaction energies (kcal/mol) for the water–acene systems. 48

3.6 Net DFT interaction energies (kcal/mol) for the water–acene systems. 51

3.7 Net RPA interaction energies (kcal/mol) for the water–acene systems. 53

5.1 Fitted values for the damping function 68

5.2 Mean absolute relative errors (MARE) of binding energies for the S22X5 set. 70

6.1 Percentage MARE of binding energies for the S22X5 set. (MAEs in kcal/mol) . . . 83

A1 List of commonly used abbreviations 92

B1 DCACP2 parameters. 95

B2 S22X5 set interaction energies at R_{eq} for the corrected PBE functional in kcal/mol. 96

B3 S22X5 set interaction energies at $1.5R_{eq}$ for the PBE functional (kcal/mol). 97

B4 S22X5 set interaction energies at $2R_{eq}$ for the PBE functional (kcal/mol). 98
B5 S22X5 set interaction energies at R_{eq} for the BLYP functional(kcal/mol). 99
B6 S22X5 set interaction energies at $1.5R_{eq}$ for the BLYP functional (kcal/mol). 100
B7 S22X5 set interaction energies at $2R_{eq}$ for the BLYP functional (kcal/mol). 101
C1 DFT–SAPT interaction energies (kcal/mol) for water–MgO (single–layer $4X4$). . . . 111
C2 DFT–SAPT interaction energies (kcal/mol) for water–MgO (double–layer $4X4$). . . 112
C3 DFT–SAPT interaction energies for water–MgO ($6X6$) 115
C4 MP2C–F12 binding energies (kcal/mol) for water interacting with MgO(100) clusters 117
C5 Multipole moments (in au) for the Mg and O atoms in the cluster models. 118
C6 Electrostatic interaction energies (kcal/mol) for water/MgO(100) clusters 118

LIST OF FIGURES

1.1 Damped dispersion energy (kcal/mol) between two carbon atoms. 3

2.1 Acenes used in Chapter 3 15

2.2 Water–acene geometry used in Chapter 3 16

2.3 Potential energy curves for water–coronene and water–HBC 26

3.1 Acenes studied. 33

3.2 Placement of the water molecule relative to the acene (water–anthracene). 33

3.3 Labeling scheme of the carbon and hydrogen atoms. 34

3.4 Differences between Mulliken charges (me) in the presence and absence of the water. 44

3.5 Long-range interactions of water–benzene calculated with various methods. 54

4.1 Water hexamers used in the current study. 59

4.2 Net interaction energies of isomers of $(H_2O)_6$ (kcal/mol) 61

4.3 2–Body interaction energies (kcal/mol) 62

4.4 Comparison of the individual contributions to the 2–body energy (kcal/mol) 63

4.5 2–body BLYP exch-rep + induction + DCACP corr. vs SAPT exch-rep + induction . 64

4.6 3–body energies (kcal/mol) from the BLYP, BLYP/DCACP, and CCSD(T) methods. 65

5.1 $(H_2O)_6$ isomer energies in kcal/mol. 71

5.2 $(H_2O)_6$ isomer energies in kcal/mol. 72

5.3 Percentage errors in the $(H_2O)_2$ interaction energies relative to CCSD(T) 74

5.4 Percentage errors in the $(H_2O)_2$ interaction energies relative to CCSD(T) 75

6.1 Interaction energy of the sandwich form of the benzene dimer. 81

6.2 DCACP/BLYP corrections compared to exp. C_6R^{-6} and DFT–SAPT dispersion. . . 82
6.3 Relative energies of $(H_2O)_6$ isomers energies (kcal/mol). 85
6.4 Relative energies of $(H_2O)_6$ isomers energies (kcal/mol). 86
6.5 Percentage error in the $(H_2O)_2$ interaction energy relative to the CCSD(T) results. . 87
6.6 Percentage error in the $(H_2O)_2$ interaction energy relative to the CCSD(T) results. . 88
B1 Geometries of dimers used for the parametrization 95
C1 Geometry representing a water molecule on a $6X6$ $(MgO)_{18}$. 104
C2 Potential energy curves for a water molecule approaching to the $2X2$ MgO cluster. . 106
C3 Water– $2X2$ MgO cluster interaction energy components. 107
C4 Potential energy curves of a water molecule to the $2X2$ cluster 108
C5 Potential energy curves for approach of a water molecule to the MgO $4X4$ cluster. . 109
C6 Potential energy curves of a water molecule to the $4X4$ MgO double layer 110
C7 Potential energy curves of a water molecule to the $6X6$ layer 114
C8 Change in the interaction energy with MgO cluster size. 116
C9 Potential energy curves for DMC compared with MP2C-F12 117

1.0 INTRODUCTION

The development of density functional theory (DFT) methods provided chemists with a useful tool for modeling a variety of systems. Although DFT was formally introduced in 1964,[1,2] correcting the deficiency of the DFT methods in modeling dispersion interactions was not a very active area of research until a decade ago. Nevertheless, significant progress have been made in including the dispersion interactions within the DFT framework. I organize my thesis as follows. Chapters 2 and 3 include tests done for the interaction of a water molecule with different types of acenes using various dispersion–corrected DFT methods. Chapter 4 contains in depth investigation of the dispersion–corrected atom–centered pseudopotential (DCACP) method using isomers of the water hexamer. Chapters 5 and 6 provides two different ways of improving the DCACP methodology.

1.1 THEORY OVERVIEW

Non–bonding interactions such as dispersion (van der Waals) and hydrogen-bonding play a vital role in determining the structure and functionality of many systems including DNA, proteins, adsorption of molecules on surfaces and the packing of crystals.[3–6] However, modeling them with computational methods is not an easy task. Kohn–Sham density functional theory (DFT)[1,2,7,8] emerged as a popular method to investigate the electronic structure of many body systems since it provides a good balance between the accuracy and computational cost. In principal DFT is exact, however in practice one needs to approximate the unknown form of the exchange–correlation functional. Until recently, this was done with the local (LDA)[2] and semi–local generalized gradient

corrected (GGA)[9] functionals which fail to correctly describe the long–range dispersion interaction between molecules.[10,11] Dispersion energy arises from instantaneous charge fluctuations (correlated motion of electrons) such as induced dipoles. The correct asymptotic behavior ($-C_6R^{-6}$) of these long–range interactions is not described by local and semi-local approximations in DFT which greatly limits their applicability to systems where dispersion interactions are important. A vast number of strategies have been introduced to address this problem.[12–29] The next sections will include an overview of these methods used in this thesis.

1.1.1 DFT+D

Atom-atom type $C_6^{ij}R_{ij}^{-6}$ (and possibly also $C_8^{ij}R_{ij}^{-8}$) corrections are the most popular method for incorporating van der Waals (vdW) interactions in to DFT.[18,20–24,30,31] A similar approach was also used for correcting the Hartree–Fock method for dispersion as early as 1975.[32] Although earlier versions for this type of dispersion correction were proposed[18] DFT–D method became more recognized after the initial work of Grimme.[20] In this so–called "DFT+D" method, the DFT total energy obtained by an XC functional is augmented with a simple dispersion correction in the form of

$$E_{disp} = -s_6 \sum_{i=1}^{N-1} \sum_{j=i+1}^{N} (C_6^{ij} R_{ij}^{-6}) f_d(R_{ij}), \tag{1.1}$$

where N is the number of atoms, R_{ij} is the distance between i^{th} and j^{th} atom pairs, C_6^{ij} are pairwise dispersion coefficients, f_d is a damping function, and s_6 is a global scaling factor which depends on the density functional being used. Numerous types of damping functions were proposed to avoid the divergent behavior of the dispersion energy at short distances.[18,20,23,30,33] The effect of a damping function[18] of the type

$$f_d(R) = \frac{1}{1+\exp(-d(\frac{R}{R_{vdW}}-1))}, \tag{1.2}$$

is shown in Fig. 1.1 (C_6^{ij}=1.65 Jnm^6mol-1, R_{vdW}=3.22 Å(dashed line), d=23 and s_6=1).

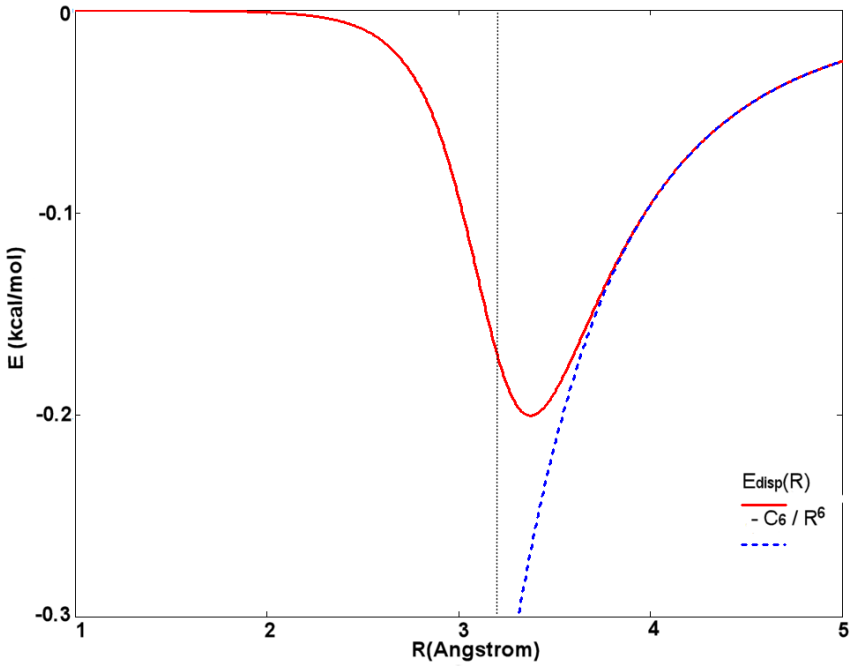

Figure 1.1: Damped dispersion energy (kcal/mol) between two carbon atoms.

The dispersion energy correction term is calculated separately from the DFT calculation. Since it is a long-range effect its influence on the electron densities should be small which allows a separate calculation for the correction. This method is general and can be combined with any exchange-correlation functional, with C_6 coefficients being determined either empirically[18,20] or *ab-initio* methods.[22–24] Obtaining an accurate set of coefficients is of vital importance. Next, I will summarize the methods used in this thesis for dispersion correction namely, DFT–D2, DFT–D3, vdW–TS, vdW–DF and RPA.

In an earlier version of the DFT–D method Wu *et al*[18] calculated empirical atomic C_6^{ij} coefficients for by least squares fitting from experimental molecular C_6^{ij} coefficients obtained by using dipole oscillator strength distributions (DOSD's). Grimme[20] initially used the C_6^{ij} coefficients from Wu *et al*[18] while averaging them over possible hybridization states (for the carbon atom). Later, in his *less empirical* DFT–D2 approach[21] using DFT/PBE0[34] calculations of atomic ionization potentials (I_p^i) and static dipole polarizabilities (α^i) he computes the dispersion coefficient for an atom with the equation:

$$C_6^i = 0.05 N I_p^i \alpha^i \tag{1.3}$$

where N has values of 2,10,18,36 and 54 based on the atom's position in the periodic table (I_p^i and α^i are in atomic units). Dispersion coefficients for elements up to Xe were made available but in some cases like the group I and II metals averaged C_6 coefficients from the preceding rare gas and group III element were used. This caused problems such as Na and Mg atoms having the same dispersion coefficients. A geometric mean combination rule of the form shown in Equation 1.4 is used to get C_6^{ij} coefficients from atomic C_6^i and C_6^j coefficients.

$$C_6^{ij} = \sqrt{C_6^i C_6^j} \tag{1.4}$$

Other than the above mentioned C_6 averaging issue, two major shortcomings of the DFT–D2 approach are that the C_6^{ij} coefficients are invariant to chemical environment and the s_6 scaling factor, which is adjusted for each density functional, results in wrong asymptotic energies at long range even if the C_6 coefficients are correct.

Grimme and coworkers solved these limitations with the newer DFT–D3 approach.[22] DFT-D3 method includes C_6 and C_8 terms for the 2 body dispersion correction and also an option for the 3 body dispersion correction.

$$E_{disp} = \sum_{AB} \sum_{n=6,8} s_n \frac{C_n^{AB}}{r_{AB}^n} f_{d,n}(r_{AB}) \tag{1.5}$$

$$f_{d,n}(r_{AB}) = \frac{1}{1 + 6(r_{AB}(s_{r,n} R_0^{AB}))^{-\alpha_n}} \tag{1.6}$$

The global scaling factor (s_n), which depends on the density functional used, is only adjusted for $n > 6$ (s_6=1) to ensure the correct asymptotic behavior. This (s_8 to be precise) is the first parameter in DFT–D3 that is empirically determined for each different density functional. Along with this change they have adopted the type of damping function (Eq. 1.6) initially used by Chai and Head–Gordon[33] which is more convenient for higher order dispersion correction. However, in a more recent paper[35] they have replaced this with the Becke–Johnson (BJ) type damping which gives finite dispersion energies at shorter distances rather than "zero" dispersion energy. They have noted that although the BJ damping is the primary choice, overall this only provides a slightly better (although more physically sound) energies for the tests they have performed.[35] I have used the damping function in Eq. 1.6 for the DFT–D3 calculations in this thesis. The $s_{r,6}$ is the second parameter (since $s_{r,8}$ is set to be equal to 1) that is empirically determined by a least squares fit to a big dataset of noncovalent interaction energies. The steepness parameters α_6 and α_8 were manually set to be 14 and 16, respectively.

Dispersion coefficients are calculated via *ab–initio* time–dependent (TD) DFT, where C_6s are calculated using the Casimir–Polder equation (Eq. 1.7) with averaged dipole polarizabilities at imaginary frequencies ($\alpha(i\omega)$). $\alpha(i\omega)$ values were computed not for free atoms but using the stable hydrides of each element (except the rare gas atoms).

$$C_6^{AB} = \frac{3}{\pi} \int_0^{\infty} \alpha^A(i\omega) \alpha^B(i\omega) d\omega \tag{1.7}$$

Grimme *et al.* propose to account for the chemical environment dependence of the dispersion coefficients by using the number coordination number of the atoms. The idea is that bond formation which induces a quenching in the atomic state that changed the excitation energies (hence the polarizabilities) is responsible for the change in the dispersion coefficients. As the coordination number of an atom increases it can be thought of as being squeezed, hence the dispersion coefficient decreases. The reference C_6^{AB} coefficient calculated by the Casimir–Polder equation is adjusted by using the coordination number for the atom pair in the system of interest. Higher order C_8 terms are then obtained using recursion relations using the C_6 values. The accuracy of the molecular C_6 coefficients obtained theoretically can be tested using the experimentally known dipole oscillator strength distributions (DOSDs). The DFT–D3 method gives an 8.4% mean absolute error for the accuracy of the molecular C_6 coefficients based on the DOSD data reported by Meath *et al*.

Two other dispersion correction schemes (Becke–Jonhson and Tkatchenko–Sheffler)[23,24] that depend on the chemical environment of the atoms were proposed before DFT–D3. Around an electron there is a depletion of density, which is named a exchange–correlation hole. The electron and its exchange hole has zero charge overall but a non–zero dipole moment. The Becke–Johnson model (which I have not used in my calculations for this theses, hence it will be summarized briefly here) proposes the aspherical shape of this exchange-correlation hole which generates a dipole moment as the source for the dispersion interaction. System dependent inter–atomic dispersion coefficients C_6^{ij} are obtained by using atomic polarizabilities and exchange(only)-hole dipole moment using the equation 1.8. The dispersion coefficients respond to chemical environment in two ways. One they are scaled using effective atomic volumes and secondly through the changes of the exchange–hole which affect the dipole moments that appear in equation 1.8. The molecular C_6s obtained using this method give 12.2% mean absolute error (MAE) based on the data of Meath and coworkers.[22] One disadvantage of the BJ methods is that the computational cost is more expensive (on the order of a hybrid DFT calculation) compared to other DFT–D methods.[36]

$$C_6^{AB} = \frac{\alpha_A \alpha_B \langle d_x^2 \rangle_A \langle d_x^2 \rangle_B}{\langle d_x^2 \rangle_A \alpha_B + \langle d_x^2 \rangle_B \alpha_A} \tag{1.8}$$

Another method for computing nonempirical dispersion coefficients, which is sensitive to chemical environment of the atom, is the vdW–TS scheme of Tkatchenko and Scheffler.[24] In this procedure C_6^{ij} terms describing the vdW interaction between two atoms or molecules are computed using equation 1.9 which they obtained thorough a series of approximation starting with the Casimer–Polder integral (Eq. 1.7).

$$C_6^{AB} = \frac{2C_6^{AA}C_6^{BB}}{\left[\frac{\alpha_B^0}{\alpha_A^0}C_6^{AA} + \frac{\alpha_A^0}{\alpha_B^0}C_6^{BB}\right]}. \tag{1.9}$$

The free–atom reference values of α_A^0 and C_6^{AA} are taken from a self–interaction corrected TDDFT calculations of Chu and Delgarno.[37] They take the advantage of the relationship between the effective volume and polarizability to calculate dispersion coefficients that depend on the chemical environment of the atom. Hirshfeld partitioning[38] of the electron density of the system is used to obtain each atoms contribution to the density. This effective density, hence the volume, is compared to the density of the free–reference atom to obtain a scaling factor which is used to define the response of the dispersion coefficient's to chemical environment. The accuracy of the molecular C_6^{ij} coefficients obtained using the vdw–TS method with respect to the experimental values is the most accurate (5.4 % MAE)[24] compared to the ones discussed so far. Among the DFT–D methods discussed so far DFT–D3 of Grimme *et al.* and BJ method use higher order dispersion coefficients (at least the C_8^{ij}) when calculating the dispersion energy but vdW–TS includes only the leading C_6^{ij} term. The reason behind this is that they assume shorter–ranged dispersion energy is included already when GGA functionals are used and some of it is also included artificially by the use of the damping function.

$$E^{ABC} = C_9^{ABC}\frac{3cos\alpha cos\beta cos\gamma + 1}{(r_{AB}r_{BC}r_{AC})^3} \tag{1.10}$$

All of these (DFT–D3, vdW–TS and BJ) methods also have versions those provide description for dispersion energy beyond the pairwise additivity.[15,22,39–41] However, Johnson *et al.* do not recommend to use their version of due to arbitrariness in the choice of damping function for the three–body interaction terms and the physical meaning if these terms in a molecular dimer,

and Grimme *et al.* decided to switch it off due to an overestimation of the three–body effects in overlapping density regions with current density functionals and this leads to deterioration in the performance of pairwise–additive only DFT–D3.[22] For including the three–body terms Axilrod–Teller–Muto equation (Eq. 1.10) has been used in all of the methods[22,39,40] but the recent version that was published by Tkatchenko and DiStasio.[15,41] This latest many–body dispersion method (MBD) includes the long–range screening effects and many–body vdW energy to the all orders of dipole interactions. In this method atoms are represented by quantum harmonic oscillators (QHO) with characteristic frequency-dependent polarizabilities obtained with the aforementioned vdW–TS method and the dispersion energy is obtained by solving the Schrödinger equation corresponding to these interacting QHOs within the dipole approximation. I will not go into more detailed description of the many–body dispersion methods since they are not used in this thesis but suffice it to say that these are found to be more important in modeling supramolecular systems[42] and crystals.[39,43]

1.1.2 Dispersion–Corrected–Atom–Centered–Pseudopotentials (DCACP's)

Pseudopotentials are very important for efficient electronic structure calculations. The advantages they offer include reducing the number of electrons used (frozen core approximation), decreasing the basis functions needed (smooth potentials near atomic core) and including relativistic effects. The details of the pseudopotential approximation will not be covered in this thesis, but the dispersion–corrected atom–centered potential DCACP approach[12,13] makes use of the separable form of pseudopotentials into a local and non–local parts (Kleinman-Bylander form).[44] The idea is that non–local part can cast the nonlocal character of the dispersion forces.

The DCACP procedure modifies the electronic density by adding to the Hamiltonian atom–centered non–local potentials of the form,

$$\mathrm{V}_l(\mathbf{r},\mathbf{r}^{'}) = \sum_{m=-l}^{l} \mathrm{Y}_{lm}(\hat{\mathbf{r}})\mathrm{p}_l(\mathrm{r};\sigma_2)\sigma_1\mathrm{p}_l(\mathrm{r}^{'};\sigma_2)\mathrm{Y}_{lm}(\hat{\mathbf{r}}^{'}), \tag{1.11}$$

where Y_{lm} denotes a spherical harmonic, and p_l is a normalized projector defined as $p_l(r;\sigma_2) \propto$

$r^l \exp[-r^2/2\sigma_2^2]$. The dispersion correction potentials are of the same functional form as the Gaussian based non–local channels of the Goedecker–Teter–Hutter (GTH) pseudopotentials.[45] The analytical form of the GTH type pseudopotentials makes it easier to optimize the parameters needed in DCACPs. The parameter σ_1 scales the magnitude of the pseudopotential, and σ_2 tunes the location of the projector's maximum from the atom center. In their application of this method, Roethlisberger and coworkers used the $l = 3$ channel, and determined the σ_1 and σ_2 parameters by use of a penalty function that minimized the differences between the DCACP and full CI or CCSD(T)[46] energies and forces evaluated at the equilibrium and midpoint geometries (the point where the interaction energy equals half that of the equilibrium value – only for the energy term) for a small set of dimers. This additional angular momentum dependent non–local part of the pseudopotential does not interfere with the original pseudopotential since it acts further away from the core region. The σ_2 parameter that determines the location of the projector's maximum for the regular GTH atomic pseudopotentials is in the range of 0.2–0.3 Å while in DCACP it varies between 1.8–3.6 Å. Also the σ_1 which determines the magnitude is much smaller in the DCACP potential compared to the regular GTH potential terms. The negligible difference in bond lengths computed with the uncorrected density functional and its DCACP version gives additional support that the new dispersion channel does not interfere with the atomic psedopotential.

The DCACP method has been implemented for the PBE,[9] BLYP[47,48] and Becke-Perdew[47,49] functionals. It adds negligible computational cost to a DFT calculation. However, unlike DFT-D methods, they permit a self-consistent treatment of electronic effects in a single DFT run and no extra effort is needed to compute the forces on the ions. Currently these pseudopotentials are available for a few elements of the periodic table.

Compared to the uncorrected GGA functionals the DCACP approach gives significantly improved interaction energies for a wide range of systems near their equilibrium structures.[12,13,50–55] However, the DCACP correction to the interaction energy falls off much more rapidly than R^{-6} with increasing distance between the monomers in a dimer.[54–56] In Chapter 4, a study of isomers of the water hexamer, we concluded that at least when used with the BLYP functional, DCACPs are correcting for limitations of the functional in describing exchange-repulsion interaction as well

as for dispersion interactions.[55]

1.1.3 van der Waals density functional (vdW–DF)

The main ingredient for the vdW–DF method is the inclusion of a long range non–local correlation energy functional of the form shown in equation 1.12.

$$E_C^{non-local} = \int\int \rho(\mathbf{r})\Phi(\mathbf{r},\mathbf{r}')\rho(\mathbf{r}')\, d\mathbf{r}\, d\mathbf{r}'. \tag{1.12}$$

The nonlocal correlation functional ($E_C^{non-local}$) involves integration over the electronic densities at two points ($\mathbf{r}$ and $\mathbf{r}'$) with the non–local kernel $\Phi(\mathbf{r},\mathbf{r}')$ relating the charge density, ρ, at $\mathbf{r}$ to that at $\mathbf{r}'$. Promising solutions toward this non–local functional for vdW electron-electron correlation was initially given by the Rutgers-Chalmers collaboration.[27,57] The vdW–DF non–local functionals represent the exchange–correlation energy (E_{XC}) functional as,

$$E_{XC}[\rho] = E_X^{GGA} + E_C^{LDA} + E_C^{non-local}, \tag{1.13}$$

where the first term on the right hand side of the equation is the exchange energy from a GGA functional, and the other two terms represent contributions from the short–range correlation energy from LDA and the long–range non–local correlation energy. The kernel Φ in equation 1.12 is a functional of the density and its gradient (vdW–DF2) where a local polarizability model is used to account for the dispersion interactions.[27,28,58,59] Since the $E_C^{non-local}$ is constructed in a way that it vanishes at the uniform electron gas limit, there is no double counting when it is used with the local LDA correlation.[58] The original vdW–DF1 functional[27,57] uses the revPBE exchange functional.[60] However since the revPBE exchange functional can bind spuriously by exchange alone and is too repulsive near equilibrium separation[61] the newer versions of this method (such as vdw–DF2) use different exchange functionals such as PW86,[62] or optimized versions of PBE or B88. The vdW–DF methods do not use empirical parameters for calculating the C_6 coefficients but other variants such as VV10[58] has parameters that affect the C_6 coefficients. The computational cost of these functionals is comparable to that of GGA due to the new algorithm of Soler and Roman-Perez that uses convolution theory.[63] Initially the computational cost scaled higher than that of

GGAs and hybrid GGAs. Recent versions of this family of functionals provide very accurate C_6 coefficients.[25,58,64] Self–consistent versions of these methods are implemented in various codes.

1.1.4 Random phase approximation (RPA)

The random phase approximation (RPA) is a many–body method which treats a subset of correlation effects (described by ring diagrams) to all orders. The RPA method has recently gained an increased popularity,[65–73] although the history of RPA goes back to Bohm's and Pines's plasma theory of electron correlation.[74] The RPA can be derived within the framework of DFT using the adiabatic connection fluctuation–dissipation (ACFD) theorem.[75,76] Being self–interaction free by incorporating the exact exchange using KS orbitals within the Hartree–Fock exchange energy expression, having the correct long–range behavior for the dispersion interactions, producing the right decay outside a metal surface and incorporating a renormalized (screened) Coulomb interaction are some of the advantages that RPA theory offers.

The expression for the correlation energy in RPA is

$$E_c^{RPA} = \int_0^\infty \frac{d\omega}{2\pi} Tr\{ln(1-\chi_0(i\omega)v)+\chi_0(i\omega)v\}. \tag{1.14}$$

In equation 1.14 v is the Coulomb interaction kernel $(1/|r-r'|)$ and χ_0 is the Kohn–Sham (non–interacting) response function evaluated at imaginary frequencies $i\omega$ by using the formula

$$\chi_0(r,r';i\omega) = 2\sum_i^{occ}\sum_a^{unocc} \frac{\phi_i^*(r)\phi_a(r)\phi_a^*(r')\phi_i(r')}{i\omega+\varepsilon_i-\varepsilon_a}. \tag{1.15}$$

$$E_{tot}^{RPA} = E_{tot}^{DFT} - E_{xc}^{DFT} + E_x + E_c^{RPA} \tag{1.16}$$

RPA can be self–consistently calculated but since it is computationally demanding. In general it is computed non–self–consistently as a post DFT calculation. The post–DFT RPA energy is calculated as shown in Equation 1.16 where exchange–correlation energy from the RPA method replaces the exchange–correlation energy obtained by using the chosen density functional. However also, due to RPA not performing well for small inter–electronic distances, some groups suggested using the range–separated versions of the RPA.[77,78] In the range–separated RPA , the short–range

interactions are described via an exchange–correlation density functional while long–range exchange and correlation are treated by HF and RPA, respectively.

2.0 BENCHMARK CALCULATIONS OF WATER-ACENE INTERACTION ENERGIES: EXTRAPOLATION TO THE WATER-GRAPHENE LIMIT AND ASSESSMENT OF DISPERSION-CORRECTED DFT METHODS

This work was published as[*]: Glen R. Jenness, Ozan Karalti, and Kenneth D. Jordan *Physical Chemistry Chemical Physics*, 12, (2010), 6375–6381[†]

2.1 INTRODUCTION

In a previous study (*J. Phys. Chem. C*, 2009, **113**, 10242–10248) we used density functional theory based symmetry-adapted perturbation theory (DFT–SAPT) calculations of water interacting with benzene (C_6H_6), coronene ($C_{24}H_{12}$), and circumcoronene ($C_{54}H_{18}$) to estimate the interaction energy between a water molecule and a graphene sheet. The present study extends this earlier work by use of a more realistic geometry with the water molecule oriented perpendicular to the acene with both hydrogen atoms pointing down. We also include results for an intermediate $C_{48}H_{18}$ acene. Extrapolation of the water–acene results gives a value of -3.0 ± 0.15 kcal mol^{-1} for the binding of a water molecule to graphene. Several popular dispersion-corrected DFT methods are applied to the water–acene systems and the resulting interacting energies are compared to results of the DFT–SAPT calculations in order to assess their performance.

The physisorption of atoms and molecules on surfaces is of fundamental importance in a

[*]Reproduced by permission of the PCCP Owner Societies

[†]G. R. J. contributed the majority of the numerical data. O. K. contributed the dispersion corrected DFT calculations.

wide range of processes. In recent years, there has been considerable interest in the interaction of water with carbon nanotube and graphitic surfaces, in part motivated by the discovery that water can fill carbon nanotubes.[79] Computer simulations of these systems requires the availability of accurate force fields and this, in turn, has generated considerable interest in the characterization of the water–graphene potential using electronic structure methods.[80–84]

Density functional theory (DFT) has evolved into the method of choice for much theoretical work on the adsorption of molecules on surfaces. However, due to the failure of the local density approximation (LDA) and generalized gradient approximations (GGA) to account for long-range correlation (hereafter referred to as dispersion or van der Waals) interactions, density functional methods are expected to considerably underestimate the interaction energies for molecules on graphitic surfaces. In recent years, several strategies have been introduced for "correcting" DFT for dispersion interactions. These range from adding a pair-wise $C_6^{ij}R_{ij}^{-6}$ interactions,[20,21,24,64] to fitting parameters in functionals so that they better describe long-range dispersion,[12,13,26,56] to accounting explicitly for long-range non-locality, *e.g.*, with the vdW–DF functional.[27] Although these approaches have been quite successful for describing dispersion interactions between molecules, it remains to be seen whether they can accurately describe the interactions of water and other molecules with carbon nanotubes or with graphene, given the tendency of DFT methods to overestimate charge-transfer interactions[85] and to overestimate polarization in extended conjugated systems.[86] Thus, even if dispersion interactions were properly accounted for, it is not clear how well DFT methods would perform at describing the interaction of polar molecules with extended acenes and graphene.

Second-order Möller–Plesset perturbation theory (MP2) does recover long-range two-body dispersion interactions and has been used in calculating the interaction energies of water with acenes as large as $C_{96}H_{24}$.[80] However, MP2 calculations can appreciably overestimate two-body dispersion energies.[87,88] This realization has led to the development of spin-scaled MP2 (SCS–MP2),[89,90] empirically-corrected MP2,[91] and "coupled" MP2 (MP2C)[92] methods for better describing van der Waals interactions. However, it is not clear that even these variants of the MP2 method would give quantitatively accurate interaction energies for water or other molecules ad-

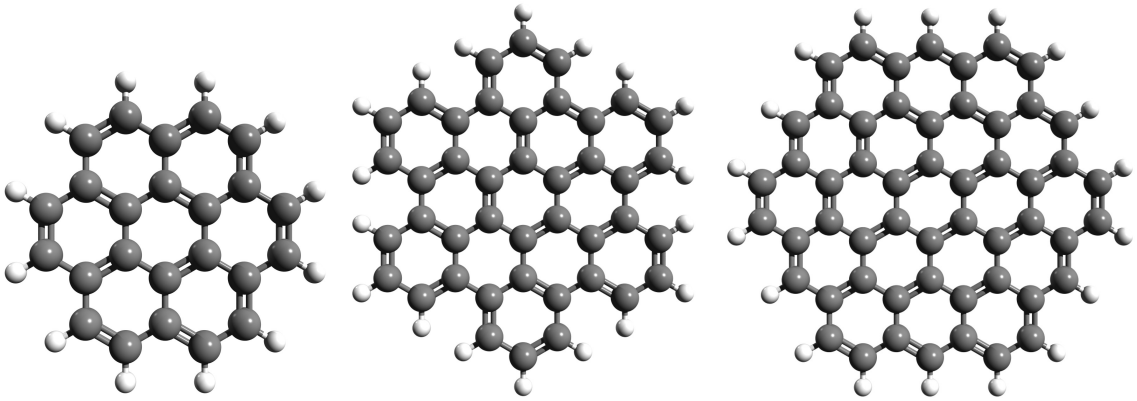

(a) Coronene (b) Hexabenzocoronene (HBC) (c) Dodecabenzocoronene (DBC)

Figure 2.1: Acenes used in the current study.

sorbed on large acenes since the HOMO–LUMO energy gap decreases with the size of the acene. In addition to these issues, the MP2 method is inadequate for systems with large three-body dispersion contributions to the interaction energies.[93]

Given the issues and challenges described above, we have employed the DFT-based symmetry-adapted perturbation theory (DFT–SAPT) method of Heßelmann *et al.*[94] to calculate the interaction energies between a water molecule and benzene, coronene, hexabenzo[bc,ef,hi,kl,no,qr]-coronene (referred to as hexabenzocoronene or HBC), and circumcoronene (also referred to as dodecabenzocoronene or DBC). As will be discussed below, the DFT–SAPT approach has major advantages over both traditional DFT and MP2 methods. The DFT–SAPT method also provides a dissection of the net interaction energies into electrostatic, exchange-repulsion, induction, and dispersion contributions, which is valuable for the development of classical force fields and facilitates the extrapolation of the results for the clusters to the water–graphene limit. In the current paper, we extend our earlier study[84] of water–acene systems to include more realistic geometrical structures. The DFT–SAPT results are also used to assess various methods for including dispersion effects in DFT calculations.

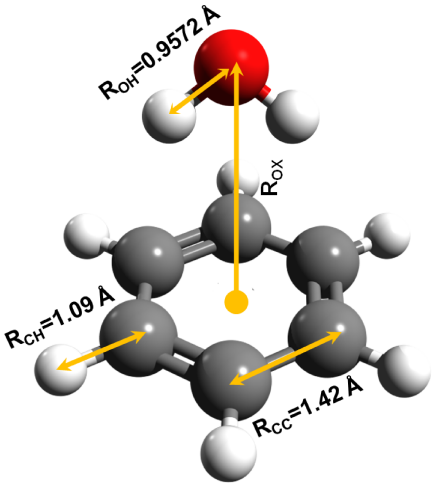

Figure 2.2: Geometry used in the current study, illustrated in the case of water–benzene.

2.2 THEORETICAL METHODS

The coronene, HBC, and DBC acenes used in this study are depicted in Figure 2.1. For each of the acenes, including benzene, all CC bond lengths and CCC angles (1.420 Å and 120°, respectively) were taken to match the experimental values for graphite.[99] The dangling bonds were capped with hydrogen atoms with CH bond lengths and CCH angles of 1.09 Å and 120°, respectively. This facilitates extrapolation of the interaction energies to the limit of a water molecule interacting with graphene. The geometry of the water monomer was constrained to the experimental gas phase geometry (OH bond length of 0.9572 Å and HOH angle of 104.52°).[100] The water molecule was placed above the middle of the central ring, with both hydrogens pointing towards the acene. Note that this is a different water orientation than used for most of the calculations reported in Reference 84. The orientation and distance of the water molecule relative to the ring system were obtained from a series of single-point DFT–SAPT calculations on water–coronene. These calculations give a minimum energy structure with the water dipole oriented perpendicular to the acene ring system, and an oxygen-ring distance of 3.36 Å, which is close to that obtained

Table 2.1: Methods and programs used in the current study.

Method	Scheme	Program
DFT–SAPT[94]	Uses linear response functions from TD-DFT to calculate dispersion energies *via* the Casimir–Polder integral	MOLPRO[95]
DFT+D[20,21]	Adds empirical $C_6^{ij}R_{ij}^{-6}$ corrections to DFT energies	GAMESS[96]
DCACP[12,13,56]	Uses pseudopotential terms to recover dispersion	CPMD[97]
C_6/Hirshfeld[24]	Adds to DFT energies $C_6^{ij}R_{ij}^{-6}$ corrections determined using Hirshfeld partitioning	FHI-AIMS[98]

in prior theoretical studies of water–coronene.[83,101–104] However, the potential energy surface is quite flat (our calculations give an energy difference of only 0.02 kcal mol^{-1} between $R_{OX} = 3.26$ Å and 3.36 Å), and thus small geometry differences are relatively unimportant.

The DFT–SAPT method, and the closely related SAPT(DFT) method of Szalewicz and coworkers,[105] evaluate the electrostatic and exchange-repulsion contributions using integrals involving the Coulomb operator and the Kohn–Sham orbitals, and are thus free of the problems inherent in evaluating the exchange-repulsion contributions using common density functionals. The induction and dispersion contributions are calculated using response functions from time-dependent DFT. In the present study, the calculations made use of the LPBE0AC functional,[94] which replaces the 25% exact Hartree–Fock exchange of the PBE0 functional[34] with the localized Hartree–Fock exchange functional of Sala and Görling[106] and includes an asymptotic correction. In general, DFT–SAPT calculations give interaction energies close to those obtained from CCSD(T) calculations.[107,108] For more details, we refer the reader to Reference 108.

The DFT–SAPT calculations were carried out with a modified aug-cc-pVTZ basis set in which

the exponents of the diffuse functions were scaled by 2.0 to minimize convergence problems due to near linear dependency in the basis set. In addition, for the carbon atoms the *f* functions were removed and the three *d* functions were replaced with the two *d* functions from the aug-cc-pVDZ basis set. Similarly, for the acene hydrogen atoms the *d* functions were removed and the three *p* functions were replaced with the two *p* functions from the aug-cc-pVDZ basis set. The full aug-cc-pVTZ basis set with the diffuse functions scaled by the same amount as the acene carbon and hydrogen atoms was employed for the water molecule. For water–benzene, the DFT–SAPT calculations with the modified basis set give an interaction energy only 0.05 kcal mol^{-1} smaller in magnitude than that obtained with the full, unscaled, aug-cc-pVTZ basis set. Density fitting (DF) using Weigend's cc-pVQZ JK-fitting basis set[109] was employed for the first order and the induction and exchange-induction contributions. For the dispersion and exchange-dispersion contributions, Weigend and co-worker's aug-cc-pVTZ MP2-fitting basis set[110] was used. The DF–DFT–SAPT calculations were carried out with the `MOLPRO` *ab initio* package.[95]

We also examined several approaches for correcting density functional calculations for dispersion, including the dispersion-corrected atom-centered potential (DCACP) method of Roethlisberger,[12,13,56] the DFT+dispersion (DFT+D) method of Grimme,[20,21] and the C_6/Hirshfeld partitioning scheme of Tkatchenko and Scheffler.[24] The DCACP procedure uses modified Göedecker pseudopotentials[45] to incorporate dispersion effects. These calculations were carried out using the `CPMD` program,[97] utilizing a planewave basis set and periodic boundary conditions. These calculations employed a planewave cutoff of 4082 eV and box sizes of $42 \times 42 \times 28$ a.u. for water–benzene and water–coronene, and $46 \times 46 \times 28$ a.u. for water–HBC and water–DBC to minimize interactions between unit cells.

The DFT+D method adds damped empirical $C_6^{ij} R_{ij}^{-6}$ atom-atom corrections[20,21] to the "uncorrected" DFT energies. The DFT+D calculations were performed with the same Gaussian-type-orbital basis sets as used in the DFT–SAPT calculations and were carried out using the `GAMESS` *ab initio* package[96] (using the implementation of Peverati and Baldridge[111]). The dispersion corrections were added to the interaction energies calculated using the PBE,[9] BLYP,[47,48] and B97–D[21] GGA functionals. The B97-D functional is Grimme's reparameterization of Becke's B97 func-

tional[112] for use with dispersion corrections.

The calculations involving the C_6/Hirshfeld method of Tkatchenko and Scheffler[24] were performed with the `FHI-AIMS` package.[98] The C_6/Hirshfeld method, like the DFT+D method, incorporates dispersion *via* atom-atom $C_6^{ij}R_{ij}^{-6}$ terms. However, unlike the DFT+D method, the C_6/Hirshfeld scheme calculates the C_6^{ij} coefficients using frequency-dependent polarizabilities for the free atoms, scaling these values by ratios of the effective and free volumes, with the former being obtained from Hirshfeld partitioning[38] of the DFT charge density. This procedure results in dispersion corrections that are sensitive to the chemical bonding environments. The tier 4 numerical atom-centered basis sets[113] native to `FHI-AIMS` were employed. These basis sets provide a $6s5p4d3f2g$ description of the carbon and oxygen atoms, and a $5s3p2d1f$ description of the hydrogen atoms. A summary of the theoretical methods employed is given in Table 2.1.

2.3 RESULTS

2.3.1 DFT–SAPT calculations

The DFT–SAPT results for the water–acene systems are summarized in Table 2.2. The net interaction energies along the water–benzene, water–coronene, water–HBC, and water–DBC sequence obtained using the DFT–SAPT procedure are -3.16, -3.05, -3.01, -2.93 kcal mol^{-1}, respectively. The interaction energies and R_{OX} values from recent studies of water–coronene summarized in Table 2.3. These earlier studies give interaction energies of water–coronene ranging from -2.56 to -3.54 kcal mol^{-1}.

From Table 2.2, it is seen that the electrostatic interaction energy decreases in magnitude, the dispersion energies increase in magnitude, and the induction energies are relatively constant along the benzene–coronene–HBC–DBC sequence. The exchange-repulsion interaction energy is 3.24 kcal mol^{-1} for water–benzene but only about 2.8 kcal mol^{-1} for the interaction of water with the larger acenes. This reflects the fact that the charge distribution in the vicinity of the carbon atoms is appreciably different for benzene than for the central carbon atoms in the larger acenes. Perhaps

Table 2.2: Contributions to the DF–DFT–SAPT water–acene interaction energies (kcal mol^{-1}).

Term	Benzene	Coronene	HBC	DBC
Electrostatics	−2.85	−1.73	−1.54	−1.39
Exchange-repulsion	3.24	2.79	2.85	2.85
Induction	−1.28	−1.29	−1.36	−1.37
Exchange-induction	0.82	0.80	0.83	0.84
δ(HF)	−0.26	−0.20	−0.23	−0.23
Net induction	−0.71	−0.69	−0.75	−0.75
Dispersion	−3.28	−3.83	−4.00	(−4.07)[a]
Exchange-dispersion	0.44	0.42	0.43	(0.43)
Net dispersion	−2.84	−3.42	−3.57	(−3.64)[a]
Total interaction energy	−3.16	−3.05	−3.01	(−2.93)[b]

[a] Estimated using $E_{disp}(water-DBC) = E_{disp}(water-HBC) + \sum C_6^{ij} R_{ij}^{-6}$, where the $C_6^{ij} R_{ij}^{-6}$ terms account for the dispersion interactions of the water molecule with the twelve additional C atoms of DBC. The C_6 coefficients were determined by fitting the DFT–SAPT water–coronene results.

[b] Total energy calculated using the estimated dispersion energy, described in footnote *a*.

Table 2.3: Interaction energies (kcal mol^{-1}) and R_{OX} values (Å) for water–coronene.

	R_{OX}	E_{int}	Approach
Rubeš *et al.*[83]	3.27	−3.54	DFT/CC//aug-cc-pVQZ
Sudiarta and Geldart[101]	3.39	−2.81	MP2//6-31G(*d*=0.25)
Huff and Pulay[104]	3.40	−2.85	MP2//6-311++G**[a]
Reyes *et al.*[102]	3.33	−2.56	LMP2//aug-cc-pVTZ(-*f*)
Cabaleiro–Lago *et al.*[103]	3.35	−3.15	SCS–MP2//cc-pVTZ
Current study	3.36	−3.05	DFT–SAPT//modified aug-cc-pVTZ(-*f*)[b]

[a] Diffuse functions were used on every other carbon atom.

[b] Modified as described in the text.

the most surprising result of the SAPT calculations is the near constancy of the induction contributions with increasing size of the acene ring system. This is not the case for models employing point inducible dipoles on the carbon atoms, and we expect that it is a consequence of charge-flow polarization,[114,115] which is not recovered in such an approach.

In classical simulations of water interacting with graphitic surfaces the dominant electrostatic contributions are generally described by interactions of the water dipoles (or atomic point charges) with atomic quadrupoles on the carbon atoms, as the quadrupole is the leading moment in an atom-centered distributed multipole representation of graphene. However for finite acenes there are also atomic charges and dipoles associated with the carbon atoms as well as with the edge H atoms. In addition, the electrostatic interaction energies obtained from the SAPT calculations include the effect of charge-penetration, which is a consequence of overlap of the charge densities of the water and acene molecules. It is useful, therefore, to decompose the net electrostatic interaction energies into contributions from charge-penetration and from interactions between the atom-centered multipole moments.

Table 2.4: Multipole moments[a] (in atomic units) for the carbon and hydrogen atoms in benzene, coronene, HBC and DBC[b].

Atom Type	q				$\|\mu\|$				Q_{20}				$\|Q_{22c}+Q_{22s}\|$			
	C_6H_6	$C_{24}H_{12}$	$C_{42}H_{18}$	$C_{54}H_{18}$	C_6H_6	$C_{24}H_{12}$	$C_{42}H_{18}$	$C_{54}H_{18}$	C_6H_6	$C_{24}H_{12}$	$C_{42}H_{18}$	$C_{54}H_{18}$	C_6H_6	$C_{24}H_{12}$	$C_{42}H_{18}$	$C_{54}H_{18}$
C1	−0.09	−0.01	−0.01	0.00	0.11	0.01	0.00	0.00	−1.14	−1.28	−1.29	−1.28	0.09	0.00	0.00	0.00
C2		−0.04	−0.01	0.00		0.11	0.02	0.01		−1.22	−1.28	−1.28		0.09	0.01	0.01
C3		−0.07	−0.03	−0.01		0.16	0.08	0.01		−1.17	−1.25	−1.28		0.02	0.08	0.01
C4			−0.08	−0.04			0.16	0.12			−1.18	−1.22			0.04	0.10
C5			−0.07	−0.07			0.13	0.16			−1.13	−1.16			0.08	0.02
C5a				−0.06				0.16				−1.18				0.12
Ha[c]			0.10				0.14				−0.15				0.09	
Hb[d]	0.09	0.10	0.09	0.11	0.14	0.14	0.14	0.15	−0.13	−0.13	−0.13	−0.13	0.11	0.08	0.10	0.06

[a] Spherical tensor notation is employed here. To convert into a Cartesian representation: $\Theta_{XX} = -\frac{1}{2}Q_{20} + \frac{1}{2}\sqrt{3}Q_{22c}$; $\Theta_{YY} = -\frac{1}{2}Q_{20} - \frac{1}{2}\sqrt{3}Q_{22c}$; $\Theta_{XY} = -\frac{1}{2}\sqrt{3}Q_{22s}$; $\Theta_{ZZ} = Q_{20}$;

[b] Benzene: C_6H_6; Coronene: $C_{24}H_{12}$; HBC: $C_{42}H_{18}$; DBC: $C_{54}H_{18}$;

[c] Ha hydrogen atoms are connected to C4 carbon atoms.

[d] Hb hydrogen atoms are connected to C1 carbons in benzene, to C3 carbons in coronene, and to C5 carbons in HBC and DBC.

Table 2.5: Electrostatic energies (kcal mol^{-1}) between atomic charges on water and multipoles.

Term	Benzene	Coronene	HBC	DBC	Graphene[a]
Charge-Charge	−1.36	−2.18	−1.89	−1.57	0.00
Charge-Dipole	1.86	3.20	2.53	2.01	0.00
Charge-Quadrupole	−2.30	−2.13	−1.55	−1.22	−0.65[b]
Total multipole	−1.80	−1.11	−0.91	−0.77	−0.65
Charge-penetration	−1.05	−0.62	−0.62	−0.62	−0.62[c]
DFT–SAPT	−2.85	−1.73	−1.54	−1.39	(−1.27)[d]

[a] Modeled by $C_{216}H_{36}$ as described in the text.

[b] Calculated by using atomic quadrupoles of $Q_{20} = -1.28$ a.u. on each carbon atom.

[c] The charge-penetration in the electrostatic interaction between water–graphene is assumed to be the same as between water and DBC.

[d] Taken to be the sum of the charge-penetration (from water–DBC) and charge-quadrupole interactions for the water–$C_{216}H_{36}$ model.

Table 2.6: Net interaction energies (kcal mol^{-1}) for water–acene systems.

Method	Benzene	Coronene	HBC	DBC	MAE[a]
DF–DFT–SAPT	−3.17	−3.05	−3.00	(−2.94)[b]	
B97-D	−3.24	−3.62	−3.70	−3.61	0.50
PBE+D	−3.69	−3.61	−3.61	−3.49	0.56
BLYP+D	−3.12	−3.37	−3.48	−3.39	0.32
DCACP-BLYP	−3.08	−3.24	−3.08	−3.10	0.13
C_6/Hirshfeld-BLYP	−2.50	−3.04	−3.11	−3.06	0.22
C_6/Hirshfeld-PBE	−3.77	−4.09	−4.16	−4.07	0.98

[a] Mean absolute error (MAE) relative to DFT–SAPT results.

[b] Calculated using the estimated dispersion term from Table 2.2.

For each of the acenes studied we used Stone's Gaussian distributed multipole analysis (GDMA) program[116] to calculate atomic charges, dipoles and quadrupoles on the acene atoms. Moments higher than the quadrupole make a negligible contribution to the interaction energies and thus were neglected from the multipole analysis. Table 2.4 summarizes the GDMA moments for the acenes obtained from MP2/cc-pVDZ charge densities (the MP2 calculations were carried out using `Gaussian03`[117]). As expected, the values of the charges and dipoles on the inner carbons decrease in magnitude as the size of the acene increases. For coronene the atomic charges and dipoles are near zero for the central six C atoms, whereas for DBC the atomic charges and dipoles are near zero for the inner three rings of carbon atoms. In order to estimate the interaction energies in the absence of charge-penetration, the three point charges from the Dang–Chang model[118] of the water monomer were allowed to interact with the multipole moments on the atoms of the acenes (the use of higher multipoles on the hydrogen and oxygen atoms of the water molecule does not significantly impact the electrostatic interactions between water and the acenes). The results for the

various water–acene systems for $R_{OX} = 3.36$ Å are summarized in Table 2.5[‡]. The charge-charge, charge-dipole and charge-quadrupole interactions are large in magnitude ($\geq$1.2 kcal mol^{-1}) for all acenes considered, with the charge-charge and charge-quadrupole contributions being attractive and the charge-dipole contributions being repulsive. Interestingly, the charge-dipole and charge-quadrupole contributions roughly cancel for water–HBC and water–DBC. The charge-quadrupole contribution decreases in magnitude with increasing size of the acene. This is a consequence of the fact that the short-range electrostatic interactions with the carbon quadrupole moments are attractive while long-range interactions with the carbon quadrupoles are repulsive. The differences of the SAPT and GDMA electrostatic energies provide estimates of the charge-penetration contributions which are found to be -0.62 kcal mol^{-1} for water–coronene, water–HBC, and water–DBC for $R_{OX} = 3.36$ Å.

2.3.2 Dispersion-corrected DFT calculations

The interaction energies of the water–acene complexes (at $R_{OX} = 3.36$ Å) obtained using the various dispersion-corrected DFT methods are reported in Table 2.6. Of the dispersion-corrected DFT methods investigated, the DCACP method is the most successful at reproducing the DFT–SAPT values of the interaction energies at $R_{OX} = 3.36$ Å. For water–coronene, water–HBC, and water–DBC the interaction energies obtained with the C_6/Hirshfeld method combined with the BLYP functional are also in good agreement with the DFT–SAPT values, although this approach underestimates the magnitude of the interaction energy for water–benzene by about 0.7 kcal mol^{-1}. Interestingly, with the exception of the PBE+D approach, all the dispersion-corrected DFT methods predict a larger in magnitude interaction energy for water–coronene than for water–benzene, opposite from the results of the DFT–SAPT calculations. This could be due to the overestimation of charge-transfer in the DFT methods, with the overestimation being greater for water–coronene. Figure 2.3.2 reports the potential energy curves for the water–coronene and water–HBC systems calculated with the various dispersion-corrected DFT methods. From Figures 3(a) and 3(b) it is

[‡]Due to a small conversion error, the actual electrostatic interactions for water-DBC in Table 2.5 differ from those published in Reference 53. These values should be replaced with the following (in kcal mol^{-1}): charge-charge=-1.44; charge-dipole=1.97; charge-quadrupole=-1.24; Total multipole=-0.71

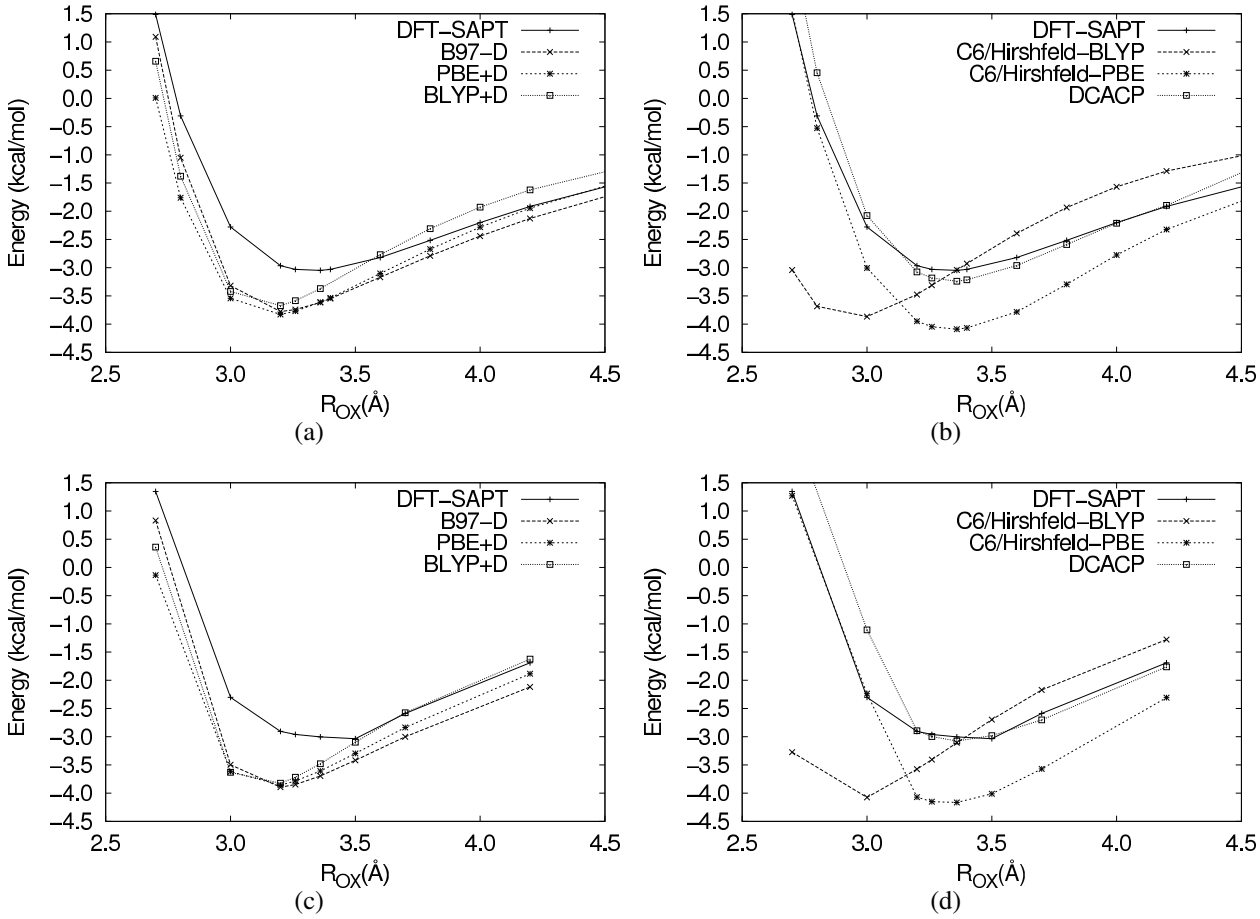

Figure 2.3: Potential energy curves for approach of water to (a,b) coronene and (c,d) HBC.

seen that the DFT+D methods and C_6/Hirshfeld methods both tend to overbind the complexes. The DFT+D methods with all three functionals considered and the C_6/Hirshfeld calculations using the BLYP functional locate the potential energy minimum at much smaller R_{OX} values than found in the DFT–SAPT calculations. It is also seen that the potential energy curves calculated using the DCACP procedure differ significantly from the DFT–SAPT potential for $R_{OX} \geq 4.2$ Å. This is on account of the fact that the dispersion corrections in the DCACP method fall off much more abruptly than R^{-6} at large R. It appears that part of the success of the DCACP method is actually due to the pseudopotential terms improving the description of the exchange-repulsion contribution to the interaction energies.

2.3.3 Extrapolation to the DFT–SAPT results to water–graphene

The exchange-repulsion, induction, exchange-dispersion, and charge-penetration contributions between water and an acene are already well converged, with respect to the size of the acene, by water–DBC. The contributions that have not converged by water–DBC are the non-charge-penetration portion of the electrostatics and the dispersion (although the latter is nearly converged). The non-charge-penetration contribution to the electrostatic energy for water–graphene was estimated by calculating the electrostatic energy of water–$C_{216}H_{36}$ using only atomic quadrupoles on the carbon atoms of the acene. The carbon quadrupole moments were taken to be $Q_{20} = -1.28$ a.u., the value calculated for the innermost six carbon atoms of DBC. We note that this value is about twice as large in magnitude as that generally assumed for graphene.[119] This gives an estimate of -0.65 kcal mol^{-1} for the non-charge-penetration contribution to the electrostatic energy between a water monomer and graphene.

Finally we estimate, using atomistic $C_6^{ij}R_{ij}^{-6}$ correction terms, that the dispersion energy is about 0.05 kcal mol^{-1} larger in magnitude in water–graphene then for water–DBC. Adding the various contributions we obtain a net interaction energy of -2.85 kcal mol^{-1} for water–graphene assuming our standard geometry with $R_{OX} = 3.36$ Å. Rubeš *et al.*, extrapolating results obtained using their DFT/CC method, predicted an interaction energy of -3.17 kcal mol^{-1} for water–graphene. Interestingly, while Rubeš *et al.* conclude the R_{OX} is essentially the same for water–

coronene, water–DBC, and water–graphene, our DFT–SAPT calculations indicate that R_{OX} increases by about 0.15 Å in going from water–coronene to water–HBC, with an energy lowering of about 0.05 kcal mol^{-1} accompanying this increase of R_{OX} for water–HBC. We further estimate, based on calculations on water–benzene, that due to the basis set truncation errors, the DFT–SAPT energies could be underestimated by as much as 0.1 kcal mol^{-1}. Thus, we estimate that the "true" interaction energy for water–graphene at the optimal geometry is -3.0 ± 0.15 kcal mol^{-1}, consistent with the result of Rubeš *et al.*[83]

2.4 CONCLUSIONS

In this study, we have used the DFT–SAPT procedure to provide benchmark results for the interaction of a water molecule with a sequence of acenes up to $C_{54}H_{18}$ in size. All results are for structures with the water molecule positioned above the central ring, with both hydrogen atoms down, and with the water–acene separation obtained from geometry optimization of water–coronene. The magnitude of the interaction energy is found to fall off gradually along the benzene–coronene–HBC–DBC sequence. This is on account of the fact that the electrostatic contribution falls off more slowly with increasing ring size than the dispersion energy grows. We combine the DFT–SAPT results with long-range electrostatic contributions calculated using distributed multipoles and long-range dispersion interactions calculated using $C_6^{ij} R_{ij}^{-6}$ terms to obtain an estimate of the water–graphene interaction energy. This gives a net interaction energy of -2.85 kcal mol^{-1} for water–graphene assuming our standard geometry. We estimate that in the limit of an infinite basis set and with geometry reoptimization, a value of -3.0 ± 0.15 kcal mol^{-1} would result for the binding of a water molecule to a graphene sheet.

We also examined several procedures for correcting DFT calculations for dispersion. Of the methods examined, the BLYP/DCACP approach gives interaction energies that are in the best agreement with the results from the DFT–SAPT calculations. In an earlier work, it was shown that the BLYP functional overestimates exchange-repulsion contributions,[85] leading us to conclude that

the pseudopotential terms added in the DCACP procedure must also be correcting the exchange-repulsion contributions.

Although the focus of this work has been on the interaction of a water molecule with a series of acenes, the strategy employed is applicable for characterizing the interaction potentials of other species with acenes and for extrapolating to the graphene limit. Although there is a large number of theoretical papers addressing the interactions of various molecules with benzene, relatively little work using accurate electronic structure methods has been carried out on molecules other than water interacting with larger acenes.

2.5 ACKNOWLEDGEMENTS

This research was supported by the National Science Foundation (NSF) grant CHE-518253. We would also like to thank Roberto Peverati for advice in using the DFT+D implementation in GAMESS, Mike Schmidt for providing us with an advanced copy of the R4 release of GAMESS, and to Wissam A. Al-Saidi for stimulating discussions.

3.0 EVALUATION OF THEORETICAL APPROACHES FOR DESCRIBING THE INTERACTION OF WATER WITH LINEAR ACENES

This work was published as[*]: Glen R. Jenness, Ozan Karalti, and Kenneth D. Jordan *The Journal of Physical Chemistry A*, 115, (2011), 5955–5964[†]

3.1 INTRODUCTION

The interaction of a water monomer with a series of linear acenes (benzene, anthracene, pentacene, heptacene, and nonacene) is investigated using a wide range of electronic structure methods, including several "dispersion"-corrected density functional theory (DFT) methods, several variants of the random phase approximation (RPA), DFT-based symmetry-adapted perturbation theory with density fitting (DF–DFT–SAPT), MP2, and coupled-cluster methods. The DF–DFT–SAPT calculations are used to monitor the evolution of the electrostatics, exchange-repulsion, induction, and dispersion contributions to the interaction energies with increasing acene size, and also provide the benchmark data against which the other methods are assessed.

Graphene and graphite are prototypical hydrophobic systems.[120] Interest in water interacting with graphitic systems has also been motivated by the discovery that water can fill carbon nanotubes.[79] One of the challenges in modeling such systems is that experimental data for characterizing classical force fields are lacking. Even the most basic quantity for testing force fields,

[*]Reproduced by permission of the PCCP Owner Societies

[†]O. K. contributed the dispersion corrected DFT and RPA calculations. G. R. J. contributed the calculations with DFT–SAPT and wave–function methods.

the binding energy of a single water molecule to a graphene or graphite surface, is not known experimentally. Several studies have appeared using electronic structure calculations to help fill this void.[53,80–84,101,103,104,121–123] However, this is a very challenging problem since most DFT methods rely on either local or semi–local density functionals that fail to appropriately describe long-range dispersion interactions, which are the dominant attractive term in the interaction energies between a water molecule and graphene (or the acenes often used to model graphene).

In a recent study we applied the DF–DFT–SAPT procedure[94] to a water molecule interacting with a series of "circular" acenes (benzene, coronene, hexabenzo[bc,ef,hi,kl,no,qr]coronene, and circumcoronene).[53] These results were used to extrapolate to the binding energy of a water molecule interacting with the graphene surface and also proved valuable as benchmarks for testing other more approximate methods. Water–circumcoronene is essentially the limit of the size system that can be currently be studied using the DF–DFT–SAPT method together with sufficiently flexible basis sets to give nearly converged interaction energies. In the present study we consider a water molecule interacting with a series of "linear" acenes, specifically, benzene, anthracene, pentacene, heptacene, and nonacene, which allows us to explore longer-range interactions than in the water–circumcoronene case and also explore in more detail the applicability of various theoretical methods with decreasing HOMO/LUMO gap of the acenes. The theoretical methods considered include DF–DFT–SAPT, several methods for correcting density functional theory for dispersion, including the DFT–D2 and DFT–D3 schemes of Grimme and co-workers,[21,22] vdW–TS scheme of Tkatchenko and Scheffler,[24] the van der Waals density functional (vdW–DF) functionals of Lundqvist, Langreth and co-workers,[28,124] and the dispersion-corrected atom-centered pseudopotential (DCACP) method of Rothlisberger and co-workers.[12,56] Due to computational costs, only a subset of these methods were applied to water–nonacene.

The results of these methods are compared to those from several wavefunction based methods, including second-order Möller–Plesset perturbation theory (MP2),[125] coupled-cluster with singles, doubles and perturbative triples [CCSD(T)],[46,126,127] spin-component-scaled MP2 (SCS–MP2),[89] "coupled" MP2 (MP2C),[92] and several variants of the random phase approximation (RPA).[128–130] For comparative purposes, we also report interaction energies calculated using the recently intro-

duced DFT/CC method,[83,131] which combines DFT interaction energies with atom-atom corrections based on coupled-cluster calculations on water–benzene.

3.2 THEORETICAL METHODS

The base DFT calculations for the DFT–D2 and DFT–D3 procedures and the CCSD(T), various MP2, and DFT–SAPT calculations were performed with the MOLPRO[95] *ab initio* package (version 2009.1). The DFT/CC corrections were calculated using a locally modified version of MOLPRO. The dispersion corrections for the DFT–D2 and DFT–D3 procedures[21,22] were calculated using the DFT-D3 program[22] of Grimme and co-workers. The DCACP calculations were performed with the CPMD[97] code (version 3.11.1). The vdW–DF energies were computed non-self-consistently using an in-house implementation of the Román–Pérez and Soler[63] methodology and employing densities from plane-wave DFT calculations carried out using the VASP code.[132–135] The RPA and vdW–TS calculations, including the base DFT (or Hartree–Fock) calculations required for both methods, were carried out with the FHI-AIMS[98] program (version 010110). The calculations with MOLPRO used Gaussian-type orbital basis sets, those with FHI-AIMS employed numerical atom-centered basis sets,[113] and those with CPMD and VASP used plane-wave basis sets. Details about the basis sets used are provided below.

3.2.1 Geometries

For the acenes, the same geometrical parameters were employed as in our earlier study of a water molecule interacting with circular acenes,[53] *i.e.*, the CC and CH bond lengths were fixed at 1.42 Å and 1.09 Å, respectively, and the CCC and CCH bond angles were fixed at 120°. Obviously, the linear acenes in their equilibrium geometries have a range of CC bond lengths and CCC bond angles; the fixed values given above were used as it facilitates comparison with our results for the circular acenes. The experimental gas-phase geometry was used for the water monomer (OH bond length of 0.9572 Å and HOH angle of 104.52°).[100] The water monomer was positioned above the

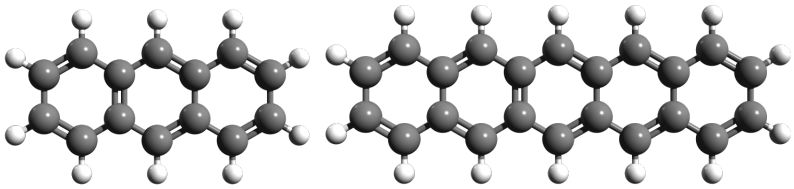

(a) Anthracene ($C_{14}H_{10}$) (b) Pentacene ($C_{22}H_{14}$)

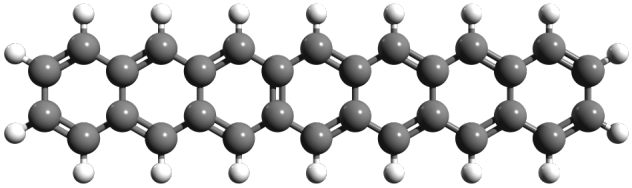

(c) Heptacene ($C_{30}H_{18}$)

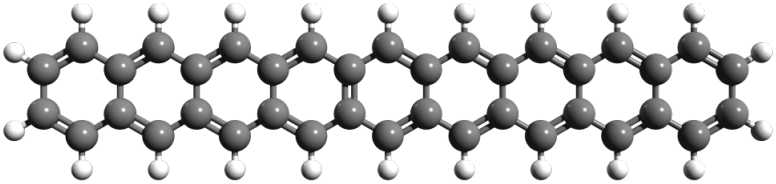

(d) Nonacene ($C_{38}H_{22}$)

Figure 3.1: Acenes studied.

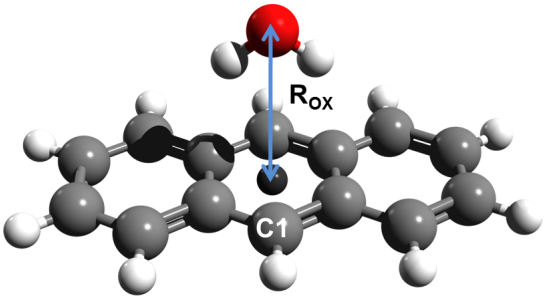

Figure 3.2: Placement of the water molecule relative to the acene (water–anthracene).

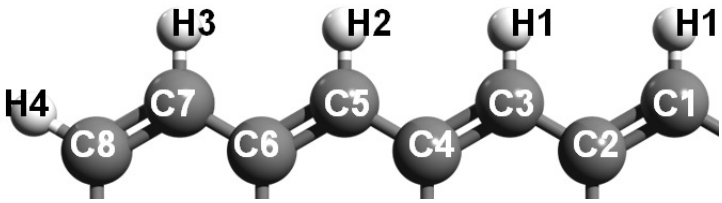

Figure 3.3: Labeling scheme of the carbon and hydrogen atoms.

central ring so that the water C_2 rotation axis is perpendicular to the plane of the acene and the oxygen atom is directly above the acene center-of-mass at a distance of 3.36 Å (obtained from our earlier optimization of water–coronene). 3.2 depicts the orientation of the water monomer relative to the acene, illustrated for the water–anthracene case. For water–anthracene, we also carried out a full geometry optimization at the MP2/aug-cc-pVDZ level to determine the sensitivity of the interaction energy to geometry relaxation. These calculations reveal that the net interaction energy is altered by less than 5% in going from our standard geometry to the fully relaxed geometry.

3.2.2 Wavefunction-based methods

The majority of the calculations using Gaussian-type orbitals were carried out using the aug-cc-pVTZ (AVTZ) basis set,[136,137] although for a subset of systems and methods, the aug-cc-pVQZ (AVQZ) basis set[136,137] and the explicitly correlated F12 methods[138–140] were used to investigate the convergence of the interaction energies with respect to the size of the basis set.

The various MP2 calculations were carried out with density fitting (DF) for both the Hartree–Fock and MP2 contributions (referred to as DF–HF and DF–MP2, respectively). The calculations involving the aug-cc-pVxZ (AVxZ, where x=T or Q) basis sets utilized the corresponding AVxZ JK- and MP2-fitting sets of Weigend and co-workers[109,110] for the DF–HF and DF–MP2 calculations, respectively.

As has been noted numerous times in the literature, the MP2 method frequently overesti-

Table 3.1: Summary of methods and programs used in the current study.

Method	Scheme	Program
DFT–SAPT[94]	Dispersion energies calculated *via* the Casimir–Polder integral using TDDFT response functions	MOLPRO[95]
MP2C[92]	Replaces uncoupled Hartree–Fock dispersion terms in MP2 with coupled Kohn–Sham dispersion terms	MOLPRO
DFT–D2[21]	Adds damped atom-atom $C_6^{ij}R_{ij}^{-6}$ corrections to DFT energies	DFT-D3[22]
DFT–D3[22]	Adds damped atom-atom $C_6^{ij}R_{ij}^{-6} + C_8^{ij}R_{ij}^{-8}$ corrections to the DFT energies	DFT-D3
vdW–TS[24]	Adds damped atom-atom $C_6^{ij}R_{ij}^{-6}$ corrections, with C_6^{ij} coefficients determined from Hirshfeld partitioning of the DFT charge densities	FHI-AIMS[98]
DFT/CC[83,131]	Applies distance-dependent atom-atom corrections from CCSD(T) calculations on model systems to standard DFT energies	MOLPRO[a]
DCACP[12,13,56]	Adds atom-centered pseudopotential terms to correct DFT energies	CPMD[97]
vdW–DF1,[124] vdW–DF2[28]	Incorporates dispersion interactions *via* an integral over a product of a non-local kernel $\Phi(\mathbf{r},\mathbf{r}')$ and the densities $n(\mathbf{r})$ and $n(\mathbf{r}')$ at two points	In-house code densities from VASP[132–135]
RPA	Calculates interaction energies using the random phase approximation	FHI--AIMS

[a] Denotes a locally modified version.

mates dispersion interactions.[141] Cybulski and Lytle,[87] and Pitoňák and Heßelmann[92,142] have suggested simple (and closely related) solutions to this problem. Here we explore the MP2C method of the latter authors where the uncoupled Hartree–Fock (UCHF) dispersion contribution (calculated *via* a sum-over-states expression) is replaced with the coupled Kohn–Sham (CKS) dispersion contribution from a time-dependent DFT (TDDFT) calculation (we include this method under wavefunction-based methods even though it uses the TDDFT procedure in evaluating the dispersion contribution). The 1*s* orbitals on the carbon and oxygen atoms were frozen in the evaluation of the response functions required for the dispersion calculations. The MP2C method generally gives interaction energies of near CCSD(T) quality, but with the computational cost scaling as $O(\mathscr{N}^4)$ (where $\mathscr{N}$ is the number of basis functions) rather than as $O(\mathscr{N}^7)$ as required for CCSD(T).[92] For water–benzene, water–anthracene, and water–pentacene, DF–MP2 and DF–MP2C calculations were also carried out with the explicitly-correlated F12 method,[138,143] for the first two cases in conjunction with the AVTZ and AVQZ basis sets, and for water–pentacene, with the AVTZ basis set only.

CCSD calculations were carried out for water–benzene, water–anthracene and water–pentacene. CCSD(T) calculations, which include triple excitations in a non–iterative manner, were carried out for water–benzene and water–anthracene. To reduce the computational cost, the water–pentacene CCSD calculations were performed with the truncated AVTZ basis set described in Ref. 53 (and hereafter referred to as Tr-AVTZ). We then estimated the full CCSD/AVTZ interaction energy for water–pentacene *via*

$$E_{int}^{CCSD/AVTZ} = E_{int}^{CCSD/Tr-AVTZ} + \left(E_{int}^{MP2/AVTZ} - E_{int}^{MP2/Tr-AVTZ}\right). \tag{3.1}$$

In addition for water–benzene and water–anthracene, CCSD and CCSD(T) calculations were carried using the F12 method[139,140] and the cc-pVTZ-F12 (VTZ-F12) basis set.[144]

Interaction energies were also calculated using the spin-component scaled MP2 (SCS–MP2) of Grimme,[89] in which the antiparallel and parallel spin correlation terms are scaled by a numerical factors of $\frac{6}{5}$ and $\frac{1}{3}$, respectively. The choice of the antiparallel scaling parameter was motivated by the fact that the MP2 methods typically underestimates correlation in two-electron systems

by about 20%; the parallel scaling parameter was obtained empirically by fitting to high-level QCISD(T)[145] values of the reaction energies for a set of 51 reactions.[89]

All reported wavefunction-based interaction energies include the Boys–Bernardi counterpoise correction,[146] with the monomer energies being calculated in the full dimer-centered basis set.

3.2.3 DF–DFT–SAPT

The DF–DFT–SAPT method makes use of DFT orbitals in evaluating the electrostatics and first-order exchange-repulsion corrections to the interaction energy,[147] with the induction and dispersion contributions (along with their exchange counterparts) calculated from response functions.[148,149] In the absence of CCSD(T) results for the larger acenes, the DF–DFT–SAPT[94] results are used as benchmarks for evaluating the performance of other methods. Tekin and Jansen[108] have shown that for systems dominated by CH-π and π-π interactions, the DF–DFT–SAPT/AVTZ method generally reproduces complete basis set limit CCSD(T) interaction energies to within 0.05 kcal mol^{-1}. Similar accuracy is expected in applying this approach to the water–acene systems. Indeed, for water–benzene the interaction energy calculated using the DF–DFT–SAPT/AVTZ method agrees to within 0.03 kcal mol^{-1} of the CCSD(T)-F12/VTZ-F12 result (although, as discussed below, this excellent agreement is due to a partial cancelation of errors in the DF–DFT–SAPT calculations). The DF–DFT–SAPT, like the DF–MP2C procedure described above, scales as O($\mathscr{N}^4$).[94]

The LPBE0AC functional[94] was used for the DF–DFT–SAPT calculations. For the asymptotic correction inherent in LPBE0AC, the experimental vertical ionization potentials (IP) from the NIST Chemistry Webbook[150] were used when available. As the experimental IPs for heptacene and nonacene were not available, these quantities were estimated using the Hartree–Fock Koopmans' Theorem (KT)[151] modified *via*

$$\mathrm{IP_X} = \mathrm{IP_X^{KT}} + \left(\mathrm{IP_{Pentacene}^{Experimental}} - \mathrm{IP_{Pentacene}^{KT}}\right), \tag{3.2}$$

where X is either heptacene or nonacene. This results in 0.92 eV correction to the KT ionization energies. Although this approach of estimating the IP could lead to errors of a few tenths of an

eV, these errors do not significantly impact the resulting water–acene interaction energies. For example, a change of 0.1 eV in the IP of benzene results in a 0.01 kcal mol^{-1} change in the interaction energy of water–benzene. For the density fitting, the cc-pV(x+1)Z JK-fitting set of Weigend[109] was employed for all non-dispersion terms, and the AVxZ MP2-fitting set of Weigend and co-workers[110] was used for the dispersion contributions.

We were unable to successfully complete the calculation of the dispersion energy of water–nonacene using the DF–DFT–SAPT procedure. However the DF–MP2C procedure uses a closely related scheme for evaluating the dispersion energy and gives the same dispersion contributions for water–heptacene and water–nonacene, and moreover gives a dispersion contribution for water–heptacene within 0.1 kcal mol^{-1} of the DF–DFT–SAPT result when used with the LPBE0AC functional.

3.2.4 DFT-based methods

Among the dispersion-corrected DFT methods, the DFT–D2 scheme,[21] which involves the addition of damped atom-atom $C_6^{ij}R_{ij}^{-6}$ correction terms to the DFT intermolecular energies, is the simplest scheme. A drawback to the DFT–D2 scheme is the lack of sensitivity of the C_6^{ij} coefficients to the chemical environment. This is partially addressed in the DFT–D3[22] method which introduces dispersion coefficients that depend on the coordination number of the atoms involved and also includes damped $C_8^{ij}R_{ij}^{-8}$ contributions.[22] In the present study, the DFT–D2 and DFT–D3 schemes are used with the PBE,[9] revPBE,[60] and BLYP[47,48] density functionals together with the AVTZ basis set. The resulting interaction energies are corrected for BSSE using the counterpoise procedure.

The vdW–TS method[24] also applies damped atom-atom $C_6^{ij}R_{ij}^{-6}$ corrections to DFT energies, but it differs from DFT–D2 in that the C_6^{ij} coefficients are adjusted using effective atomic volumes obtained from Hirshfeld partitioning[38] of the charge densities. The vdW–TS calculations were performed with tier 3 and tier 4 numerical atom-centered basis sets[113] for hydrogen and carbon/oxygen, respectively. These basis sets have been designed for use in `FHI-AIMS`. The tier 3 basis set provides a 5s3p2d1f description of the hydrogen atoms, and the tier 4 basis set provides

a $6s5p4d3f2g$ description of the carbon/oxygen atoms. The largest vdW–TS calculation, that on water–nonacene, employed 3864 basis functions.

The DFT/CC method of Rubeš and co-workers[83,131] adds to the DFT energy atom-atom correction terms parameterized to differences between CCSD(T)/CBS and PBE interaction energies for water–benzene. The DFT/CC method has been successfully used to categorize both solid[152] and molecule–surface interactions.[83,121,131] The reference energies used for the DFT/CC calculations were taken from Refs. 4 and 69. The base PBE energies for DFT/CC method were calculated with the AVTZ basis set and were corrected for BSSE using the counterpoise procedure.

The dispersion-corrected atom-centered potential (DCACP) method of Roethlisberger and coworkers[12,56] modifies Goedecker–Teter–Hutter (GTH) pseudopotentials[45] by adding an f channel to correct for deficiencies in the density functional employed. The calculations with the DCACPs were carried out with a plane-wave basis set and using periodic boundary conditions. This approach was applied to acenes through heptacene and all calculations employed a planewave cutoff of 3401 eV and a box size of $30 \times 16 \times 16$ Å. The high cut-off energy was necessitated by use of the GTH pseudopotentials.

The vdW–DF1[124] and vdW–DF2[28] GGA functionals of Langreth and coworkers represent the exchange-correlation energy functional as

$$\mathrm{E_{XC}}[\rho] = \mathrm{E_X} + \mathrm{E_C^{LDA}} + \mathrm{E_C^{non-local}}, \tag{3.3}$$

where the nonlocal correlation functional $\left(\mathrm{E_C^{nonlocal}}\right)$ involves integration over the electronic densities (ρ) at two points ($\mathbf{r}$ and $\mathbf{r}'$) with a non-local kernel ($\Phi(\mathbf{r},\mathbf{r}')$),

$$\mathrm{E_C^{non-local}} = \frac{1}{2}\int\int \rho(\mathbf{r})\Phi(\mathbf{r},\mathbf{r}')\rho(\mathbf{r}')\, d\mathbf{r}\, d\mathbf{r}'. \tag{3.4}$$

As recommended by the developers, for vdW–DF1 and vdW–DF2, the revPBE and modified PW86[49] (called PW86R[153]) exchange density functionals were used, respectively. The vdW–DF calculations were performed with charge densities from `VASP`[132–135] calculations obtained using `VASP`-native pseudopotentials together with a planewave cutoff of 800 eV and a supercell with $\sim$ 10 Å of vacuum in all directions.

3.2.5 RPA-based methods

The random phase approximation (RPA) method is a many-body method which treats a subset of correlation effects (described by ring diagrams) to all orders.[154] There are multiple variants of the RPA method, and in this work three different RPA schemes, denoted RPA, RPA+2OX, and RPA/(HF+PBE), are considered. In each case the energy includes exact exchange contributions computed using the Hartree–Fock expression using either the Hartree–Fock or Kohn–Sham orbitals. The RPA plus second-order exchange (RPA+2OX) approach[128,129] adds a second-order exchange energy correction to the total RPA energy. In the RPA/(HF+PBE) scheme, suggested to us by Ren and Blum,[130] the RPA/PBE correlation correction is added to the Hartree–Fock energy. For the RPA and RPA+2OX schemes the interaction energies obtained using orbitals from HF, PBE, revPBE and BLYP calculations are reported. The RPA calculations were performed with a modified tier 3 numerical atom-centered basis set with the highest angular momentum basis functions from the full tier 3 basis set (*i.e.* the f functions from hydrogen, the g functions from oxygen, and the f and g functions from carbon) being deleted. In addition, the core 1s orbitals were frozen.

3.3 RESULTS AND DISCUSSION

Before turning to the discussion on the interaction energies obtained using the various theoretical methods, it is instructional to examine the trends in the energy gaps between the highest occupied molecular orbital (HOMO) and lowest unoccupied molecular orbital (LUMO) as a function of the length of the acene. The orbital energies have been calculated at the Hartree–Fock level using the 6-31G* basis set.[155,156] This basis was chosen to avoid the low-lying unfilled orbitals corresponding to approximate continuum functions[157] that would be present with a basis set including diffuse functions. The resulting HOMO–LUMO gaps are 12.7, 7.9, 5.8, 4.7, and 4.1 eV along the sequence benzene, anthracene, pentacene, heptacene, and nonacene. This leads one to anticipate growing multiconfigurational character in the wavefunctions with increasing length of the acene. It has even been suggested that the linear acenes larger than pentacene have triplet

ground states,[158] although more recent theoretical work indicates that they have singlet ground states[159] as assumed in our study. Ref. 159 also demonstrates the expected increase in the multiconfigurational character with increasing length of the acene, raising the possibility that some theoretical methods may not properly describe the water–acene interaction energies for the larger acenes.

3.3.1 DF–DFT–SAPT Results

From 3.2, which summarizes the results of the DF–DFT–SAPT calculations, it is seen that the net interaction energy between the water molecule and the acene is nearly independent of the size of the acene. The electrostatic and exchange-repulsion contributions both experience a sizable reduction in magnitude in going from benzene to anthracene, with these changes being of opposite sign and approximately compensating for one another. The exchange-repulsion contribution is essentially constant from anthracene to nonacene, whereas the electrostatic interaction energy continues to decrease in magnitude along the sequence of acenes, with the change in the electrostatic energy in going from water–heptacene to water–nonacene being only 0.03 kcal mol^{-1}. The induction energy, discussed in more detail below, is nearly constant across the series of acenes while the dispersion energy grows in magnitude from water–benzene to water–heptacene, and being essentially the same for water–heptacene and water–nonacene. The fall off in the electrostatic contribution is approximately compensated by the growing dispersion contribution with increasing length of the acene.

For benzene, anthracene, pentacene, and heptacene, the atomic multipoles through hexadecapoles were calculated using a distributed multipole analysis (DMA),[116,160–162] performed with the `GDMA`[116] program and using MP2/cc-pVDZ charge densities from `Gaussian03`[117] calculations. The resulting atomic multipoles (through the quadrupoles) are reported in the supporting information (SI). The analysis was not done for nonacene as the atomic multipole moments for the carbon atoms of the central ring are well converged by heptacene. The charges, dipole moments, and quadrupole moments associated with the carbon atoms of the central ring undergo appreciable changes in going from benzene to anthracene, but they are essentially unchanged along

Table 3.2: Contributions to the DF–DFT–SAPT interaction energies (kcal/mol).

Term	Benzene	Anthracene	Pentacene	Heptacene	Nonacene
$E^{(1)}_{Elst}$	−2.82	−2.29	−2.07	−2.01	−1.98
$E^{(1)}_{Exch}$	3.25	2.85	2.84	2.85	2.85
$E^{(2)}_{Ind}$	−1.28	−1.22	−1.24	−1.26	−1.28
$E^{(2)}_{ExInd}$	0.83	0.76	0.76	0.77	0.77
δ_{HF}	−0.26	−0.21	−0.21	−0.20	−0.21
Net Induction	−0.71	−0.67	−0.69	−0.69	−0.72
$E^{(2)}_{Disp}$	−3.38	−3.66	−3.72	−3.79	(−3.78) [a]
$E^{(2)}_{ExDisp}$	0.46	0.43	0.43	0.43	(0.43)[b]
Net Dispersion	−2.92	−3.23	−3.29	−3.36	(−3.36)
DF–DFT–SAPT	−3.20	−3.34	−3.21	−3.21	−3.21

[a] As discussed in 3.2.3, the DF–DFT–SAPT calculation of the dispersion energy of water–nonacene was unsuccessful. The dispersion energy for water–nonacene was taken to be the same as that for water–heptacene as DF–MP2C calculations give the same dispersion energy for these two systems.
[b] The exchange-dispersion energy of water–nonacene has been assumed to be the same as that for water–heptacene.

Table 3.3: Electrostatic interaction energies of water–linear acenes

Term	Benzene	Anthracene	Pentacene	Heptacene
Charge-Charge	−1.31	−2.36	−2.34	−2.26
Charge-Dipole	1.79	3.33	3.27	3.15
Charge-Quadrupole	−2.27	−2.72	−2.55	−2.44
Charge-Octopole	−0.03	0.17	0.26	0.28
Charge-Hexadecapole	−0.05	−0.09	−0.11	−0.11
Total multipole	−1.87	−1.67	−1.47	−1.39
Charge-penetration	−0.95	−0.62	−0.60	−0.62
DF–DFT–SAPT	−2.82	−2.29	−2.07	−2.01

the anthracene–pentacene–heptacene sequence. The electrostatic interaction between water and the acene can be divided into contributions from the permanent atomic moments and charge-penetration which is the result of the charge density of one monomer "penetrating" the charge density of the other monomer.[3] The charge-penetration contributions were estimated by subtracting from the SAPT electrostatic interaction energies the electrostatic interaction energies calculated using the distributed moments through the hexadecapoles of the acenes and the point charges of the DPP2 model[163] for the water monomer. As seen from 3.3, this procedure gives a charge-penetration energy of -0.95 kcal mol^{-1} for water–benzene and about -0.6 kcal mol^{-1} for a water monomer interacting with the larger acenes. These results are essentially unchanged upon use of moments for the acenes obtained using the larger cc-pVTZ basis set[136] or when employing higher atomic multipoles on the water monomer.

The net induction energy is defined as $E_{ind}^{(2)} + E_{ex-ind}^{(2)} + \delta(HF)$, where the $\delta(HF)$ accounts in an approximate manner for the higher-order induction and exchange–induction contributions. The net

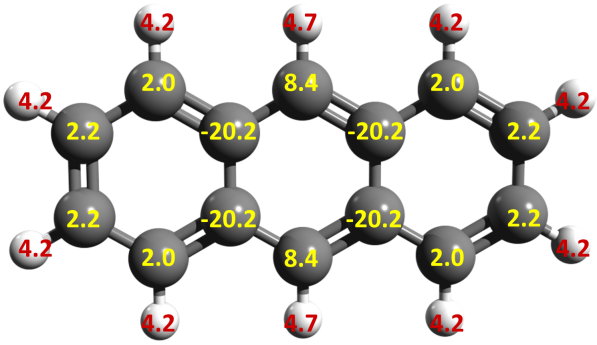

(a)

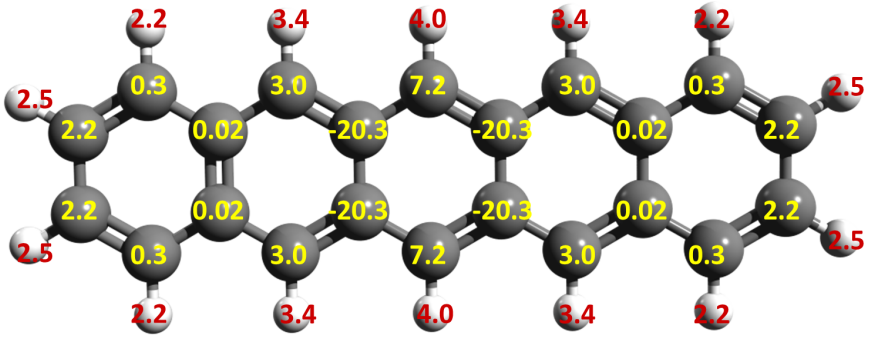

(b)

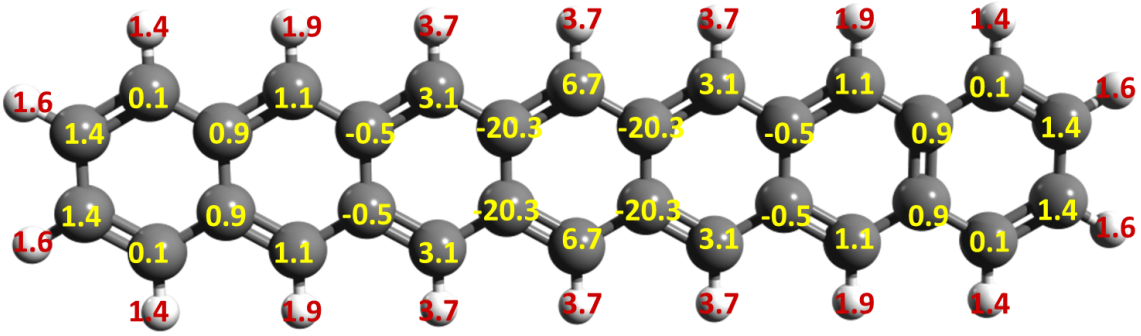

(c)

Figure 3.4: Differences between Mulliken charges (me) in the presence and absence of the water.

induction energies are about -0.7 kcal mol^{-1} for each of the water–acene systems. At first sight the near constancy of the induction energy is somewhat surprising. The net induction energies can be decomposed into a sum of three contributions, atomic polarization, charge-flow polarization, and intermonomer charge-transfer.[3] The nature of the charge-flow polarization is illustrated in 3.4 where we report the change in the atomic charges of anthracene, pentacene, and heptacene caused by the presence of the water molecule. These results were obtained from Mulliken population analysis[164] of the Hartree–Fock/cc-pVDZ wavefunctions of the water–acene complexes. As expected, the electric field from the water molecule causes flow of electron density from remote carbon atoms to the central ring. Using the atomic charges from the Mulliken analysis, we estimate that charge-flow polarization and intermonomer charge-transfer combined contribute roughly half of the induction energy for the water–acene systems, and that these contributions are relatively independent of the size of the acene. Thus, the insensitivity of the induction energy with the size of the acene can be understood in terms of the relatively small contributions of atomic polarization in these complexes.

The dispersion contribution grows by 0.31 kcal mol^{-1} in magnitude in going from water–benzene to water–anthracene, by 0.06 kcal mol^{-1} in going from water–anthracene to water–pentacene, and by another 0.07 kcal mol^{-1} in going to water–heptacene. For water–anthracene the dispersion contribution to the interaction energy is nearly identical to that for water–heptacene. These changes are small compared to the net dispersion contributions (defined as $E^{(2)}_{disp} + E^{(2)}_{ex-disp}$).

3.3.2 Basis set sensitivity of the interaction energies

Before considering in detail the interaction energies obtained with the other methods, it is useful to first consider the sensitivity of the results to the basis sets employed. In 3.4, we report for water–benzene and water–anthracene interaction energies obtained using the DF–MP2, DF–MP2C and DF–DFT–SAPT methods, in each case with both the AVTZ and AVQZ basis sets. In addition, for the DF–MP2 and DF–MP2C methods, F12 results are included. The DF–DFT–SAPT interaction energies increase by 0.06–0.10 kcal mol^{-1} in magnitude in going from the AVTZ to the AVQZ basis set, whereas the corresponding increase in the DF–MP2 and DF–MP2C interaction

Table 3.4: Influence of the basis set on the water–acene interaction energies (kcal/mol).

Theoretical Method	AVTZ	AVQZ
Water–benzene		
DF–MP2	−3.28	−3.39
DF–MP2–F12	−3.47	−3.47
DF–MP2C	−3.06	−3.20
DF–MP2C–F12	−3.25	−3.27
DF–DFT–SAPT	−3.20	−3.30
Water–anthracene		
DF–MP2	−3.66	−3.77
DF–MP2–F12	−3.85	−3.84
DF–MP2C	−3.17	−3.29
DF–MP2C–F12	−3.35	−3.37
DF–DFT–SAPT	−3.34	−3.40

energies is 0.09–0.15 kcal mol^{-1}. Moreover, with the latter two methods, the interaction energy increases by another 0.05–0.08 kcal mol^{-1} in magnitude in going from the AVQZ basis set to the F12/AVTZ procedure. The changes in the DF–MP2 and DF–MP2C interaction energies in going from the F12/AVTZ to the F12/AVQZ approaches are 0.02 kcal mol^{-1} or less. These results justify the use of the DF–DFT–SAPT/AVTZ approach to provide the benchmark results for assessing other theoretical methods.

Thus for the MP2 and MP2C methods, the CBS-limit interaction energies are about 0.2 kcal mol^{-1} larger in magnitude than the results obtained using the AVTZ basis set. A similar sensitivity to the basis set is found for the CCSD(T) interaction energy of water–benzene as seen from 3.5. Moreover, the DF–MP2C and CCSD(T) procedures give nearly identical interaction energies (we revisit the DF–MP2C interaction energies in the next section). It is also found that the DF–DFT–SAPT calculations with the AVTZ basis set give interaction energies within a few hundredths of a kcal mol^{-1} of the MP2C and CCSD(T) results obtained using the AVQZ/F12 method.

Although the interaction energies calculated with the DF–DFT–SAPT method are less sensitive to the basis set than those calculated with the DF–MP2C or CCSD(T) methods, it is clear that in the CBS-limit the DF–DFT–SAPT interaction energies would be about 0.1 kcal mol^{-1} larger in magnitude than those obtained using the AVTZ basis set, resulting in slight overbinding of the water–acene complexes.

3.3.3 Wavefunction-based results

Although the Hartree–Fock approximation predicts a monotonic fall off in the magnitude of the interaction energy with increasing size of the acene, this is not the case for the DF–DFT–SAPT method, the various DF–MP2 methods, or for the CCSD method. In each of these methods, the interaction energy increases in magnitude in going from water–benzene to water–anthracene and then drops off for the larger acenes. The origin of this behavior is clear from analysis of the results in 3.2 and Table S1. Namely, the carbon atoms of benzene carry a greater negative charge than do the carbon atoms of the central ring of the large acenes, causing the exchange-repulsion energy to

Table 3.5: Net interaction energies (kcal/mol) for the water–acene systems.

Method	Benzene	Anthracene	Pentacene	Heptacene	Nonacene
DF–DFT–SAPT	−3.20	−3.34	−3.21	−3.21	−3.21
DF–HF	−0.74	−0.48	−0.29	−0.23	−0.21
DF–MP2	−3.28	−3.66	−3.63	−3.62	−3.61
DF–MP2–F12	−3.47	−3.85	−3.80		
DF–SCS–MP2	−2.61	−2.87	−2.82	−2.80	−2.79
DF–MP2C	−3.06	−3.17	−3.06	−3.02	−3.01
DF–MP2C–F12	−3.25	−3.35	−3.23		
CCSD	−2.63	−2.77	−2.69		
CCSD–F12a	−2.80	−2.89			
CCSD–F12b	−2.76	−2.85			
CCSD(T)	−3.05	−3.26			
CCSD(T)–F12a	−3.21	−3.37			
CCSD(T)–F12b	−3.17	−3.33			

be greater in the case of water–benzene. This is the factor primarily responsible for the smaller in magnitude interaction energy in water–benzene than in water–anthracene.

The interaction energies for the wavefunction based methods are presented in 3.5. For water–benzene, water–anthracene, and water–pentacene the DF–MP2–F12 calculations overestimate the binding energies by 0.27–0.59 kcal mol^{-1} in magnitude, with the discrepancy growing with increasing size of the acene. On the other hand, the DF–SCS–MP2 method underestimates the magnitude of the total interaction energies by 0.39 to 0.61 kcal mol^{-1}. Comparison of the CCSD and CCSD(T) results for water–benzene and water–anthracene shows that the inclusion of triple excitations increases the interaction energies in magnitude by 0.4–0.5 kcal mol^{-1}. Thus it appears that the underestimation of the magnitude of the interaction energies with the DF–SCS–MP2 method is due to the neglect of triple excitations.

The close agreement of the DF–MP2C, DF–DFT–SAPT and CCSD(T) interaction energies for the water–acene systems warrants further discussion. A detailed analysis of wavefunction–based SAPT [SAPT(HF)][165,166] calculations on water–benzene reveals that intramonomer correlation a -0.1 kcal mol^{-1} contribution to the dispersion portion of the interaction energy and a positive contribution to both the exchange and electrostatic contributions to the interaction energy, with the net change in the exchange plus electrostatics interaction being 0.65 kcal mol^{-1}. On the other hand, in the DF–MP2C approach there is a change of $+0.2$ kcal mol^{-1} in the dispersion energy upon replacing the uncoupled Hartree–Fock dispersion contribution with the coupled Kohn–Sham value.

Thus the good agreement between interaction energies obtained with the DF–MP2C method and DF–DFT–SAPT approaches appears to be is due in part to a cancelation of errors in the former. A closer examination of the SAPT(HF) results for intramonomer correlation on the dispersion energy reveals that there are both large positive and negative corrections. It appears that although the DF–MP2C method does not recover the 0.65 kcal mol^{-1} contribution of correlation effects to the exchange and electrostatic energies, this is compensated by the failure to recover the -0.68 kcal mol^{-1} change in the dispersion energy due to intramonomer triple excitations.

3.3.4 DFT-based results

3.6 reports interaction energies obtained using the PBE, revPBE, and BLYP density functionals with and without correcting for long-range dispersion. In considering these results, it should be kept in mind that while GGA functionals do not capture long-range dispersion interactions, they can describe short-range dispersion, and also that some dispersion-corrected DFT methods, such as DCACP and DFT–D actually correct for deficiencies in DFT other than the absence of long-range dispersion interactions.[55]

From 3.6 it can be seen that while the PBE functional recovers about half of the total interaction energies for the water–acene systems, the revPBE and BLYP functionals predict binding only in the water–benzene case. The failure to obtain bound complexes with the BLYP and revPBE functionals is due to their larger (compared to PBE) exchange-repulsion contributions.[85] Indeed this behavior of the revPBE functional was the motivation for the switch from revPBE in vdW–DF1 to PW86 in vdW–DF2.[28]

The DFT–D2 method does well at reproducing the DF–DFT–SAPT interaction energies with mean absolute errors (MAEs) of 0.39, 0.15 and 0.02 kcal mol^{-1} for PBE, revPBE, and BLYP, respectively. For all of the density functionals considered, the DFT–D3 approach overestimates the magnitude of the interaction energies by about 0.5 kcal mol^{-1}. This overestimation is partially reduced if one uses the DFT–D3 parametrization based on the TZVPP[167] basis set[22] (denoted as DFT–D3/TZ in 3.6).

The vdW–TS procedure based on the PBE functional overestimates the magnitude of the total interaction energies, with a MAE of 0.67 kcal mol^{-1}, while the vdW–TS procedure based on the BLYP functional considerably underestimates the magnitude of the interaction energies. Given the fact that the vdW–TS method employs dispersion corrections that depend on the chemical environments, it is surprising that it performs poorer than DFT–D2 for the water–acene systems.

The DFT/CC method gives interaction energies very close to the DF–DFT–SAPT results (MAE of 0.05 kcal mol^{-1}). The DCACP/BLYP approach also gives interaction energies in excellent agreement with the DF–DFT–SAPT results (MAE of 0.06 kcal mol^{-1}) while the DCACP/PBE approach, on the other hand, does not fair as well (MAE of 0.68 kcal mol^{-1}). Both the vdW–DF1

Table 3.6: Net DFT interaction energies (kcal/mol) for the water–acene systems.

Method	Benzene	Anthracene	Pentacene	Heptacene	Nonacene[a]	MAE[b]
DF–DFT–SAPT	−3.20	−3.34	−3.21	−3.21	−3.21	
PBE	−1.87	−1.50	−1.36	−1.32	−1.31	1.76
PBE+D2	−3.66	−3.69	−3.60	−3.57	−3.56	0.38
PBE+D3	−3.60	−3.75	−3.67	−3.65	−3.64	0.43
PBE+D3/TZ[c]	−3.41	−3.54	−3.45	−3.43	−3.42	0.21
revPBE	−0.23	0.14	0.29	0.32	0.33	3.41
revPBE+D2	−3.21	−3.50	−3.44	−3.42	−3.42	0.16
revPBE+D3	−3.50	−3.75	−3.68	−3.66	−3.65	0.41
revPBE+D3/TZ[c]	−3.41	−3.66	−3.58	−3.56	−3.55	0.31
BLYP	−0.27	0.21	0.35	0.37	0.38	3.44
BLYP+D2	−3.13	−3.29	−3.23	−3.22	−3.22	0.03
BLYP+D3	−3.59	−3.83	−3.77	−3.75	−3.75	0.50
BLYP+D3/TZ[c]	−3.23	−3.47	−3.41	−3.39	−3.39	0.14
vdW–TS/PBE	−3.77	−4.01	−3.94	−3.92	−3.89	0.67
vdW–TS/BLYP	−2.50	−2.77	−2.68	−2.65	−2.64	0.59
DFT/CC	−3.23	−3.38	−3.31	−3.29	−3.29	0.06
DCACP/PBE	−2.70	−2.62	−2.48	−2.45		0.68
DCACP/BLYP	−3.08	−3.30	−3.25	−3.23		0.05
vdW–DF1	−2.89	−3.30	−3.38	−3.27		0.14
vdW–DF2	−3.21	−3.38	−3.29	−3.27		0.05

[a] Only a subset of methods were applied to nonacene to check for convergence with respect to system size in the interaction energies.
[b] Mean absolute error (MAE) relative to DF–DFT–SAPT. MAEs were calculated only for benzene through nonacene when water–nonacene interaction energies are available, else they were calculated for benzene through heptacene.
[c] D3/TZ denotes DFT–D3 parameters optimized with Ahlrichs' TZVPP basis set.

and vdW–DF2 functionals give interaction energies close to the DF–DFT–SAPT values, with the vdW–DF2 proving more successful at reproducing the trend in the interaction energies along the sequence of acenes obtained from the DF–DFT–SAPT calculations.

3.3.5 RPA-based results

As seen from 3.7, the RPA calculations using HF orbitals give interaction energies about 0.9 kcal mol^{-1} smaller than the DF–DFT–SAPT results. The errors are reduced to about 0.6 kcal mol^{-1} when using RPA based on DFT orbitals for each of the three functionals considered. The underestimation of the interaction energies is apparently a consequence of the limitations in the RPA method at describing short-range correlation effects (which are not recovered by a sum over ring diagrams only). Interestingly, Scuseria and co-workers have shown that the RPA method based on Hartree–Fock orbitals corresponds to an approximate coupled-cluster doubles approximation.[68] The present PBA/HF calculations on water-benzene, water-anthracene, and water-pentacene gives binding energies 0.25–0.38 kcal mol^{-1} smaller in magnitude than the corresponding CCD results (which, in turn, are nearly identical to the CCSD results in 3.5.

The RPA+2OX method does not correctly reproduce the trend in the interaction energies along the sequence of acenes. It appears that the small HOMO/LUMO gaps in the DFT calculations on the larger acenes result in nonphysical second-order exchange corrections. There is a significant improvement in the interaction energies as calculated with the RPA/(HF+PBE) method, which gives interaction energies 0.2–0.3 kcal mol^{-1} smaller in magnitude than the DF–DFT–SAPT results, which in turn are expected to be about 0.1 kcal mol^{-1} smaller in magnitude than the exact interaction energies for the geometries employed. However, it is possible that the improved results obtained with this approach are fortuitous as it obviously does not address the problem of RPA not properly describing short-range correlation effects.

Table 3.7: Net RPA interaction energies (kcal/mol) for the water–acene systems.

Method	Benzene	Anthracene	Pentacene	Heptacene	Nonacene[a]	MAE[b]
DF–DFT–SAPT	−3.20	−3.34	−3.21	−3.21	−3.21	
RPA/HF	−2.38	−2.42	−2.31	−2.27	−2.25	0.91
RPA/PBE	−2.60	−2.70	−2.62	−2.59		0.61
RPA/revPBE	−2.52	−2.69	−2.61	−2.59		0.64
RPA/BLYP	−2.54	−2.73	−2.66	−2.63		0.60
RPA+2OX/HF	−2.56	−2.53	−2.38	−2.37		0.78
RPA+2OX/PBE	−3.18	−2.91	−2.66	−2.25		0.49
RPA+2OX/revPBE	−3.15	−3.01	−2.76			0.28
RPA+2OX/BLYP	−3.19	−3.03	−2.78			0.25
RPA/HF+PBE	−2.90	−3.11	−3.05	−3.02		0.22

[a] Only a subset of methods were applied to nonacene to check for convergence with respect to system size in the interaction energies.
[b] Mean absolute error (MAE) relative to DF–DFT–SAPT. MAEs were calculated using results for benzene through nonacene when water–nonacene interaction energies are available, else they were calculated for benzene through heptacene.

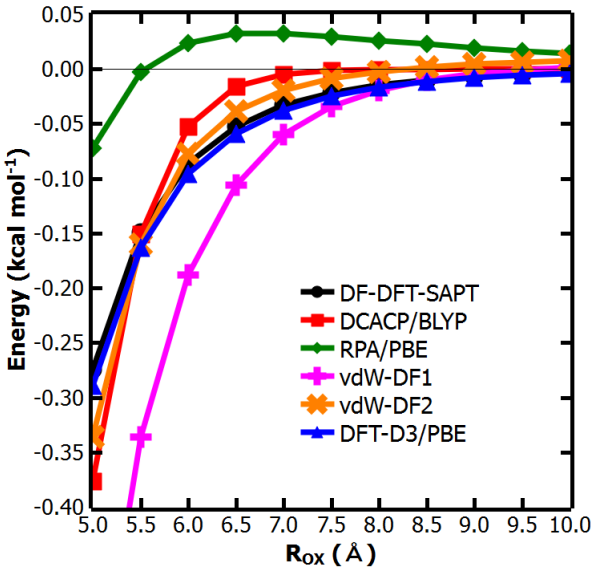

Figure 3.5: Long-range interactions of water–benzene calculated with various methods.

3.3.6 Long-range interactions

All of the results discussed above have been for a water–acene complex with the water–acene separation close to the potential energy minima (for the assumed orientation). 3.5 plots the long-range interaction energies of various theoretical methods. For the DF–DFT–SAPT method the sum of the dispersion and exchange-dispersion contributions is plotted, and for the DCACP/BLYP the difference between the interaction energies with and without the DCACP correction is plotted. For the DFT–D3/PBE method the dispersion contribution is plotted. For the vdW–DF1, vdW–DF2, and RPA approaches, the differences of the correlation energies of the dimers and the correlation energies of the monomers are plotted (using only the non-local correlation terms in the case of the vdW–DF methods).

From 3.5, it is seen that the DFT–D3/PBE curve closely reproduces the DF–DFT–SAPT dispersion curve, indicating that this method is properly describing the dispersion energy in the asymptotic region. Both the vdW–DF2 and DCACP/BLYP methods give dispersion contributions that

fall off too rapidly for $R_{OX} \geq 5.5$ Å (as noted in Ref. 58, the vdW–DF2 tends to underestimate the C_6 coefficients[58]). The vdW–DF1 curve, while being close to the SAPT curve for $R \gtrsim 8$ Å, is much more attractive than the DF–DFT–SAPT curve for $R_{OX} \leq 7.5$ Å.

The long-range interaction energy from the RPA/PBE calculations is repulsive from $R_{OX} = 5.5$ to 10 Å (the longest distance considered). This is due to the fact that the correlation correction in the RPA method also describes the intramonomer correlation, which alters the electrostatic interaction between the water monomer and the benzene molecule.

3.4 CONCLUSIONS

In the current study we examined the applicability of a large number of theoretical methods for describing a water molecule interacting with a series of linear acenes. The DF–DFT–SAPT calculations, which provide the benchmark results against which the other methods are compared, give interaction energies of water–benzene, water–anthracene, water–pentacene, and water–heptacene, ranging from -3.20 to -3.24 kcal mol^{-1}. This small spread in interaction energies is largely due to the fact that the decreasing magnitude of the electrostatic interaction energy with increasing size of the acene is partially compensated by the growing (in magnitude) dispersion contribution. The DF–MP2C–F12/AVTZ approach, gives interaction energies in excellent agreement with the DF–DFT–SAPT results, although this good agreement appears to be due, in part, to a cancelation of errors in the DF–MP2C method.

Four of the DFT–corrected methods considered — BLYP–D2, DCACP/BLYP, DFT/CC and vdW–DF2 — are found to give interaction energies for the water–acene systems very close to the DF–DFT–SAPT results. The revPBE–D2, BLYP–D3/TZ, vdW–DF1, and PBE–D3/TZ approaches also are reasonably successful at predicting the interaction energies at our standard geometries. However these successes do not necessarily carry over to other geometries. In particular, as seen in 3.5, both the DCACP and vdW–DF2 methods underestimate long-range dispersion interactions in magnitude.

Even though the HOMO/LUMO gap decreases with increasing size of the acene, there is no indication that any of the methods considered are encountering problems in the calculation of the water–acene interaction energy even for acenes as large as nonacene.

3.5 ACKNOWLEDGEMENT

We would like to thank Professor A. Heßelmann for his advice concerning the use of the MP2C method, Professor S. Grimme for providing us with a copy of his DFT-D3 program, and Professor P. Nachtigall for discussions on DFT/CC. G. R. J. would like to personally thank the attendees of the Telluride Many-Body Interactions 2010 Workshop for many insightful discussions. The calculations were carried out on computer clusters in the University of Pittsburgh's Center for Molecular and Materials Simulations (CMMS).

4.0 IS THE DCACP METHOD PRIMARILY CORRECTING FOR DISPERSION?

4.1 INTRODUCTION

In the present study the performance of the dispersion–corrected atom–centered potential (DCACP)[12,13] approach designed to add dispersion interaction missing in standard density functional methods is analyzed for the low–energy ring, cage, prism, and book isomers of $H_2O)_6$. It is concluded that for these clusters, the success of the DCACP method, particularly when used in conjunction with BLYP functional, not only corrects for dispersion but also corrects for errors in the non–dispersion contributions such as exchange to the interaction energies.

A major drawback of common GGA and hybrid density functional methods is the failure to describe long-range dispersion interactions which greatly limits their applicability to systems where such interactions are important. Not surprisingly, a large number of strategies have been introduced to address this problem.[12,13,18,20–24,26–29] These include adding $C_6^{ij}R_{ij}^{-6}$ (and possibly also $C_8^{ij}R_{ij}^{-8}$) atom-atom type corrections,[18,20–24] fitting parameters in functionals[26] or additional pseudopotential terms,[12,13] to reproduce energies from accurate wavefunction calculations, and incorporating a non–local energy correction.[27–29] In our work on water clusters[85] and on water interacting with acenes,[53,54] we have found that near the potential energy minima the dispersion–corrected atom–centered potential (DCACP) procedure of Roethlisberger and coworkers[12,13] gives interaction energies close to those obtained with symmetry-adapted perturbation theory (SAPT).[94,105,166] In the DCACP approach, standard pseudopotentials are augmented with terms that are presumed to account for dispersion interactions missing in calculations using the uncorrected functionals. In this note, we provide evidence that, when applied to water clusters and

used in conjunction with the BLYP functional,[47,48] the major effect of additional pseudopotential terms is to correct for deficiencies in the exchange–repulsion interactions rather than to correct for dispersion.

The DCACP procedure attempts to model long–range dispersion by adding terms to the Hamiltonian of the form,

$$V_{\mathrm{DCACP}}(\mathbf{r},\mathbf{r'}) = \sum_{m} Y_{l,m} p_l(\mathbf{r}) \sigma_1 p_l(\mathbf{r'}) Y^*_{l,m}, \tag{4.1}$$

where $Y_{l,m}$ denotes a spherical harmonic, and projectors (p_l) have the form

$$p_l \propto r^l p_l \exp(-r^2/2\sigma_2^2), \tag{4.2}$$

In their application of this method Roethlisberger and coworkers have taken $l = 3$, and have determined the σ_1 and σ_2 parameters by use of a penalty functional that minimizes the differences between the DCACP and full CI or CCSD(T) energies and forces at the equilibrium and midpoint geometry (the point where the interaction energy equals half that of the equilibrium value). The correction terms have the same analytical form as that used in the Goedecker–Teter–Hutter pseudopotentials.[45] The DCACP method has been implemented with PBE,[9] BLYP[47,48] and Becke-Perdew[47,49] functionals but most applications of the approach have been with the BLYP functional ,and we focus on this implementation in this article. We choose as our test systems, the ring, book, cage and prism isomers of $(H_2O)_6$ (shown in Fig. 4.1) which have been the subject of numerous studies.[64,85,168–173]

In a recent study,[85] using both DFT and wavefunction-based methods, we decomposed the net interaction energies of these isomers into their two-, three-, and four + five + six-body components. We further separated the two- and three-body contributions from the DFT calculations into electrostatics, exchange-repulsion, induction and intermonomer correlation contributions using the LMO-EDA procedure,[174] and compared these with analogous results from symmetry-adapted perturbation theory (SAPT).[166] The inter-monomer correlation contributions from the DFT calculations were taken as approximately corresponding to the short-range part of the dispersion inter-

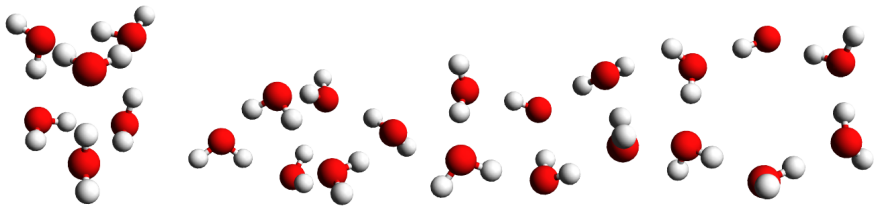

(a) Prism (b) Cage (c) Book (d) Ring

Figure 4.1: Water hexamers used in the current study.

actions. In this earlier work, it was found that the BLYP functional greatly overestimates the exchange-repulsion energies, and that at the minimum energy structures it gives dispersion contributions slightly greater in magnitude than those obtained from SAPT calculations. Obviously, the BLYP functional does not recover long-range dispersion interactions, and these results imply that it overestimates short-range dispersion interactions. Since the LMO-EDA analysis indicates that the greatest source of error in interaction energies of the $(H_2O)_6$ clusters as calculated with the BLYP functional are associated with exchange-repulsion rather than with dispersion energies, we hypothesized that the DCACP procedure mainly addresses the deficiency in the exchange–repulsion energies.

4.2 DISCUSSION

To test the hypothesis presented above, DCACP calculations were carried out on the ring, book, cage, and prism isomers of $(H_2O)_6$. Total interaction energies and their two- and three-body components were evaluated using the BLYP functional with and without the DCACP correction terms. The calculations were carried out using the BigDFT code[175] in which we have implemented the DCACP corrections in the form of Goedecker-Teter-Hutter pseudopotentials.[45] BigDFT makes use of systematic Daubechies wavelet basis sets[176] which are orthogonal in both real and Fourier

space. The BigDFT calculations were carried out using isolated boundary conditions[177] and fine grids (hgrid=0.15 and crmult=8) to ensure convergence in the energies to about 0.1 kcal/mol.

Figure 4.2 reports the net binding energies of the four $(H_2O)_6$ isomers obtained using the BLYP, BLYP/DCACP and CCSD(T) methods. As noted previously, it is seen that the BLYP functional greatly underbinds the clusters and incorrectly orders the isomers as compared to CCSD(T) calculations. The CCSD(T) results are from Ref. 13 and were obtained by combining CCSD(T)/aug-cc-pVDZ energies with the difference of the MP2/aug-cc-pV5Z and MP2/aug-cc-pVDZ energies. This approach results in small ($\leq$ 0.3 kcal/mol) BSSE errors. In contrast to the BLYP method, the BLYP-DCACP calculations give total and relative energies in good agreement with the CCSD(T) values. Clearly, the DCACP procedure is remedying a major deficiency in the BLYP functional.

Fig. 4.3 compares the 2-body interaction energies obtained using the BLYP, BLYP/DCACP, and the CCSD(T) methods. As expected the BLYP functional considerably underestimates the magnitude of the 2-body interaction energies, while the BLYP/DCACP procedure gives 2-body interaction energies close to the CCSD(T) results. 4.4 reports the individual contributions to the net two-body energies obtained from the LMO-EDA analysis of the BLYP energies and from the SAPT calculations. As discussed above the largest errors in the BLYP energies are associated with the exchange-repulsion contributions. These range from 21 kcal/mol for the ring isomer to 26 kcal/mol for the prism isomer. The overestimation of the 2-body exchange repulsion contributions is partially offset by about 10 kcal/mol error in the opposite direction in the induction energies. Perhaps the most compelling results are those shown in Fig. 4.5 , which compares the sum of BLYP exchange-repulsion, induction energies and the DCACP correction (taken as the difference of the BLYP and BLYP/DCACP 2-body energies) with the SAPT exchange-repulsion plus induction energies. For each isomer, the two sets of results are in close agreement with the SAPT exchange-repulsion + induction energies lying about 3 kcal/mol lower in energy. This provides strong support to our conjecture that the DCACP procedure is mainly correcting for errors in non-dispersion contributions to the energy.

Fig. 4.6 reports the three–body energies obtained from the BLYP, BLYP/DCACP, and CCSD(T) methods. As seen from this figure and noted previously in Ref. 13, the BLYP functional

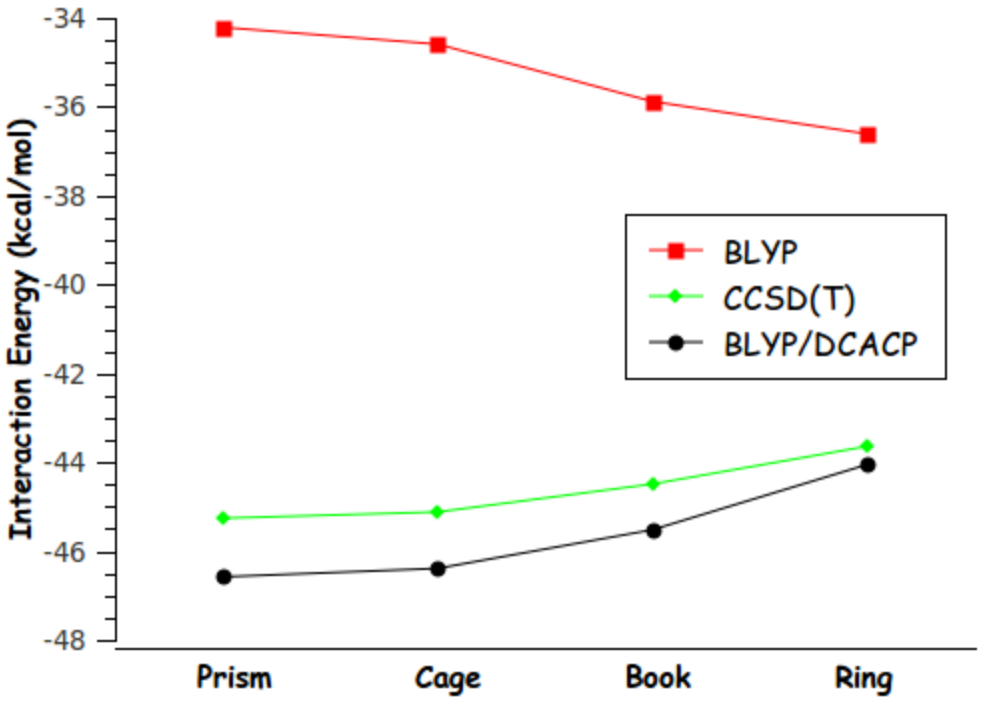

Figure 4.2: Net interaction energies of isomers of $(H_2O)_6$ (kcal/mol)

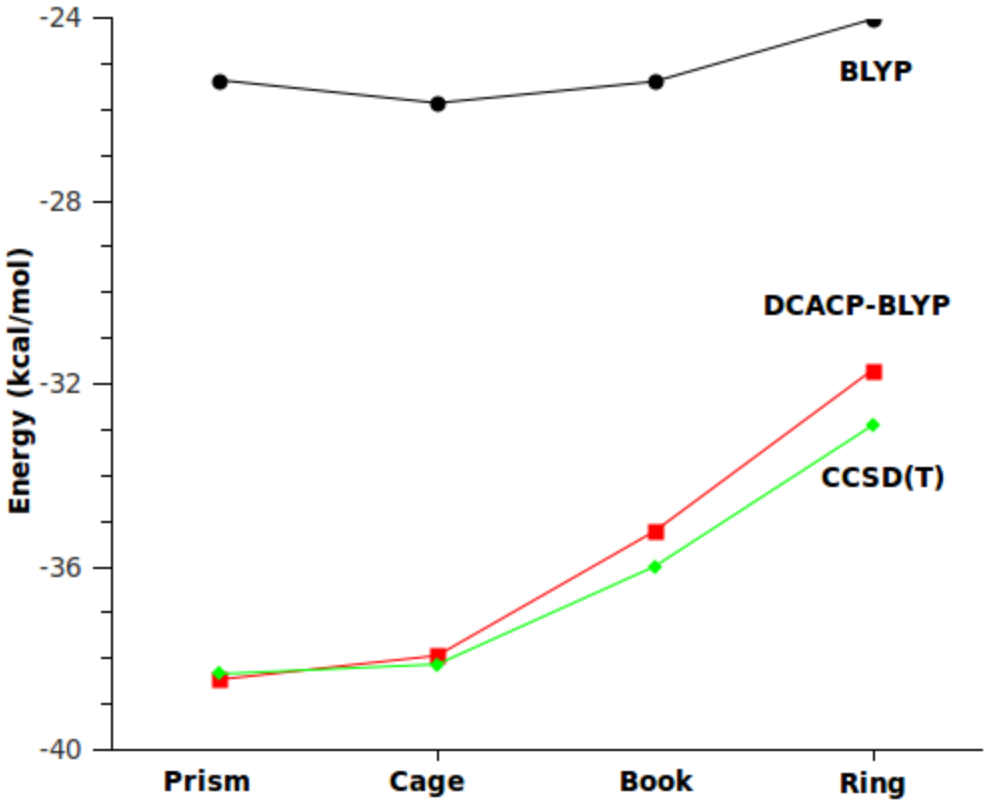

Figure 4.3: 2–Body interaction energies (kcal/mol)

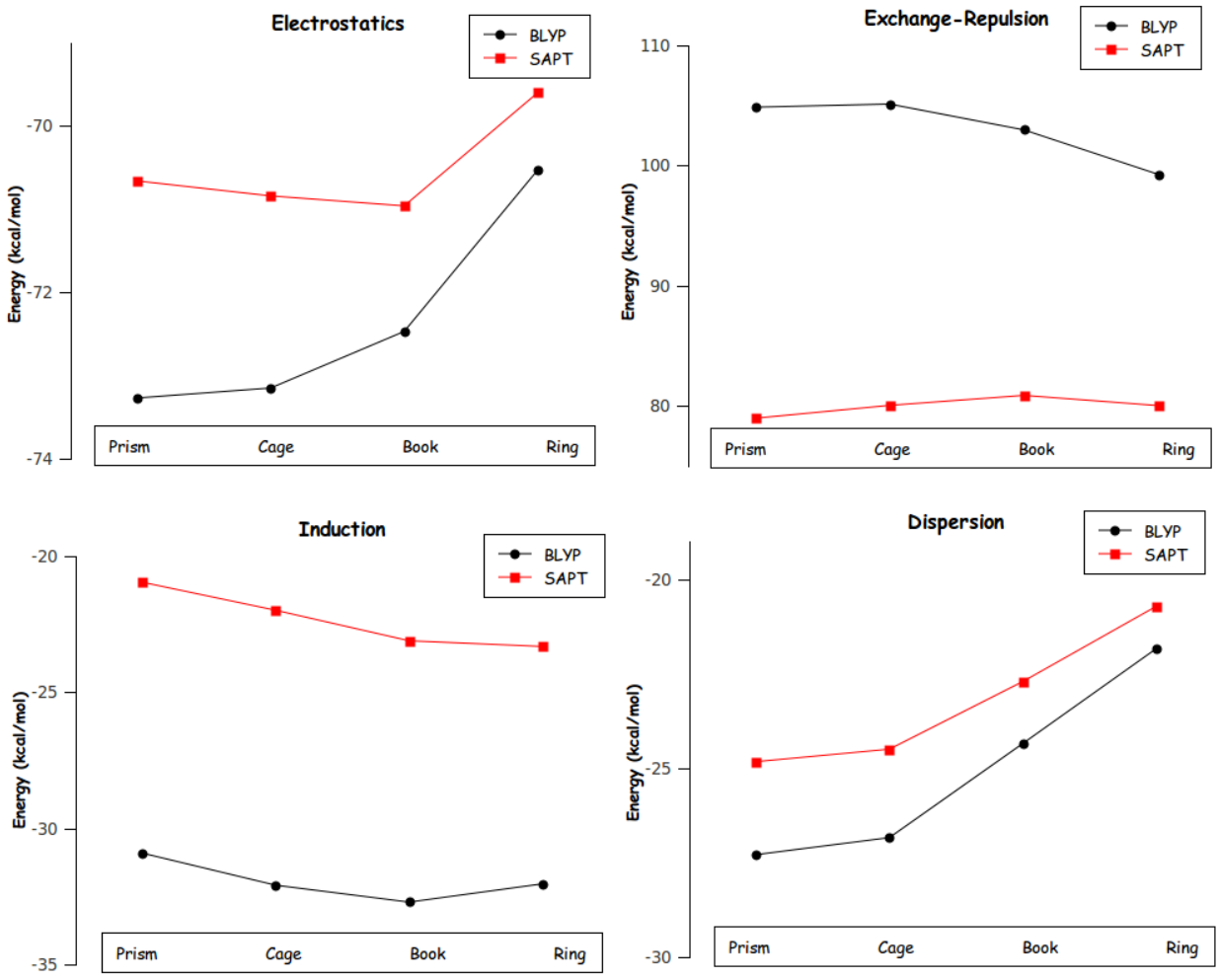

Figure 4.4: Comparison of the individual contributions to the 2–body energy (kcal/mol)

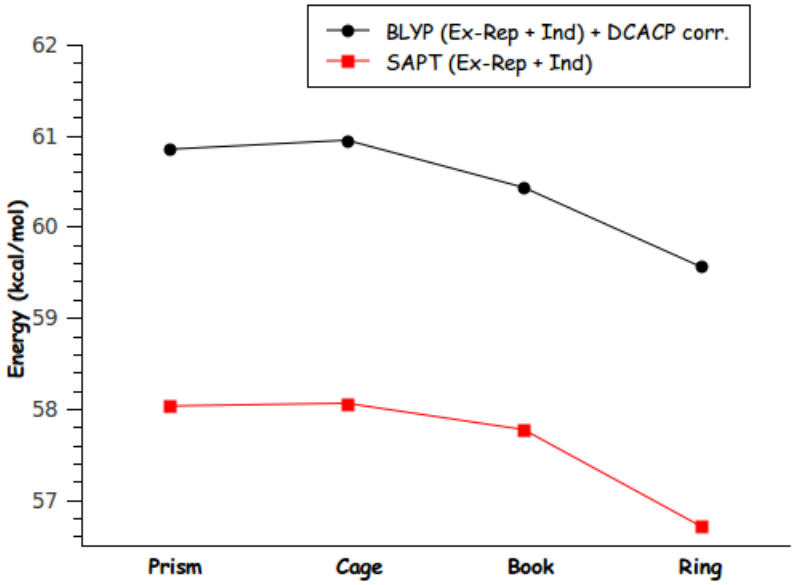

Figure 4.5: 2–body BLYP exch-rep + induction + DCACP corr. vs SAPT exch-rep + induction

overestimates the magnitude of the 3-body energies by $1-2$ kcal/mol. With the exception of the prism isomer, the DCACP correction has little impact on the 3–body energies. (The origin of the 0.9 kcal/mol decrease in the 3–body energy of the prism isomer upon inclusion of the DCACP correction is not clear.)

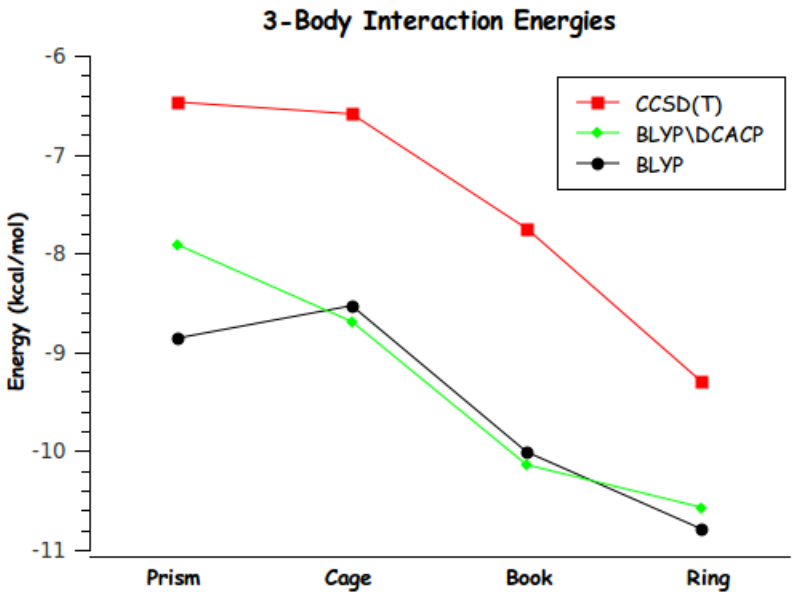

Figure 4.6: 3–body energies (kcal/mol) from the BLYP, BLYP/DCACP, and CCSD(T) methods.

4.3 CONCLUSIONS

In summary, we present results that show, when applied to water clusters and when used with the BLYP functional, the DCACP procedure is mainly correcting the limitations of the BLYP functional in describing exchange-repulsion interactions rather than for dispersion interactions as generally assumed. We expect that this conclusion holds for bulk water and for other H-bonded systems.

5.0 DCACP+D

5.1 INTRODUCTION

The dispersion–corrected atom–centered potential (DCACP)[12,13] approach, as discussed in the previous three chapters, is a simple way of correcting density functional methods for dispersion interactions. Although it provides very good accuracy for the interaction energies near equilibrium distances, the energies fall off too quickly with the distance between the two moieties increases. Also, as we have pointed in Chapter 4, at least, when used with the BLYP functional,[47,48] the DCACP method is correcting for limitations of the functional in describing exchange-repulsion interaction as well as for dispersion interactions. Actually, a similar effect is also noted for DFT+D type dispersion corrections where the short–range damping function changes (corrects) the other properties of the employed density functional.[24] Here, we propose the "DCACP+D" method (which will be referred as DCACP/PBE-D3 or DCACP/BLYP-D3 throughout the text) for improving the behavior of the long–range dispersion correction of the DCACPs. The main idea is to use pseudopotentials to correct for the corresponding density functional's deficiencies in describing the interaction other than the dispersion and then for the dispersion energy to add on pairwise corrections based on the Grimme (DFT–D3)[22] and Tkatchenko-Sheffler (DFT+vdW–TS)[24] schemes.

5.2 METHOD

The penalty functional used in this study differs from the Roethlisberger group's version. In the calibration process of the pseudopotentials we try to reproduce the reference potential energy curves by only using the energy terms (no force term is involved). As in the case of the original DCACP's, we use the $l = 3$ channel of the non–local part of the GTH pseudopotenial for the optimization. We utilize the evolutionary algorithm coded in Dakota program for the minimization process.[178] All DFT calculations were done with the CPMD program.[97] Since the reference systems used in the original DCACP show good transferability we decided to use the same set of dimers in our fitting procedure. Parallel placed $(H_2)_2$, $(N_2)_2$, cross–shaped $(CO_2)_2$ and sandwich type benzene dimer reference systems were used for the calibration of H, N, O and C pseudopotentials respectively. The dispersionless potential energy curves of the reference dimers were calculated by subtracting the DFT–SAPT[94] dispersion energies from the CCSD(T) energies. DFT–SAPT dispersion energies were calculated by adding the second–order dispersion energy and second–order exhange–dispersion energy. In the case of $(H_2)_2$ aug-cc-pV5Z basis set[136] was used for the DFT–SAPT and CCSD(T) calculations. For the $(N_2)_2$ aug–cc–pVQZ basis set[137] was used in both type of calculations. In the $(CO_2)_2$ CCSD(T)–F12a method[139] was used in conjunction with the VTZ–F12[144] basis set and DFT–SAPT calculations were done with aug-cc-pVQZ basis set. For benzene dimer CCSD(T)/aug-cc-pVQZ quality binding energies were taken from a paper of Sinnokrot et al.[179] and DFT–SAPT calculations were done with aug-cc-pVQZ basis set. DFT–D3//aug-cc-pVQZ calculations for the S22 set were obtained with Molpro, employing the initial version damping function of the DFT–D3 method.[22]

In our first method proposal for improving the DCACPs, the dispersion correction part was added on using the DFT–D3 method of Grimme.[22] and the vdW–TS method of Tkatchenko et al.[24] In the version used in this work, vdW–TS method only adds damped C_6/R^6 terms onto the DFT energy obtained using the fitted pseudopotentials while the Grimme version, in addition to the damped C_6/R^6 term, also includes C_8/R^8 terms. We have used the BLYP[47,48] and PBE[9] functionals in our calculations. Since the energies obtained by the original density functionals were modified

Table 5.1: Fitted values for the damping function

	This	work	Grimme	et al.
	PBE	BLYP	PBE	BLYP
s_{r6}	1.00	1.00	1.22	1.09
s_8	1.30	1.15	0.72	1.68

by the DCACP fitting, we had to refit the s_{r6} and s_8 values in the Grimme damping function (Eq. 5.1) and only the s_{r6} parameter in the vdW–TS scheme. The s_{r6} and s_8 values were fitted using the binding energies from the S22X5 set (non–equilibrium geometries) of Hobza et al.[180] We have used both the equilibrium geometry (R_{eq}) binding energies and twice of the R_{eq} distance binding energies to obtain the new values of s_{r6} and s_8. These values and the original s_{r6} and s_8 values for the PBE and BLYP functionals for the Grimme–type correction are given as an example in Table 5.1.

$$E_{disp} = -\left(\frac{C_6}{r^6}\frac{1}{1+6\left(\frac{r}{s_{r6}R_0}\right)^{-14}} + s_8\frac{C_8}{r^8}\frac{1}{1+6\left(\frac{r}{}R_0\right)^{-16}}\right. \tag{5.1}$$

5.3 TESTS

We have compiled the mean absolute relative errors (MARE) in the binding energies obtained by different methods for the S22X5 set of Hobza using two different separation, one at the equilibrium separation of the monomers and the other twice of that distance. These values are reported in Table 5.2. To our knowledge this is the first time mean absolute relative errors in binding energies of the S22 set for the DCACPs are reported. These calculations are done with the CPMD program with same box sizes and energy cut-off values used for our method and original DCACP calculations.

Energies are well converged with respect to the cell dimensions and energy cut–off values.

The DCACP+D method based on the Grimme–type dispersion corrections for both of the density functionals (BLYP and PBE) shows improvement on the equilibrium binding energies of the test set compared to the original DCACPs. Also in all cases a dramatic improvement is seen for binding energies at $2R_{eq}$. Although, the DCACP+D scheme augmented with the vdW–TS dispersion energies performs worse than the original DCACPs at R_{eq}, it reduces the error by half at longer distance. The poor performance of the Tkatchenko–Sheffler method compared to Grimme's can be attributed to the neglect of the C_8/R^8 terms. In the vdW–TS scheme short–range correlation (C_8/R^8 terms) is believed to be captured by the semi–local DFT functionals. However, due to the dispersionless fitting procedure we use, the functionals when used with the pseudopotentials are not describing the short–range dispersion energy as compared to the original BLYP and PBE methods. Due to this poor performance vdW–TS procedure is not included in the further tests. When compared with the original Grimme D3 method our DCACP+D scheme improves the binding energies for the PBE functional but shows a poor performance when combined with the BLYP functional. Both methods give similar accuracy at longer–range ($2R_{eq}$) for the S22 set.

Figures 5.1 and 5.2 compare the binding energies of four isomers of water hexamer (prism, cage, book, ring) obtained by CCSD(T), original DCACP and DCACP+D approaches. As a side note both the orginal BLYP and PBE functional without the dispersion corrections are not able to give the correct energy ordering in these four water hexamer isomers.[85] Firstly, all dispersion corrected methods other than the DCACP/PBE predict correct ordering of the stability of the isomers. For the BLYP functional our DCACP+D method shows overbinding for the binding energies of the isomers of water hexamers and does a poor job compared to BLYP–D3 and DCACP/BLYP methods. However, in the case of the PBE functional, our method shows a better performance than the other two schemes, in accordance with the MARE of the S22 set.

To understand the trends in the binding energies of the isomers of water hexamer we plotted the percentage errors (relative to the CCSD(T)–F12//AVQZ) these methods give for in the interaction energy curve of two rigid water molecules along a path in figures 5.3 and 5.4. A negative % error mean the method underbinds, such as in the case of BLYP functional which gives negative % errors

Table 5.2: Mean absolute relative errors (MARE) of binding energies for the S22X5 set.

	Dimer Separation	
Method	R_{eq}	$2R_{eq}$
DCACP–PBE	15	46
DCACP–PBE–D3	10	8
DCACP–PBE+vdW–TS	20	12
PBE–D3	13	8
PBE+vdW–TS	9	-
DCACP–BLYP	14	46
DCACP–BLYP–D3	12	11
DCACP–BLYP+vdW–TS	16	-
BLYP–D3	4	12

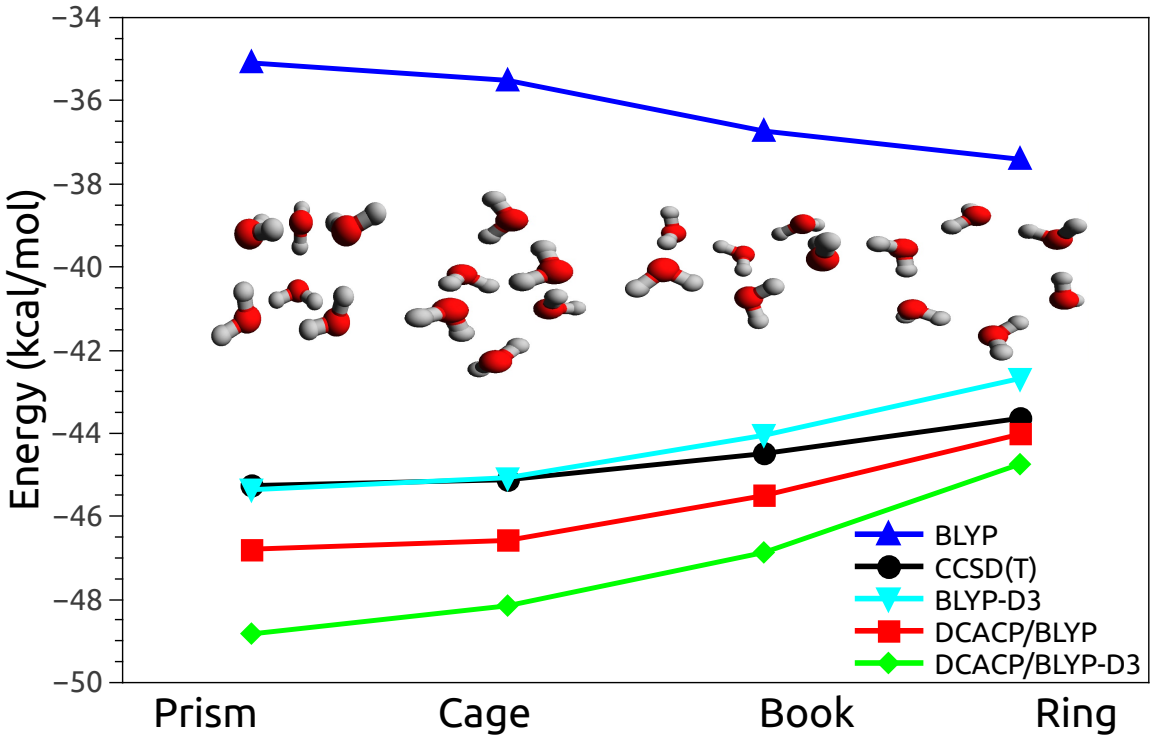

Figure 5.1: $(H_2O)_6$ isomer energies in kcal/mol.

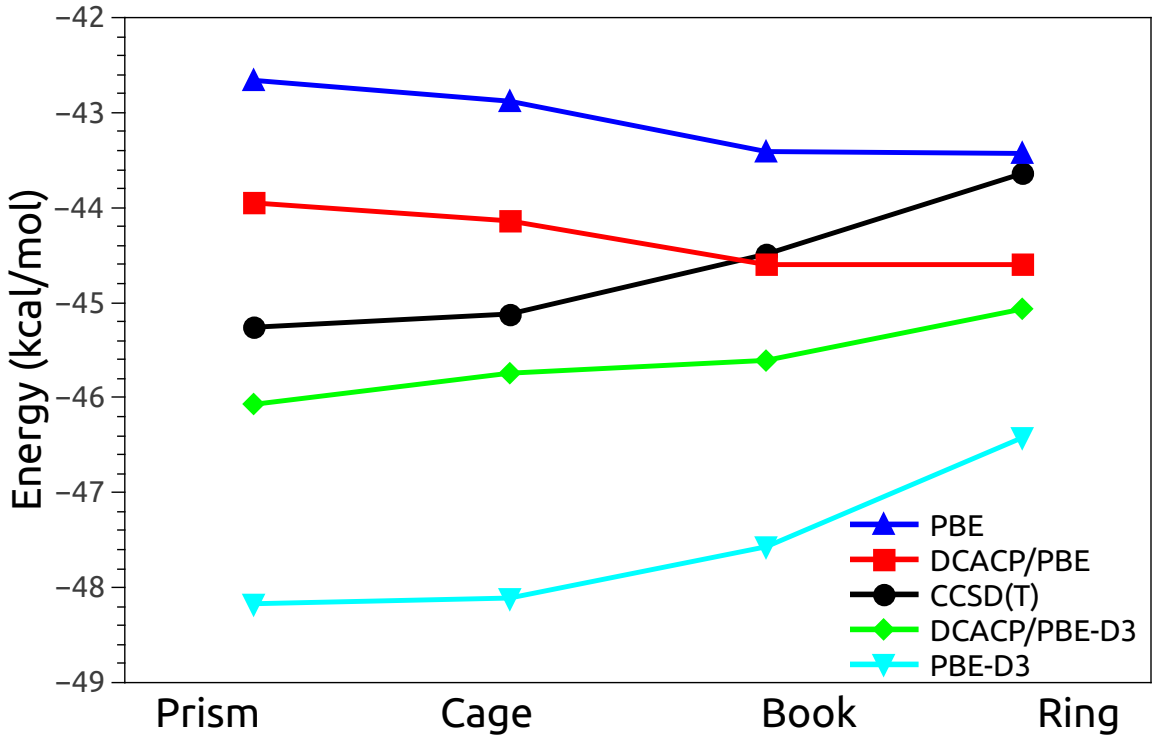

Figure 5.2: $(H_2O)_6$ isomer energies in kcal/mol.

at all distances considered. Although it not easy to make general comments for the hexamer system based on the dimer interaction energies, some clear trends are seen. The neighboring distances in the isomers of water hexamers range from 2.75 to 2.95 Angstroms. For the BLYP functional around this range both BLYP–D3 and DCACP/BLYP shows less percentage errors compared to our method. The effect on this strong interaction is mostly carried over the total binding energies. The difference between the CCSD(T) curve and the DCACP/BLYP–D3 curve increases as one moves from ring to prism isomer.In the Prism isomer one water is in close proximity (2.8 Å) to 3 other water molecules. The performance of our method around that range of bond lengths shows itself as an increased error in the binding energy for the prism isomer. The ring isomer structure contains distances between the water dimers that are overall longer than the other isomers, so that the error in the binding energy that the DCACP/BLYP–D3 method gives is almost a half of that of the prism. Also for the difference in the BLYP–D3 and CCSD(T) energies increases for the prism structure because at longer–range the errors in BLYP–D3 method increase as seen from figure 5.3. Figure 5.4 reports a clear improvement of DCACP–PBE–D3 over PBE–D3 for water dimer binding energies which is carried over as better binding energies of the hexamers are predicted by this method.

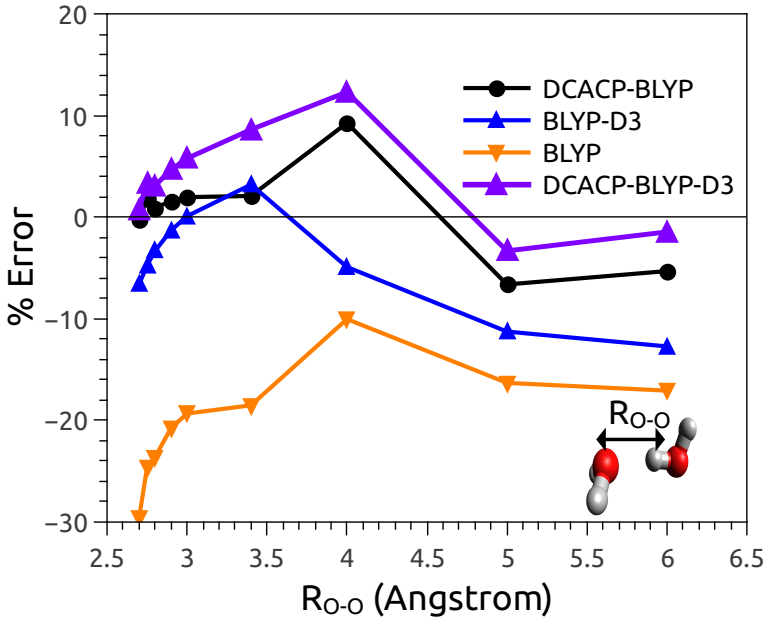

Figure 5.3: Percentage errors in the $(H_2O)_2$ interaction energies relative to CCSD(T)

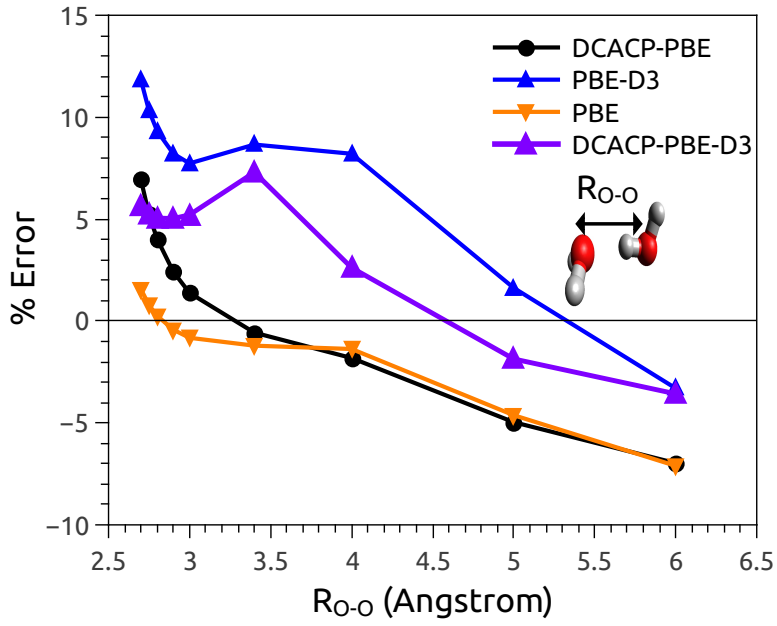

Figure 5.4: Percentage errors in the $(H_2O)_2$ interaction energies relative to CCSD(T)

5.4 CONCLUSIONS

We proposed the DCACP+D method to correct the deficiencies in the original DCACP approach to correct density functional for the missing dispersion interactions. DCACP+D method uses the psedopotentials to correct for deficiencies in the employed functional and adds the dispersion energy using atom–atom type corrections. Grimme type (D3) dispersion correction methods works better than the Tkatchenko–Scheffler method due to inclusion of C_8/R^8 terms. As seen from the results for the S22 test set, the new method (DCACP+D) performs better for compared to the original DCACPs for longer ranged distances where the DCACP interaction energies fall off too quickly. The test cases show that when used with PBE functional the DCACP+D gives slightly better interaction energies compared to the PBE–D3 method.

6.0 CORRECTING DENSITY FUNCTIONALS FOR DISPERSION INTERACTIONS USING PSEUDOPOTENTIALS

This work was published as[*]: Ozan Karalti, Xiaoge Su, Wissam A. Al–Saidi and Kenneth D. Jordan *Chemical Physics Letters*, 591, (2014), 133[†]

6.1 INTRODUCTION

We present a two–channel dispersion–corrected atom–centered potential (DCACP) method for correcting BLYP and PBE density functionals for long–range dispersion. The approach, designated DCACP2, is tested on the S22X5 test set and on isomers of the water hexamer. The DCACP2 method provides a significantly improved description of the interaction energies at distances beyond R_{eq} than does the single–channel DCACP procedure.

The dispersion–corrected atom–centered potential (DCACP)[12,13] approach is one of several methods[12–29] designed to overcome the failure of commonly used density functional methods to describe dispersion interactions at distances beyond which there is appreciable overlap of charge of the atoms or molecules of interest. The DCACP approach gives significantly improved (compared to the uncorrected GGA functionals) interaction energies for a wide range of systems near their equilibrium structures.[12,13,50–55] However, the DCACP correction to the interaction energy falls off much more rapidly than R^{-6} with increasing distance between the monomers in a

[*]Reproduced by permission of the Elsevier Science

[†]O. K. prepared the publication and contributed all of the numerical data. X. S. contributed to the coding part.

dimer.[54–56] In a study of isomers of the water hexamer we concluded that, at least when used with the BLYP functional,[47,48] the DCACP method is correcting for limitations of the functional in describing exchange-repulsion interaction as well as for dispersion interactions.[55]

The DCACP procedure modifies the electronic density by adding to the Hamiltonian atom–centered non–local potentials of the form,

$$V_l(\mathbf{r},\mathbf{r}') = \sum_{m=-l}^{l} Y_{lm}(\hat{\mathbf{r}}) p_l(r;\sigma_2)\sigma_1 p_l(r';\sigma_2) Y_{lm}(\hat{\mathbf{r}}'), \tag{6.1}$$

where Y_{lm} denotes a spherical harmonic, and p_l is a normalized projector defined as $p_l(r;\sigma_2) \propto r^l \exp[-r^2/2\sigma_2^2]$. The correction potentials are of the same functional form as the non–local channels of the Goedecker–Teter–Hutter pseudopotentials.[45] The parameter σ_1 scales the magnitude of the pseudopotential, and σ_2 tunes the location of the projector's maximum from the atom center. In their application of this method, Roethlisberger and coworkers used the $l = 3$ channel, and determined the σ_1 and σ_2 parameters by use of a penalty function that minimized the differences between the DCACP and full CI or CCSD(T)[46] energies and forces evaluated at the equilibrium and midpoint geometries (the point where the interaction energy equals half that of the equilibrium value) for a small set of dimers. The DCACP method has been implemented for the PBE,[9] BLYP[47,48] and Becke-Perdew[47,49] functionals.

In the present study we investigate an extension of the DCACP method that employs more than one angular momentum channel in the correction potential. The motivation is that this increased flexibility should better enable the procedure to correct for both exchange–repulsion errors as well as for long–range dispersion, extending the range of geometries for which the method is useful. The multiple channel DCACP method was originally introduced in Ref.[56] where in an application to $(H_2)_2$ three angular momentum channels (p, d and f) were used to fit the H pseudopotential to the full configuration–interaction energy curve. However, this three-channel H pseudopotential was not published. In this study we extend the approach to C, N, and O employing the d and f channels in the pseudopotential. The procedure is referred to as DCACP2 to indicate the use of two channels to correct the interaction energies. As in Ref. 25, we use three channels for H, although similar results would have been obtained had we used only two channels. We parametrize

the DCACP2 method to work with the BLYP and PBE functionals, and we test it on the S22x5 test set of Hobza and co–workers[180] as well as on selected isomers of the water hexamer. Neither the DCACP nor the DCACP2 procedure significantly effects the covalent bond lengths. In this context we note that von Lilienfeld recently reported a force–correcting atom–centered potential (FCACP) procedure that does improve covalent bond lengths and vibrational frequencies compared to the values obtained using uncorrected GGA functionals.[181]

6.2 METHOD

In determining the DCACP corrections we fit the potential energy curves of a set of reference dimers at several intermolecular separations. The evolutionary algorithm coded in the Dakota program was used for the optimizations.[178] We used the same dimers in our fitting procedure as employed in the design of the original DCACP procedure. Namely, parallel aligned $(H_2)_2$ and $(N_2)_2$ dimers, cross–shaped $(CO_2)_2$, and the sandwich–type benzene dimer (see Fig. 1 in the supporting information) reference systems were used for determining the parameters in the H, C, N and O DCACP2 correction potentials, respectively. CCSD(T) calculations were used to provide the reference energies. In the case of the $(H_2)_2$ and $(N_2)_2$ dimers, the CCSD(T) calculations were carried out with the aug-cc-pV5Z and aug–cc–pVQZ basis sets,[136,137] respectively. For the $(CO_2)_2$ dimer the CCSD(T)–F12a method[139] was used in conjunction with the VTZ–F12[144] basis set. In the case of benzene dimer, the fitting was to CCSD(T)/aug–cc–pVQZ binding energies taken from a paper by Sinnokrot et al.[179] Corrections for basis set superposition error (BSSE) were applied using the Boys and Bernardi counterpoise procedure[146] to the CCSD(T) interaction energies. The DFT calculations used in the fitting process and the tests of the DCACP2 method were carried out using the CPMD code,[97] taking care that the energies were well converged with respect to box size and plane–wave energy cut off. Surprisingly, the performance of the original DCACP procedure appears not to have been tested on the S22X5 test set, and we undertook such calculations as part of this study. In addition, we carried out DFT–D3[22] calculations for the S22X5 test set. The latter

calculations were performed using the Molpro program,[95] and were carried out using the aug–cc–pVQZ basis set and included counterpoise corrections for BSSE. We used a tighter grid target accuracy per atom of 10^{-8} than the default 10^{-6} for the DFT–D3 calculations. In order to test the performance of the DCACP2 method for describing long–range dispersion interactions DFT–based symmetry–adapted perturbation theory[94,105] calculations were performed for the sandwich form of the benzene dimer using the aug–cc–pVQZ basis set. These calculations employed the DFT–SAPT implementation of Hesselmann and coworkers in the Molpro code.[94]

6.3 RESULTS

In the fitting procedure, six or seven distances, one at the equilibrium geometry R_{eq}, one at a separation shorter (0.1-0.2 Å) than R_{eq} and four or five at separations greater than R_{eq}, were employed. The last point was taken as the separation (around 6–7 Å) where the interaction energy is about one tenth (or less) that at the equilibrium separation. The improvement afforded by the DCACP2–BLYP method for the sandwich form of the benzene dimer used in the fitting of pseudopotential terms for the C atom is illustrated in Fig. 6.1. The potential energy curve calculated using the DCACP2 method much more closely reproduces that calculated with the CCSD(T) method[179] than does the potential energy curve obtained using original DCACP procedure. Particularly noticeable is the improvement at short and large distances.

Of particular interest to whether the DCACP2 method accurately reproduces the correct C_6R^{-6} behavior at large distances. This is examined in Fig. 6.2, which plots for the sandwich form of the benzene dimer the differences of the DCACP and DCACP2 energies from the BLYP energy as a function of the separation between the molecules as well as $-C_6R^{-6}$ using the experimentally determined C_6 coefficient[182] and the dispersion energies obtained from the DFT–SAPT calculations. The DCACP2 correction, unlike the DCACP correction, essentially reproduces the experimental C_6R^{-6} curve from 5 to 8 Å, the longest distance considered. At shorter distances the DCACP, DCACP2 and DFT–SAPT corrections are all less attractive than C_6R^{-6}, but this is largely a con-

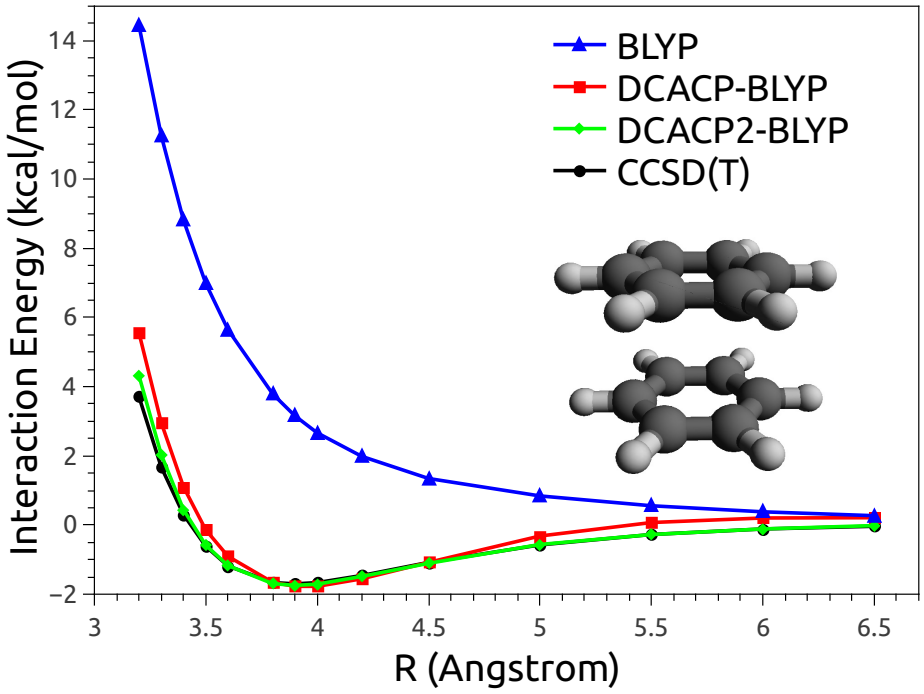

Figure 6.1: Interaction energy of the sandwich form of the benzene dimer.

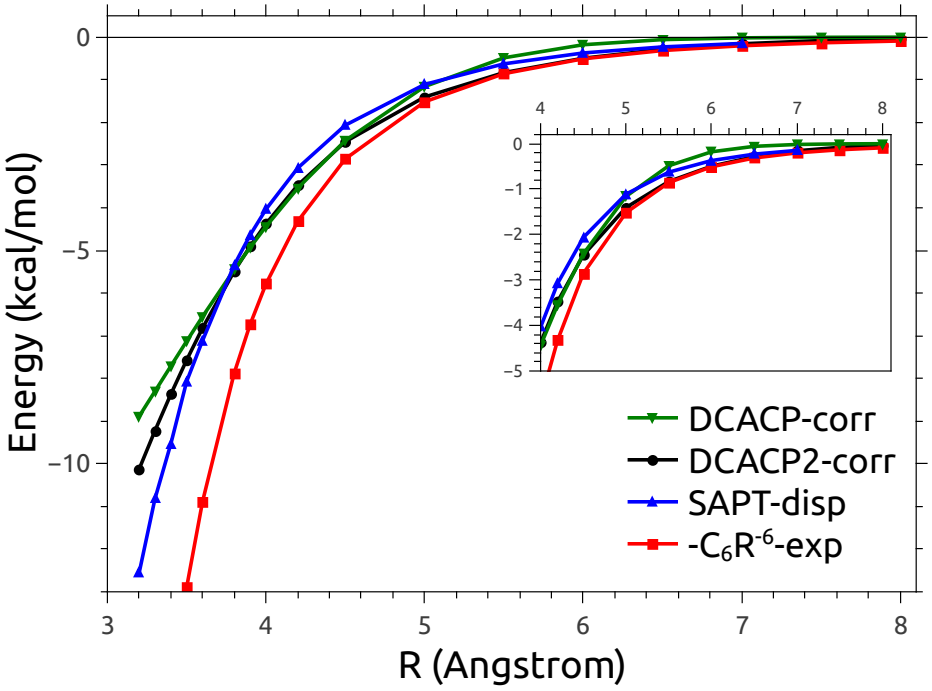

Figure 6.2: DCACP/BLYP corrections compared to exp. C_6R^{-6} and DFT–SAPT dispersion.

Table 6.1: Percentage MARE of binding energies for the S22X5 set. (MAEs in kcal/mol)

	Dimer Separation		
Method	R_{eq}	$1.5R_{eq}$	$2R_{eq}$
DCACP–PBE	15.5(0.86)	16.0(0.26)	45.7(0.16)
DCACP2–PBE	11.7(0.61)	7.9(0.18)	15.1(0.08)
PBE–D3	13.1(0.72)	15.1(0.24)	8.0(0.05)
DCACP–BLYP	13.9(0.65)	10.2(0.13)	46.1(0.13)
DCACP2–BLYP	6.7(0.33)	5.7(0.09)	10.8(0.07)
BLYP–D3	4.4(0.21)	12.5(0.18)	11.6(0.07)

sequence of exchange–dispersion interactions that are neglected in the C_6R^{-6} contribution. Most impressively the DCACP2 correction closely reproduces the dispersion energy contribution from the DFT–SAPT energies distances over the range of 3.4 to 8.0 Å. At short distances ($R \leq 3.4$ Å) the DCACP2 correction is somewhat more attractive than the DFT–SAPT dispersion correction. This is likely due to the DCACP2 method correcting for limitations of the BLYP functional in describing exchange interactions as well as in describing dispersion interactions. The small deviation of the DCACP2 correction from the SAPT dispersion energies for $4.5 \leq R \leq 6.0$ Å, may actually reflect a small error in the SAPT results as the DCACP2 potential closely reproduces the CCSD(T) potential over this range of distances.

Table 6.1 reports the mean absolute relative errors (MARE) and in parenthesis the mean absolute errors (MAE) in the interaction energies for the dimers in the S22X5 set.[180] Results are reported for separations of R_{eq}, $1.5R_{eq}$ and $2R_{eq}$. For the uncorrected BLYP and PBE functionals the MAE's for the S22 test set at R_{eq} are 4.81 and 2.61 kcal/mol, respectively.[22] These errors are considerably reduced in all three dispersion correction schemes considered. For both functionals there is a decrease in mean absolute errors for the DCACP2 procedure compared to the original

DCACP approach, especially at longer separations ($1.5R_{eq}$ and $2R_{eq}$). In the case of the PBE functional, the DCACP2 method slightly outperforms PBE–D3 at R_{eq}, has a MARE about half that of PBE–D3 at $1.5R_{eq}$ and about twice that of PBE–D3 at $2.0R_{eq}$, where the net interaction energies are quite small. For the BLYP functional the DCACP2 and BLYP–D3 methods are comparable in performance at R_{eq} and $2R_{eq}$, while the DCACP2 method has a MARE about the same as that of BLYP–D3 at $1.5R_{eq}$. Most significantly, in contrast to the D3 correction, the S22 set was not used in the fitting of the parameters of the DCACP and DCACP2 methods. At R_{eq} and $1.5R_{eq}$ all three correction schemes — D3, DCACP, and DCACP2 — perform better when used in conjunction with the BLYP functional than with the PBE functional. However, we note that several studies have recommended the use of modified PBE functionals (generally with adjustment of the exchange component) when used with dispersion corrections.[17,183,184] Hence, we anticipate that the DCACP2 method would perform better with an appropriately modified PBE functional rather than with the original PBE functional.

Figure 6.3 compares the calculated binding energies of four water hexamer isomers (prism, cage, book, ring). Rigid water monomers were used in these calculations, with the geometries being taken from Ref. 48. Results are reported for the CCSD(T)(aug-cc-pV5Z basis set), BLYP–D3, DCACP–BLYP, and DCACP2–BLYP methods. The BLYP and PBE functionals without dispersion corrections do not give the correct energy ordering of these isomers.[85,168,169] All three correction schemes when used with the BLYP functional give relative stabilities in good agreement with the CCSD(T) results,[85] with the DCACP2 method performing the best. However, significantly poorer results are obtained for the water hexamer system when using the DCACP–PBE and DCACP2–PBE functionals (Fig. 6.4). The PBE–D3 procedure does correctly predict the relative energies, but it significantly overbinds the hexamer.

To gain additional insight into the trends noted above for the $(H_2O)_6$ isomers, we also calculated the potential energy curve of the water dimer using rigid monomers, as a function the O–O separation, keeping the "flap" angles fixed. The results are reported in Figures 6.5 and 6.6. The nearest neighbor O–O distances in the isomers of the water hexamer range from 2.70 to 2.95 Å. The DCACP2–BLYP approach more accurately describes the interaction energy than does DCACP–

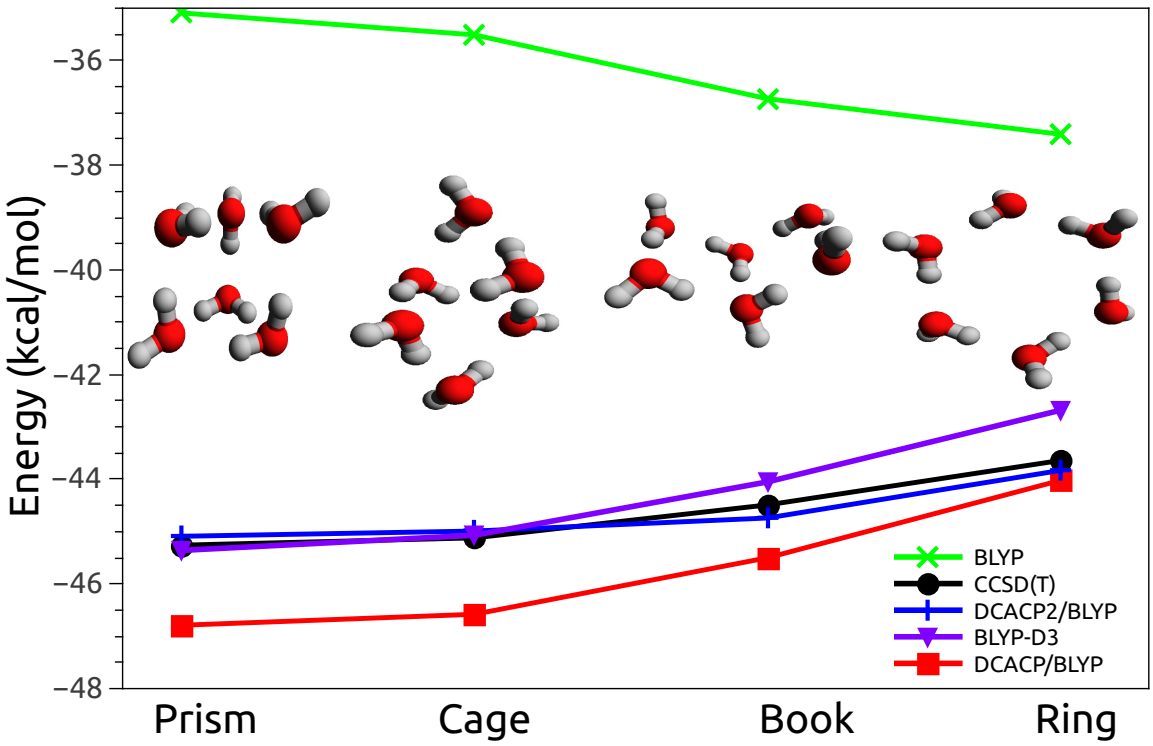

Figure 6.3: Relative energies of $(H_2O)_6$ isomers energies (kcal/mol).

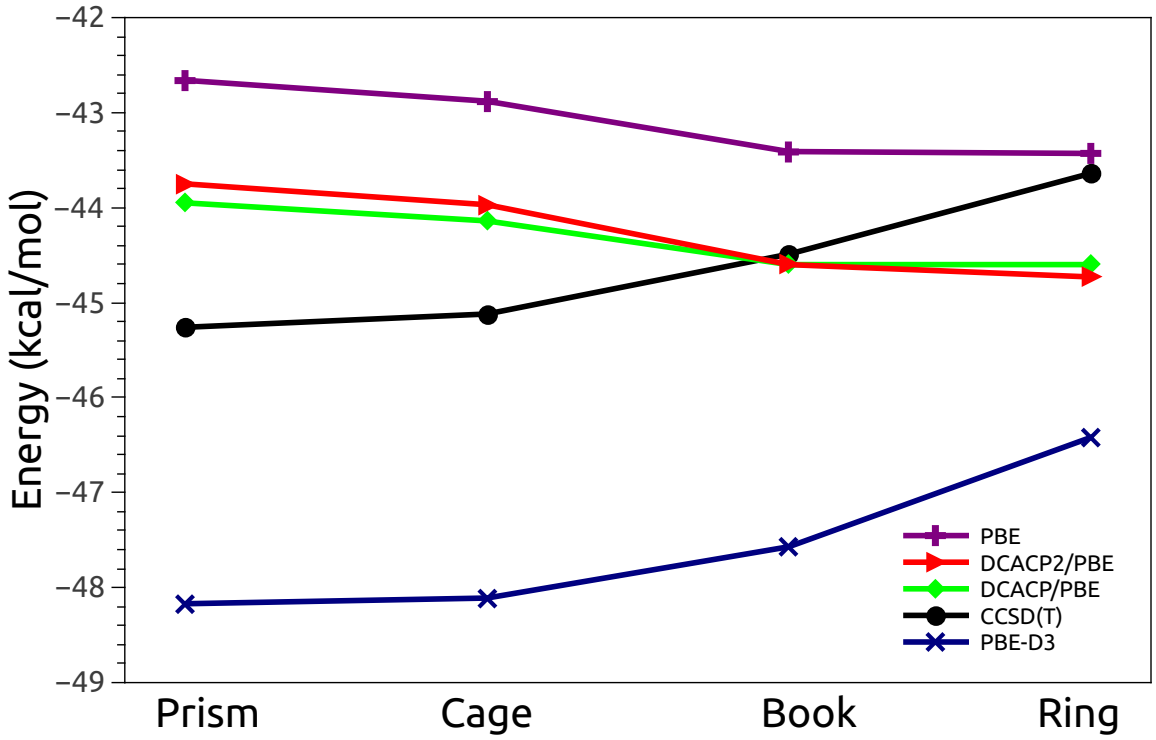

Figure 6.4: Relative energies of $(H_2O)_6$ isomers energies (kcal/mol).

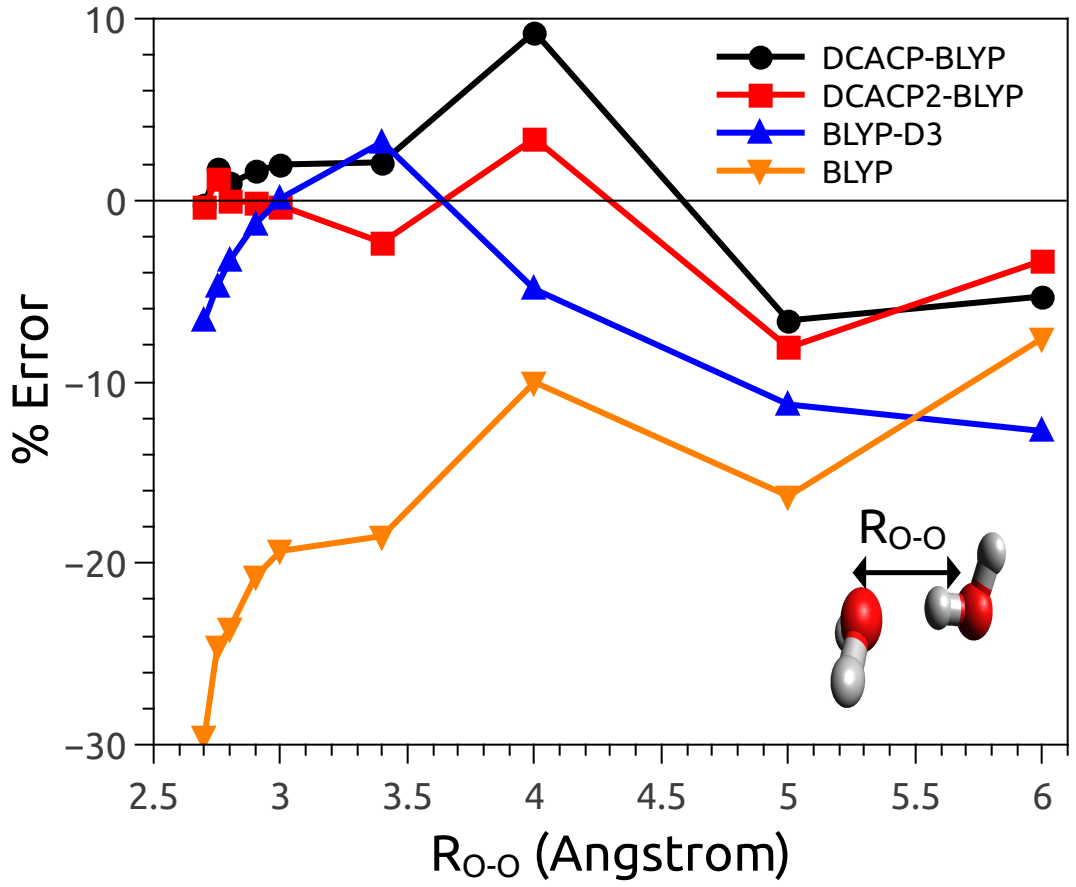

Figure 6.5: Percentage error in the $(H_2O)_2$ interaction energy relative to the CCSD(T) results.

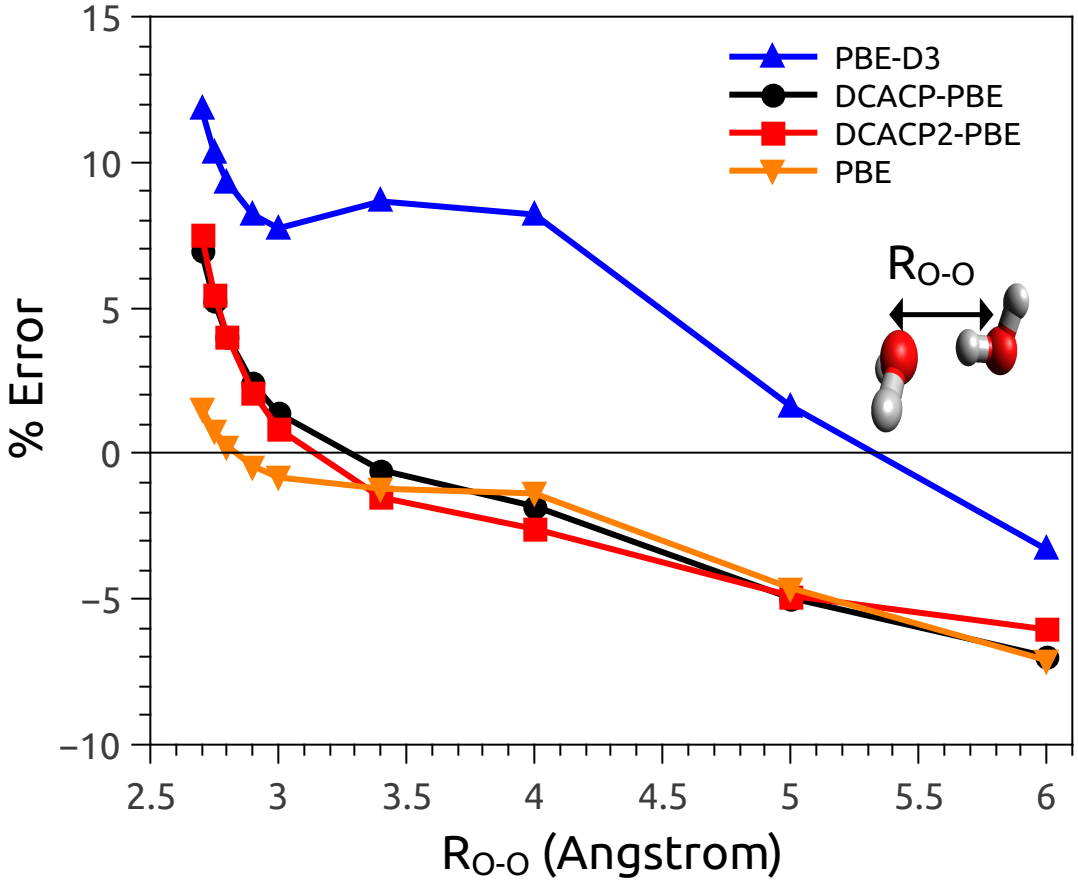

Figure 6.6: Percentage error in the $(H_2O)_2$ interaction energy relative to the CCSD(T) results.

BLYP for O–O distances ranging from 2.2 to about 5.2 Å. However, with the PBE functional, the DCACP2 and DCACP methods give nearly identical potential energy curves for the water dimer.

6.4 CONCLUSIONS

A two–channel DCACP method, designated DCACP2, has been developed for H, C, N, and O. The implementation has been made for both the BLYP and PBE density functionals through the addition of terms to the Goedecker–Teter–Hutter type pseudopotentials. The DCACP2 method, performs significantly better than the one–channel DCACP approach on the S22X5 test set, with the improvement being particularly notable with the BLYP functional. Most importantly, the DCACP2 method provides a much better description of the interaction energies at distances beyond R_{eq} than does the original DCACP procedure. The DCACP2–BLYP procedure gives absolute and relative binding energies of the ring, cage, prism and book isomers of the $(H_2O)_6$ in excellent agreement with the results of CCSD(T) calculations. Work is underway in our group to provide parameters for the DCACP2 procedure for a wider range of elements.

6.5 ACKNOWLEDGMENTS

This research was carried out with the support of a grant CHE–1111235 from the National Science Foundation. The calculations were performed on computers in University of Pittsburgh's Center for Simulation and Modeling.

7.0 CONCLUSIONS

The first part of thesis provides an overview of most of the methods used for correcting density functional theory methods for long–range dispersion interactions. Tests with various systems in Chapters 2 and 3 shows that all of these methods clearly provides better interaction energies compared to what their uncorrected density functional gives. Among those dispersion corrected methods DFT-D3's good accuracy in predicting the longer–ranged interactions and simplicity and accuracy of interaction energies at the equilibrium lengths provided by the DCACP methods catches attention. The detailed test with the isomers of the water hexamer suggests that when used with the BLYP functional the original implementation of the DCACPs not only corrects for limitations of the functional in describing dispersion interactions but also corrects for exchange-repulsion interactions. In chapters 5 and 6 we provided two methods for improving the DCACP methodology. First proposal is to fit the DCACPs to non–dispersion terms in the interaction energy and then augment it with DFT–D3 type dispersion energies. The DCACP+D method combined with the PBE functional improves the accuracy in the interaction energies near equilibrium points and also solves the wrong asypmtotic decay behavior of the original DCACPs. The DCACP2 scheme proposed in chapter 6 uses two channels in the pseudopotential rather than a single f channel for modeling the dispersion interactions. The DCACP2 method, performs significantly better than the one–channel DCACP approach on the S22X5 test set, with the improvement being particularly notable with the BLYP functional. Most importantly, the DCACP2 method provides a much better description of the interaction energies at distances beyond R_{eq} than does the original DCACP procedure. The DCACP2–BLYP procedure gives absolute and relative binding energies of the ring, cage, prism and book isomers of the $(H_2O)_6$ in excellent agreement with the results of CCSD(T) calculations.

Work is underway in our group to provide parameters for the DCACP2 procedure for a wider range of elements.

APPENDIX A

COMMONLY USED ABBREVIATIONS

Table A1: List of commonly used abbreviations

Abbreviation	Meaning
AVDZ	Dunning's aug-cc-pVDZ basis set
AVTZ	Dunning's aug-cc-pVTZ basis set
AVTZ(-f)	AVTZ basis set with *f* functions removed from heavy atoms and *d* functions from light atoms
AVQZ	Dunning's aug-cc-pVQZ basis set
AV5Z	Dunning's aug-cc-pV5Z basis set
CCSD	Coupled cluster using iterative singles and doubles
CCSD(T)	Coupled cluster using iterative singles and doubles with perturbative triples
δ(HF)	Hartree–Fock correction term for SAPT
DCACP	Dispersion Corrected Atom Centered Pseudopotentials
DF	Density fitting. Identical to resolution of the identity (RI)
DF–DFT–SAPT	DFT based SAPT of Heßelmann *et al.*[147–149] with density fitting[94]
DFT	Density functional theory
DFT+D2	Grimme's second-generation dispersion correction for DFT[21]
DFT+D3	Grimme and co-worker's third-generation dispersion correction for DFT[22]
DFT/CC	Rubeš *et al.*[83,131] coupled cluster correction method for DFT
DFT–SAPT	DFT based SAPT of Heßelmann *et al.*[147–149]
Disp	2^{nd}–order dispersion interaction
DMA	Distributed multipole analysis
EDA	Energy decomposition analysis
Elst	1^{st}-order electrostatics interaction
Exch	1^{st}-order exchange interaction
Exch-Disp	2^{nd}-order exchange–dispersion interaction
Exch-Ind	2^{nd}-order exchange–induction interaction
GDMA	Gaussian distributed multipole analysis
HF	Hartree–Fock
Ind	2^{nd}-order induction interactions
LMO–EDA	Localized molecular orbital energy decomposition analysis
MP2	Möller–Plesset 2^{nd}–order perturbation theory

MBPTn	Many-body perturbation theory through order n
RI	Resolution of the identity. Identical to density fitting (DF).
SAPT	Symmetry-adapted perturbation theory
SAPT(DFT)	DFT based SAPT of Misquitta *et al.*[105,185,186]
Tr-AVTZ	Truncated AVTZ basis set as described in Section 2.2
vdW-TS	Tkatchenko and Sheffler type dispersion correction
XC	Exchange–Correlation

APPENDIX B

SUPPORTING INFORMATION FOR CHAPTER 6

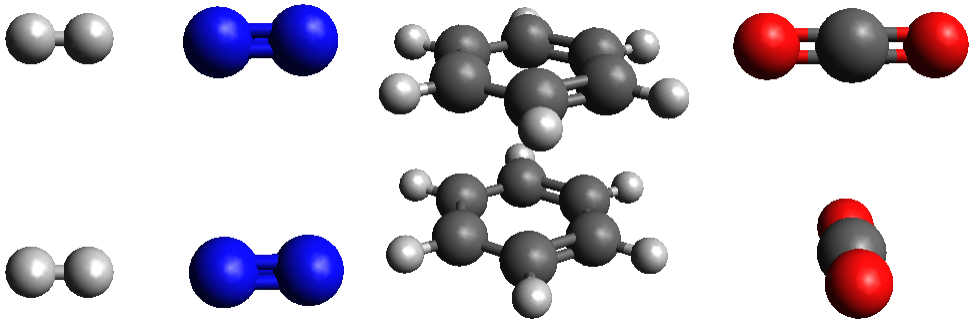

Figure B1: Geometries of dimers used for the parametrization

Table B1: DCACP2 parameters.

	BLYP		PBE	
	σ_1 $[10^{-4}]$	σ_2	σ_1 $[10^{-4}]$	σ_2
$H_{l=1}$	-1.08	4.62	-0.099	9.34
$H_{l=2}$	-3.17	2.78	-18.00	0.27
$H_{l=3}$	-0.84	1.92	0.82	2.49
$C_{l=2}$	-2.66	4.80	-1.83	4.79
$C_{l=3}$	-8.34	2.47	-8.85	2.33
$N_{l=2}$	-2.33	4.21	-0.68	5.32
$N_{l=3}$	-9.06	2.32	-3.12	2.35
$O_{l=2}$	-1.76	4.49	-1.88	9.13
$O_{l=3}$	-8.87	2.13	-12.5	1.54

Table B2: S22X5 set interaction energies at R_{eq} for the corrected PBE functional in kcal/mol.

Dimer	CCSD(T)	DCACP2	DCACP
adenine–thymine (S)	-12.22	-9.21	-7.85
adenine–thymine (WC)	-16.37	-16.08	-15.72
ammonia dimer	-3.14	-2.92	-2.89
benzene–ammonia	-2.35	-1.88	-1.83
benzene–HCN	-4.52	-4.59	-4.31
benzene–methane	-1.50	-1.29	-1.24
benzene–water	-3.27	-2.82	-2.77
benzene dimer (S)	-2.81	-2.70	-2.13
benzene dimer (T)	-2.80	-2.38	-2.36
ethene–ethyne	-1.49	-1.67	-1.65
ethene dimer	-1.48	-1.30	-1.24
formamide dimer	-15.95	-15.82	-15.59
formic acid dimer	-18.59	-19.56	-19.32
indole–benzene (S)	-5.18	-4.40	-3.69
indole–benzene (T)	-5.74	-4.75	-4.37
methane dimer	-0.53	-0.36	-0.42
phenol dimer	-7.05	-6.01	-5.74
pyrazine dimer	-4.51	-3.60	-3.02
uracil dimer (HB)	-20.46	-20.06	-19.71
uracil dimer (S)	-9.87	-7.76	-7.09
water dimer	-4.97	-5.11	-5.13
2-pyridoxine–2-aminopyridine	-16.70	-16.96	-16.64

Table B3: S22X5 set interaction energies at $1.5R_{eq}$ for the PBE functional (kcal/mol).

Dimer	DFT–D3	DCACP2	DCACP
adenine–thymine (S)	-3.49	-2.73	-2.47
adenine–thymine (WC)	-7.92	-7.03	-6.92
ammonia dimer	-1.26	-1.07	-1.07
benzene–ammonia	-0.99	-0.74	-0.73
benzene–HCN	-2.29	-2.04	-2.04
benzene–methane	-0.62	-0.46	-0.43
benzene–water	-1.46	-1.15	-1.16
benzene dimer (S)	-0.67	-0.51	-0.28
benzene dimer (T)	-1.30	-1.00	-0.88
ethene–ethyne	-0.58	-0.50	-0.48
ethene dimer	-0.28	-0.18	-0.14
formamide dimer	-8.57	-7.86	-7.89
formic acid dimer	-9.93	-9.14	-9.18
indole–benzene (S)	-1.23	-0.94	-0.66
indole–benzene (T)	-2.99	-2.42	-2.27
methane dimer	-0.09	-0.05	-0.03
phenol dimer	-3.61	-2.87	-2.79
pyrazine dimer	-1.12	-0.72	-0.88
uracil dimer (HB)	-10.73	-9.91	-9.84
uracil dimer (S)	-2.71	-2.22	-2.00
water dimer	-2.49	-2.28	-2.30
2-pyridoxine–2-aminopyridine	-8.80	-7.97	-7.88

Table B4: S22X5 set interaction energies at $2R_{eq}$ for the PBE functional (kcal/mol).

Dimer	DFT–D3	DCACP2	DCACP
adenine–thymine (S)	-0.95	-0.76	-0.58
adenine–thymine (WC)	-2.73	-2.40	-2.28
ammonia dimer	-0.36	-0.33	-0.33
benzene–ammonia	-0.29	-0.24	-0.19
benzene–HCN	-0.86	-0.81	-0.73
benzene–methane	-0.14	-0.11	-0.05
benzene–water	-0.49	-0.44	-0.40
benzene dimer (S)	-0.09	-0.04	0.03
benzene dimer (T)	-0.38	-0.30	-0.18
ethene–ethyne	-0.15	-0.14	-0.16
ethene dimer	-0.03	-0.02	0.00
formamide dimer	-3.66	-3.41	-3.37
formic acid dimer	-3.92	-3.55	-3.54
indole–benzene (S)	-0.14	-0.06	0.14
indole–benzene (T)	-1.11	-0.94	-0.78
methane dimer	-0.01	-0.01	0.00
phenol dimer	-1.40	-1.16	-1.03
pyrazine dimer	-0.21	-0.14	-0.05
uracil dimer (HB)	-4.59	-4.27	-4.19
uracil dimer (S)	-0.76	-0.68	-0.52
water dimer	-0.95	-0.93	-0.93
2-pyridoxine–2-aminopyridine	-3.47	-3.16	-3.05

Table B5: S22X5 set interaction energies at R_{eq} for the BLYP functional(kcal/mol).

Dimer	CCSD(T)	DCACP2	DCACP
adenine–thymine (S)	-12.22	-11.07	-9.26
adenine–thymine (WC)	-16.37	-16.44	-15.88
ammonia dimer	-3.14	-3.06	-3.08
benzene–ammonia	-2.35	-2.15	-2.16
benzene–HCN	-4.52	-4.21	-3.88
benzene–methane	-1.50	-1.43	-1.41
benzene–water	-3.27	-2.92	-3.11
benzene dimer (S)	-2.81	-2.59	-1.96
benzene dimer (T)	-2.80	-2.43	-2.22
ethene–ethyne	-1.49	-1.59	-1.61
ethene dimer	-1.48	-1.49	-1.37
formamide dimer	-15.95	-15.64	-15.50
formic acid dimer	-18.59	-18.94	-18.50
indole–benzene (S)	-5.18	-4.35	-3.25
indole–benzene (T)	-5.74	-5.07	-4.65
methane dimer	-0.53	-0.63	-0.79
phenol dimer	-7.05	-6.65	-6.39
pyrazine dimer	-4.51	-4.08	-3.13
uracil dimer (HB)	-20.46	-20.18	-19.77
uracil dimer (S)	-9.87	-9.35	-8.50
water dimer	-4.97	-4.99	-5.04
2-pyridoxine–2-aminopyridine	-16.70	-17.04	-16.75

Table B6: S22X5 set interaction energies at $1.5R_{eq}$ for the BLYP functional (kcal/mol).

Dimer	DFT–D3	DCACP2	DCACP
adenine–thymine (S)	-3.49	-3.34	-2.90
adenine–thymine (WC)	-7.92	-7.24	-7.29
ammonia dimer	-1.26	-1.03	-1.11
benzene–ammonia	-0.99	-0.75	-0.79
benzene–HCN	-2.29	-2.01	-2.05
benzene–methane	-0.62	-0.47	-0.46
benzene–water	-1.46	-1.12	-1.20
benzene dimer (S)	-0.67	-0.56	-0.31
benzene dimer (T)	-1.30	-1.12	-1.02
ethene–ethyne	-0.58	-0.48	-0.47
ethene dimer	-0.28	-0.21	-0.20
formamide dimer	-8.57	-7.97	-8.14
formic acid dimer	-9.93	-9.51	-9.69
indole–benzene (S)	-1.23	-1.04	-0.75
indole–benzene (T)	-2.99	-2.60	-2.51
methane dimer	-0.09	-0.04	-0.02
phenol dimer	-3.61	-3.21	-3.30
pyrazine dimer	-1.12	-1.04	-0.88
uracil dimer (HB)	-10.73	-10.34	-10.43
uracil dimer (S)	-2.71	-2.47	-2.29
water dimer	-2.49	-2.30	-2.43
2-pyridoxine–2-aminopyridine	-8.80	-8.31	-8.36

Table B7: S22X5 set interaction energies at $2R_{eq}$ for the BLYP functional (kcal/mol).

Dimer	DFT–D3	DCACP2	DCACP
adenine–thymine (S)	-0.93	-0.91	-0.62
adenine–thymine (WC)	-2.40	-2.49	-2.43
ammonia dimer	-0.31	-0.33	-0.33
benzene–ammonia	-0.23	-0.26	-0.16
benzene–HCN	-0.75	-0.77	-0.72
benzene–methane	-0.09	-0.12	-0.03
benzene–water	-0.41	-0.45	-0.35
benzene dimer (S)	-0.08	-0.09	0.06
benzene dimer (T)	-0.29	-0.35	-0.20
ethene–ethyne	-0.13	-0.13	-0.12
ethene dimer	-0.03	-0.03	0.00
formamide dimer	-3.38	-3.33	-3.51
formic acid dimer	-3.59	-3.62	-3.67
indole–benzene (S)	-0.13	-0.12	0.13
indole–benzene (T)	-0.93	-0.97	-0.77
methane dimer	-0.01	-0.01	0.00
phenol dimer	-1.24	-1.22	-1.13
pyrazine dimer	-0.20	-0.24	-0.14
uracil dimer (HB)	-4.39	-4.16	-4.17
uracil dimer (S)	-0.76	-0.70	-0.64
water dimer	-0.85	-0.86	-0.88
2-pyridoxine–2-aminopyridine	-3.15	-3.13	-3.22

APPENDIX C

ADSORPTION OF A WATER MOLECULE ON THE MGO(100) SURFACE AS DESCRIBED BY CLUSTER AND SLAB MODELS

This work was published as[*]: Ozan Karalti, Dario Alfè, Michael J. Gillan and Kenneth D. Jordan *Physical Chemistry Chemical Physics*, 14, (2012), 7846–7853[†]

C.1 INTRODUCTION

The interaction of a water molecule with the (100) surface of MgO as described by cluster models is studied using MP2, coupled MP2 (MP2C) and symmetry–adapted perturbation theory (SAPT) methods. In addition diffusion Monte Carlo (DMC) results are presented for several slab models as well as for the smallest, $2X2$ cluster model. For the $2X2$ model it is found that the MP2C, DMC, and CCSD(T) methods all give nearly the same potential energy curve for the water–cluster interaction, whereas the potential from the SAPT calculations differs slightly from the potentials of the other methods. The interaction of the water molecule with the cluster models of the MgO(100) surface is weakened upon expanding the number of layers from one to two and also upon expanding the description of the layers from $2X2$ to $4X4$ to $6X6$. The SAPT calculations reveal that both these expansions of the cluster model are accompanied by reductions in the magnitudes of the induction and dispersion contributions. The best estimate of the energy for binding an isolated water model to the surface obtained from the cluster model calculations is in good agreement with that obtained from the DMC calculations using a 2–layer slab model with periodic boundary conditions.

The adsorption of atoms and molecules on surfaces is of fundamental importance in a wide range of processes. MgO is an important component of the Earth's subsurface and is used as a constituent in some superconducters and glasses as well as a catalyst. The nature of water adsorption on the MgO(100) surface has attracted considerable attention, being the subject of several experimental and theoretical studies.[187–195] It appears that even at low coverages, molecularly adsorbed water is H–bonded to surface OH groups resulting from water dissociation and, as a result, an experimental value for the interaction energy of an isolated water molecule with the surface is not available. On the computational side, the water/MgO system has been investigated using semi–empirical methods,[194] density functional theory (DFT),[187] a mixed Hatree-Fock/coupled–cluster procedure combined with an embedded cluster model,[190] and a study of the quantum nuclear effects on the adsorption energy.[188]

In the present work, we calculate the interaction energy between a water monomer and various cluster models of the MgO(100) surface. The methods used include density–fitted Möller–Plesset second–order perturbation theory (DF-

[*]Reproduced by permission of the PCCP Owner Societies

[†]D. A. contributed the QMC calculations and O. K. contributed the rest of the publication.

MP2),[196,197] density–fitted coupled MP2 (DF-MP2C),[92,142] and explicitly correlated DF–MP2 (DF–MP2–F12),[138] DF–MP2C (DF-MP2C–F12), and CCSD(T) (CCSD(T)-F12).[138,140] In addition, calculations using the wavefunction–based[166,198] and density–fitted density–functional theory–based[94] symmetry–adapted perturbation theory (SAPT) are carried out. These are referred to as WF-SAPT and DFT-SAPT, respectively. The SAPT calculations are particularly useful for elucidating the factors at play in the adsorption of the water monomer as they provide physical dissections of the net interaction into electrostatics, exchange-repulsion, induction, and dispersion contributions. This information should prove especially valuable in designing force fields for simulating water on the MgO(100) surface. Due to the computational cost, the coupled cluster and WF–SAPT methods were applied only to the smallest cluster model.

In addition to the methods discussed above, the interaction energy between water and the MgO(100) surface was calculated using the diffusion Monte Carlo (DMC) method together with slab models and periodic boundary conditions. For comparative purposes the DMC model was also applied to a water monomer interacting with the smallest cluster model of the surface.

C.2 COMPUTATIONAL DETAILS

The MgO cluster models considered are single–layer $2X2$, $4X4$, and $6X6$, and double–layer $4X4$ (the nXn nomenclature indicates that the cluster contains n rows of n atoms in the layer). The lattice constant used in the geometries of the $(MgO)_n$ clusters were taken from a slab–model optimized with DFT-PBE using the VASP code.[134] The single–layer cluster models of the bare surface have D_{2h} symmetry and the double-layer cluster model have D_{2d} symmetry. All nearest neighbor MgO bond lengths are 2.115 Å. With one exception , described below, the geometry of the water monomer (OH bond lengths of 0.989 Å and HOH bond angle of 103.2°) was also taken from a DFT-PBE optimized geometry, without allowing the Mg and O atoms of slabs to move, as was the orientation of the monomer relative to the surface (see Fig. C1).

Due to the computational cost, WF–SAPT calculations were carried out only for the $2X2$ cluster model, and the main approach for analyzing the interaction energies for the sequence of cluster models is the DFT–SAPT method. This method and the closely related SAPT(DFT) method of Szalewicz and co–workers[105] determine the electrostatic and exchange–repulsion contributions to the interaction energy from integrals over the Coulomb operator evaluated using Kohn–Sham orbitals. Thus these approaches are free of the problems inherent in evaluating exchange–repulsion using common density functional methods. The induction and dispersion contributions were calculated using response functions from time–dependent DFT. The DFT–SAPT calculations made use of the LPBE0AC functional,[94] which replaces the 25% Hartree–Fock exchange of the PBE0 functional[34] with the 25% localized Hartree–Fock exchange of Sala and Görling[106] and includes an asymptotic correction.[199] The correction scheme requires ionization potentials of the fragments. For water the experimental IP reported in the NIST Chemistry Web Book,[150] was used, and for the $(MgO)_n$ clusters, Koopmans' theorem IP's from Hartree–Fock calculations with the same basis set as employed in the DFT–SAPT calculations were used.

For the single–layer $2X2$ and $4X4$ cluster models, the DFT–SAPT calculations were performed using the aug–cc–pVQZ basis set[137] on all atoms. For the double–layer $4X4$ model, a mixed aug–cc–pVQZ/aug–cc–pVDZ[136] basis set was used. This was generated by employing the aug–cc–pVQZ basis set for the water molecule and the two closest magnesium and two closest oxygen atoms in the top layer (the atoms marked by Xs in Fig. C1), with the aug–cc–pVDZ basis set being used for the remaining atoms. For the monomer SCF calculations and for the evaluation of the first–order electrostatics ($E^{(1)}_{Elst}$) and exhange ($E^{(1)}_{Exch}$) interactions, and the second–order induction ($E^{(2)}_{Ind}$) and exchange-induction ($E^{(2)}_{Ex-Ind}$) terms the cc–pVQZ JK–fitting set of Weigend[109] was used for the oxygen and hydrogen atoms, and the MP2-fitting set of Weigend and co–workers[110] was used for the magnesium atoms. For the second-order dispersion and exchange-dispersion terms, the aug–cc–pVQZ MP2–fitting set of Weigend and co–workers[110] was used for all atoms. In the case of the mixed basis set calculations double–zeta versions of the fitting sets were used on the atoms employing the aug–cc–pVDZ basis sets.

The DF–MP2 and DF–MP2C calculations were carried out using the same basis sets and auxiliary fitting sets as

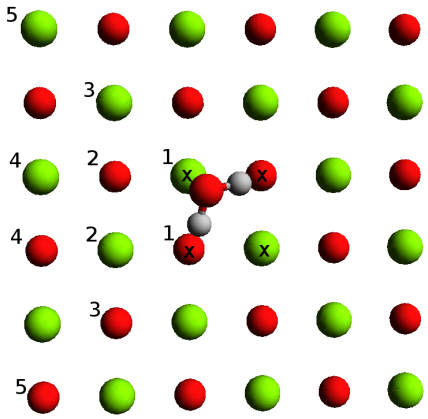

Figure C1: Geometry representing a water molecule on a $6X6$ $(MgO)_{18}$.

used in the DFT–SAPT calculations (the mixed basis set described above was used for the single–layer $6X6$ cluster model). These two approaches and the CCSD(T) method were also used in combination with F12a corrections.[139] The F12a calculations used the cc–pVQZ–F12 (VQZ–F12) basis sets of Peterson and co-workers[144] for the single–layer $2X2$ and $4X4$ cluster models and a combination of the cc–pVDZ–F12 (VDZ–F12) and VQZ–F12 basis sets for the larger clusters following the same strategy described above for the DFT–SAPT calculations. For the oxygen and hydrogen atoms, the auxiliary basis sets implemented in MOLPRO2010.1 were used.[109] For the magnesium atoms, the cc–pVDZ and cc–pVQZ MP2–fitting sets of Weigend and co-workers were used as the auxiliary basis sets for the calculations using the VDZ-F12 and VQZ-F12 basis sets, respectively. The various MP2 and CCSD(T) calculations were carried out with the non–valence core orbitals frozen. All calculations other than the quantum Monte Carlo calculations were performed with the MOLPRO2010.1 package.[95]

In reporting the results of the SAPT calculations the dispersion and exchange–dispersion contributions were combined as were the induction, exchange–induction and δ(HF) contributions.[94] In the SAPT procedure the induction and exchange–induction contributions are calculated to second–order in the intermolecular interaction. The higher order induction and exchange–induction interactions are accounted for by the so–called δ(HF) term.[94]

The quantum Monte Carlo calculations were performed with the CASINO code,[200] using the diffusion Monte Carlo (DMC) method, together with trial wavefunctions that enforce fixed nodal surfaces.[201] The trial wavefunctions employed were of the Slater–Jastrow type:

$$\Psi_T(\mathbf{R}) = D^{\uparrow} D^{\downarrow} e^{J} \,, \qquad \text{(C.1)}$$

where $D^{\uparrow}$ and $D^{\downarrow}$ are Slater determinants of up- and down–spin single–electron orbitals, and e^{J} is a Jastrow factor, which is the exponential of a sum of one-body (electron–nucleus), two-body (electron–electron), and three body (electron–electron-nucleus) terms, that are parametrized functions of electron–nucleus, electron-electron and electron–electron–nucleus separations, and are designed to satisfy the cusp conditions. The parameters in the Jastrow factor are varied to minimize the variance of the local energy.[202,203] Imaginary time evolution of the Schrödinger equation has been performed with the usual short time approximation with a time step of 0.005 a.u. and the locality approximation.[204] Dirac–Fock pseudo-potentials (PP) of Trail and Needs were used for O and H,[205] and a density functional theory (DFT) PP generated with the local density approximation (LDA) was employed for Mg.[206] The O and Mg PPs replace the $1s^2$ cores. The single particle orbitals were obtained from DFT plane–wave (PW) calculations using the LDA and a PW cutoff of 300 Ry (4082 eV), and re–expanded in terms of B–splines,[207] using the natural B–spline grid

spacing given by $a = \pi/G_{\max}$, where $G_{\max}$ is the length of the largest vector employed in the PW calculations. The plane–wave calculations were performed using the PWSCF package.[208]

For the slab model LDA and DMC calculations, periodicity was used only in the two directions parallel to the MgO surface. For these calculations long–range electrostatics were treated using the Ewald method.[209] The MgO distances in the slab models were taken from an optimization of bulk MgO carried out using DFT calculations with the PBE functional.[9] The geometry of the water on the MgO slab also obtained from a PBE–DFT optimization in which only the water degrees of freedom are allowed to relax. The other geometries on the binding energy curve were obtained by rigidly displacing the water molecule. Computed in this way, the binding energy curve does not account for contributions due to relaxation of the slab which are expected to be quite small.

The slab model calculations employed a supercell with two 4X4 MgO layers. Exploratory calculations with larger slab models showed that the 2–layer 4X4 model was adequate for achieving nearly converged results of the water–surface interaction energies.

C.3 RESULTS

$2X2$ cluster model calculations were carried out for all theoretical methods described above, while for the larger clusters, calculations were performed only for the DFT–SAPT, MP2–F12, and MP2C–F12 methods. Potential energy curves for approach of a water molecule to the (100) MgO surface were calculated for each of the cluster models of the surface.

C.3.1 $2X2$ Cluster model

The calculated potential energy curves for water adsorption on the $2X2$ cluster model are shown in Fig. 2(a). The DMC results are not included in this figure, but will be considered below. Of the methods reported, the CCSD(T)–F12 method is expected to most accurately describe the interaction potential and will be used as the reference for assessing the performance of the other theoretical methods. At this level of theory, the potential energy minimum has the water O atom located 2.15 $\AA$ from the closest Mg atom of the surface, with the binding energy being -25.0 kcal/mol. For the MP2 and MP2C methods, the potential energy curves calculated using the aug-cc-pVQZ basis set are as much as 1 kcal/mol above the corresponding curves obtained with the VQZ–F12 method, and, for this reason, we focus on the VQZ–F12 results in the following discussion. The potential energy curve from the MP2C–F12 calculations is very close to that obtained from the CCSD(T)–F12 calculations over the range of distances considered (1.98–6.50 $\AA$). Here and elsewhere in this study distances are measured between the O atom of water and the closest Mg atom of the surface. However, at short distances the MP2–F12 potential lies as much as 2 kcal/mol above the CCSD(T)–F12 potential. Thus the MP2C–F12 procedure is more reliable than the MP2–F12 procedure for describing the interaction of the water molecule with the surface. For $R \geq 2.3$ $\AA$ the DFT–SAPT potential energy curve is very close to the MP2/aug–cc–pVQZ potential, but at shorter distances the DFT–SAPT potential energy curve is more attractive and has a different shape from the MP2C-F12 and CCSD(T)-F12 potentials. This problem is exacerbated in the WF–SAPT approach for which the potential is about 5 kcal/mol too attractive at $R = 2$ $\AA$. This is a consequence of the strong overlap of the electron distributions of H_2O and $(MgO)_2$ near the potential energy minimum which leads to a breakdown in the perturbative expansion in the WF–SAPT procedure. In the case of the DFT–SAPT method, it is not clear whether the error in the interaction energy at short distance reflects a problem with the procedure used to calculate the induction and dispersion contributions or whether it reflects an inadequacy of using DFT orbitals to calculate the electrostatic and exchange interactions.

The individual components of the DFT-SAPT interaction energies for the single–layer $2X2$ model are reported in Figure C3. Near the minimum energy structure the exchange–repulsion and the electrostatic interaction contributions are about 85 and -73 kcal/mol, respectively. As a result, the electrostatics plus exchange–repulsion contribution is

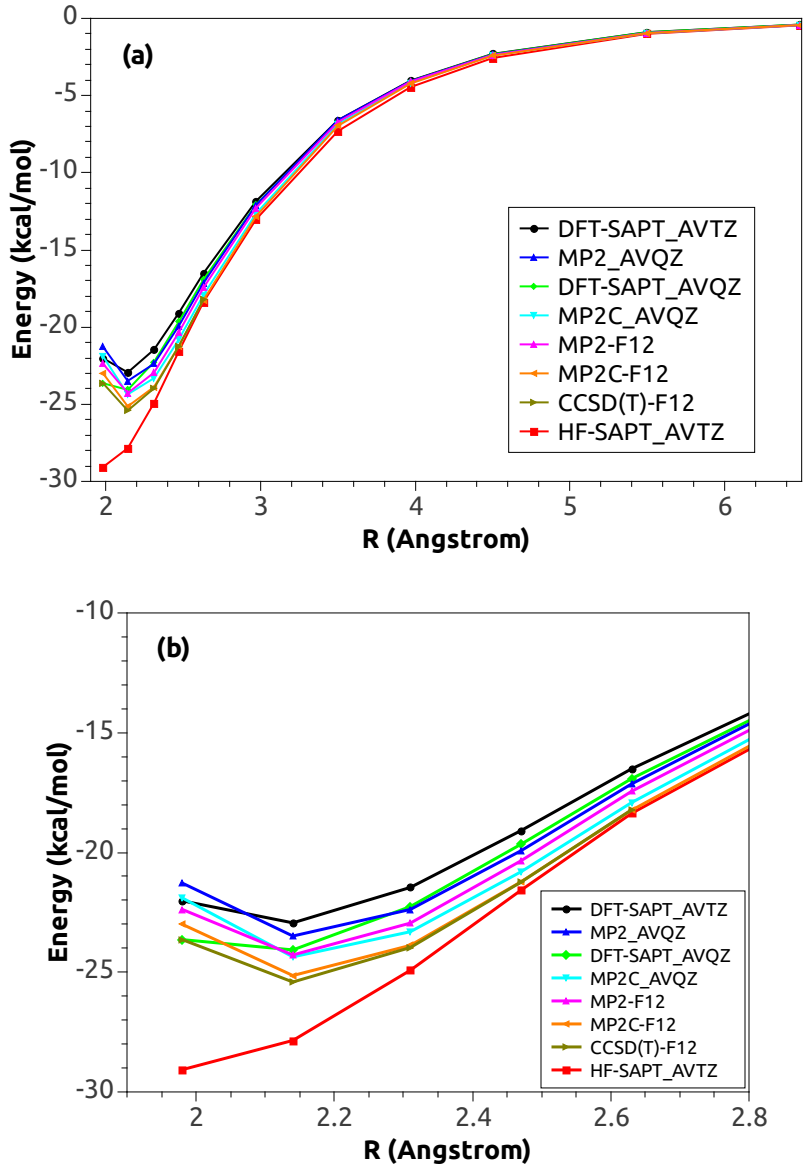

Figure C2: Potential energy curves for a water molecule approaching to the 2X2 MgO cluster.

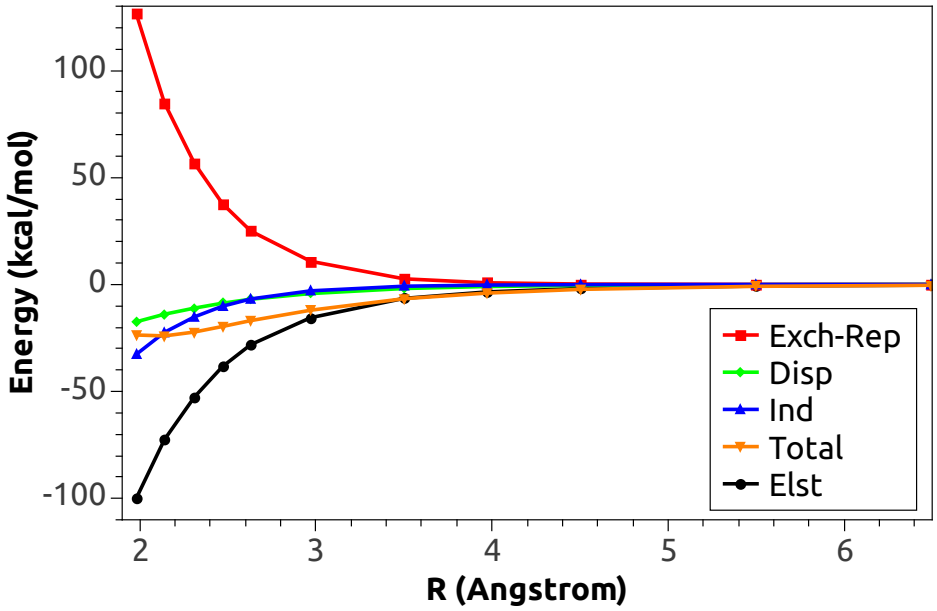

Figure C3: Water– $2X2$ MgO cluster interaction energy components.

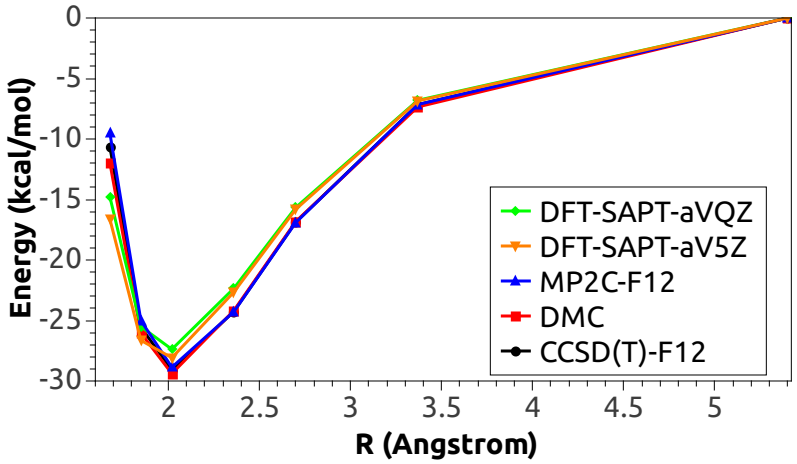

Figure C4: Potential energy curves of a water molecule to the $2X2$ cluster.

repulsive and the induction (-22 kcal/mol) and dispersion (-14 kcal/mol) contributions are crucial for the binding of the water molecule to the cluster.

In Fig. C4 we compare the near–complete basis set limit CCSD(T)–F12, MP2C–F12, DFT–SAPT, and DMC potential energy curves of a water monomer interacting with the single–layer $2X2$ model of the MgO surface. (These calculations were carried out with a slightly different geometry of the water monomer than used in the rest of this study.) Interestingly the MP2C–F12, CCSD(T)–F12, and DMC potentials are nearly identical whereas the DFT–SAPT potential differs noticeably from the others even when calculated using the aug–cc–pV5Z basis set.[137] Specifically, the DFT–SAPT potential lies appreciably above other potentials for distances about 2–2.5 $\AA$, but drops below the other potentials for $R \leq 1.8$ $\AA$. CCSD(T)–F12 calculations were also carried out accounting for correlation of the 2s and 2p orbitals of the Mg atoms (not shown in the figure). Near the minimum of the potential energy curve inclusion of correlation effects involving the Mg 2s and 2p orbitals results in a 0.7 kcal/mol increase in the magnitude of the interaction energy.

C.3.2 $4X4$ Cluster models

The MP2–F12, MP2C–F12, and DFT–SAPT potential energy curves for a water molecule interacting with the $4X4$ cluster model of the surface are shown in Figure C5. For each method the binding energy at the potential energy minimum is about half that obtained for the $2X2$ model. At the potential energy minimum the binding energy obtained with the DFT–SAPT and MP2–F12 methods are about 1.5 and 0.5 kcal/mol smaller in magnitude than obtained in the MP2C–F12 calculations. The weaker binding with the DFT–SAPT than with the MP2–F12 method is primarily a reflection of the limitation of the aug-cc-pVQZ basis set used for the DFT–SAPT calculations. The individual contributions to the interaction energy determined from the DFT-SAPT calculations are tabulated in Table C1. At $R = 2.14$ $\AA$, which corresponds to the equilibrium separation of the H_2O–$(MgO)_2$ system, both the electrostatics and exchange–repulsion of H_2O–$(MgO)_8$ are reduced in magnitude compared to the H_2O–$(MgO)_2$ system, with the net electrostatics plus exchange–repulsion contributions being 6 kcal/mol more positive for the $4X4$ case. As a result, at

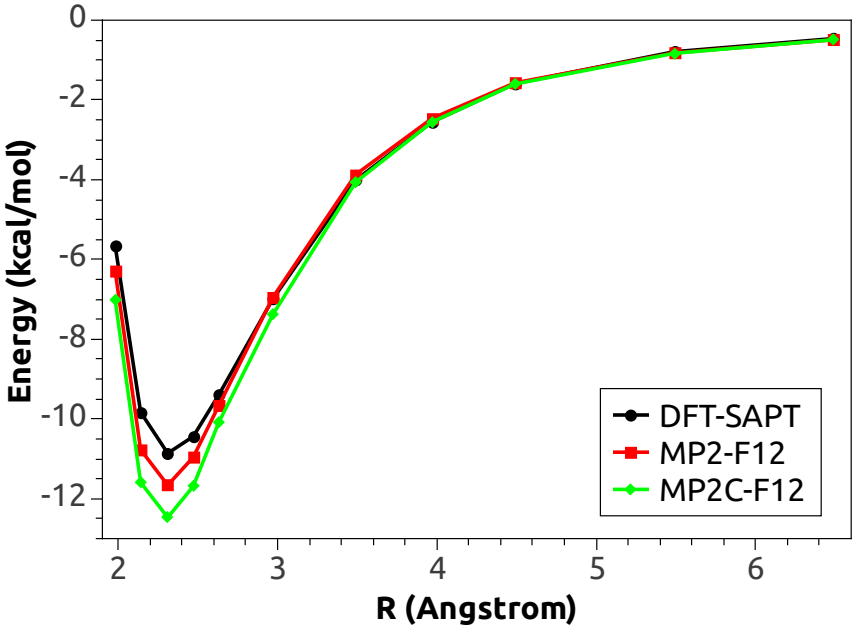

Figure C5: Potential energy curves for approach of a water molecule to the MgO 4X4 cluster.

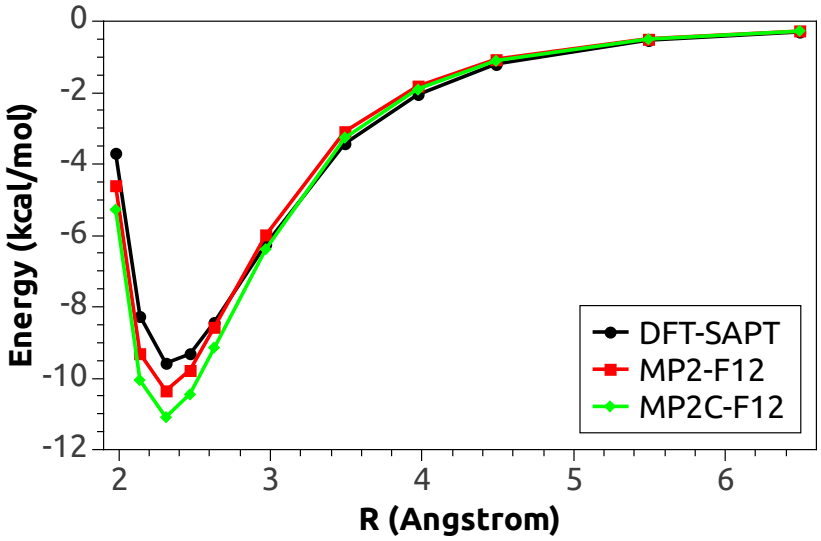

Figure C6: Potential energy curves of a water molecule to the 4X4 MgO double layer.

the equilibrium structure the water molecule is displaced further from the 'surface' in the 4X4 than 2X2 cluster model (2.31 vs. 2.14 $\AA$) which further weakens the interaction, primarily due to a reduction in the magnitude of the induction and dispersion interactions, with the change in the induction energy being more important. It should be noted that the breakdown in the DFT–SAPT procedure found for the 2X2 model is not seen for the 4X4 model, presumably due to the reduction of the magnitude of the electrostatics and exchange interactions in the larger cluster model.

Figure C6 and Table C2 report the interaction energies of a water monomer with the double–layer 4X4 cluster model. Compared to the single–layer 4X4 model, the net interaction energy at the potential minimum is about 1 kcal/mol smaller in magnitude in the two–layer model, but the equilibrium distance remains nearly the same as for the single–layer 4X4 model. In going from the single–layer to the double–layer 4X4 model, the electrostatic and exchange–repulsion interactions of the water molecule with the surface change by 1.7 and -1.7 kcal/mol respectively at the equilibrium distance of 2.31 $\AA$. Hence there is no net change in the electrostatics plus exchange–repulsion. On the other hand, the induction and dispersion contributions change by 0.8 and 0.2 kcal/mol, leading to about a 10% weaker interaction in the double–layer model.

C.3.3 6X6 Cluster model

The DFT–SAPT, MP2-F12 and MP2C–F12 interaction potentials for a water molecule interacting with the 6X6 cluster model of the surface are reported in Fig. C7, and the decomposition of the DFT–SAPT interaction energies is reported in Table C3. The distance of the minimum of the resulting potential energy curves is close to those obtained with the one– and two–layer 4X4 cluster models. The MP2C-F12 binding energies of a water molecule interacting with the MgO(100) surface as described by the various cluster models are reported in Table C4. Examination of the DFT–SAPT results reveals that in going from the single–layer 4X4 to single–layer 6X6 model the electrostatic plus

Table C1: DFT–SAPT interaction energies (kcal/mol) for water–MgO (single–layer 4X4).

R (Angs)	Elst	Exch-Rep	Disp	Ind	Total
1.98	−75.6	108.1	−17.8	−20.4	−5.7
2.14	−52.7	70.6	−14.2	−13.5	−9.8
2.31	−36.7	46.1	−11.3	−8.9	−10.9
2.47	−25.5	30.0	−9.0	−5.8	−10.4
2.63	−17.8	19.4	−7.2	−3.8	−9.4
2.97	−8.9	8.1	−4.6	−1.7	−7.0
3.49	−3.2	1.9	−2.2	−0.5	−4.0
3.97	−1.7	0.5	−1.2	−0.2	−2.6
4.49	−1.0	0.1	−0.6	−0.1	−1.6
5.49	−0.6	0.0	−0.2	0.0	−0.8
6.49	−0.4	0.0	−0.1	0.0	−0.5

Table C2: DFT–SAPT interaction energies (kcal/mol) for water–MgO (double–layer 4X4).

R (Angs)	Elst	Exch-Rep	Disp	Ind	Total
1.98	−73.3	105.6	−17.0	−19.0	−3.7
2.14	−50.8	68.6	−13.6	−12.5	−8.3
2.31	−35.0	44.4	−10.9	−8.1	−9.6
2.47	−24.0	28.7	−8.7	−5.3	−9.3
2.63	−16.5	18.5	−6.9	−3.4	−8.4
2.97	−7.9	7.6	−4.4	−1.5	−6.3
3.49	−2.5	1.7	−2.1	−0.4	−3.4
3.97	−1.2	0.5	−1.2	−0.2	−2.1
4.49	−0.6	0.1	−0.6	−0.1	−1.2
5.49	−0.3	0.0	−0.2	0.0	−0.5
6.49	−0.2	0.0	−0.1	0.0	−0.3

exchange contribution to the interaction energy changes by only -0.3 kcal/mol, whereas the induction plus dispersion contribution decreases by 1.0 kcal/mol in magnitude. Table C4 also includes MP2C–F12 results for the double–layer and triple–layer $2X2$ models of the surface. From these results it is seen that adsorption energies essentially converged at the two layers. The convergence of the adsorption energy along the $2X2$, $4X4$, and $6X6$ sequence of single–layer cluster models is shown in Fig. C8. Combining the results (at the minima of the potential energy scans) of the single–layer, and double–layer $4X4$ models and the single–layer $6X6$ model, we estimate the binding energy of a water molecule for a double–layer $6X6$ cluster model to be about -10.6 kcal/mol, which is in reasonable agreement with the -11.1 kcal/mol DMC result for a water molecule interacting with a 2–layer model of the MgO(100) surface. A comparison of the potential energy curve estimated for the double–layer $6X6$ model using MP2C–F12 energies and from the DMC calculations for the 2–layer slab with periodic boundary conditions is presented in Fig. C9. Overall the agreement between the two potential energy curves is good, with the small discrepency near the potential energy minimum probably reflecting a limitation of the strategy used to estimate the 2–layer $6X6$ cluster model results and also not including the core correlation effects for the Mg atoms.

We note that the temperature programmed desorption measurements of Ref. 5, which gave a value of 15 kcal/mol energy for desorbing from the Mg (100) surface at low coverages, probably detected water molecules that were H–bonded to OH groups on the surface, thereby, enhancing their binding energies.[195]

C.3.4 GDMA calculations

The electrostatic interaction energy from the DFT–SAPT calculations includes the effects of charge–penetration. In order to estimate the charge–penetration contribution to the electrostatic energy, we calculated atomic charges, dipoles, and quadrupoles using Stone's generalized distributed moment analysis (GDMA)[116] of the MP2/cc-pVDZ[136] densities for the $(MgO)_n$ cluster models.(The MP2 calculations were performed using Gaussian 03.[117]) The resulting moments are summarized in Table C5. This analysis shows that the charge on the interior Mg and O atoms has no simple trend in the different cluster models. The magnitude of the dipole moment on the central atoms decreases along the sequence of models and it becomes zero for the single–layer $6X6$ cluster model. The corresponding dipoles on the O atoms are 0.05, 0.03, and 0.26 au. (The absolute values of the dipoles are reported.) The changes in the quadrupole moments with cluster model are more striking. For example, for the central Mg atoms, the value of the Q_{20} component of the quadrupole is -0.39, -0.07, -0.02, and -0.05 au for the single–layer $2X2$, single–layer $4X4$, double–layer $4X4$, and single–layer $6X6$ cluster models, respectively. The corresponding results for the central O atoms are -0.89, -1.48, -0.74, and -1.40 au. The same trend for the quadrupole moments is also observed in going from the central atoms of the $6X6$ to the edge atoms. Using the moments from the GDMA analyses of H_2O and the $(MgO)_n$ cluster models we calculated the electrostatic interaction energies, with the results being tabulated in Table C6. The resulting interaction energies are 32.3, 22.1, 22.3 and 22.5 kcal/mol smaller in magnitude than the DFT–SAPT electrostatic interaction energies for the single–layer $2X2$, single–layer $4X4$, double–layer $4X4$, and single–layer $6X6$ cluster models, respectively. These differences can be taken as estimates of the charge–penetration contributions to the electrostatic interaction energies. The greater charge–penetration contribution in the $2X2$ model arises in part from the shorter separation of the water molecule from the surface in this case. Calculations using a $2X2$ cluster model with GDMA moments from the interior $2X2$ sub–cluster in the $4X4$ cluster model actually gives even stronger binding of the water molecule to the cluster than obtained with the original $2X2$ model. Thus the main factor causing the weakening of the electrostatic interaction between the water molecule and the surface as one goes from the $2X2$ to the $4X4$ cluster model is the unfavorable electrostatic interaction with the non–central Mg and O atoms rather than changes of the charge distribution of the atoms in the central $2X2$ region caused by the presence of surrounding ions.

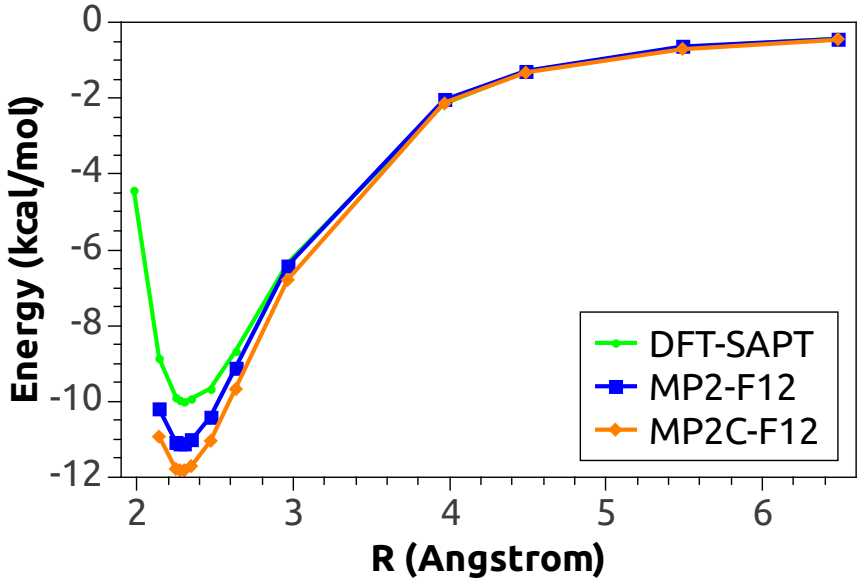

Figure C7: Potential energy curves for approach of a water molecule to the MgO 6X6 cluster.

Table C3: DFT–SAPT interaction energies (kcal/mol) for water–MgO (single–layer 6X6).

R (Angs)	Elst	Exch-Rep	Disp	Ind	Total
1.98	−75.3	107.0	−16.3	−19.9	−4.43
2.14	−52.3	69.8	−13.1	−13.2	−8.86
2.25	−40.4	51.6	−11.2	−9.9	−9.88
2.28	−38.6	49.0	−10.9	−9.4	−9.96
2.31	−36.2	45.3	−10.5	−8.7	−10.01
2.47	−25.0	29.4	−8.4	−5.7	−9.66
2.63	−17.3	19.0	−6.7	−3.7	−8.68
2.97	−8.4	7.9	−4.3	−1.6	−6.35
3.49	−2.8	1.8	−2.1	−0.4	−3.48
3.97	−1.3	0.5	−1.2	−0.2	−2.15
4.49	−0.7	0.1	−0.6	−0.1	−1.29
5.49	−0.4	0.0	−0.2	0.0	−0.66
6.49	−0.3	0.0	−0.1	0.0	−0.43

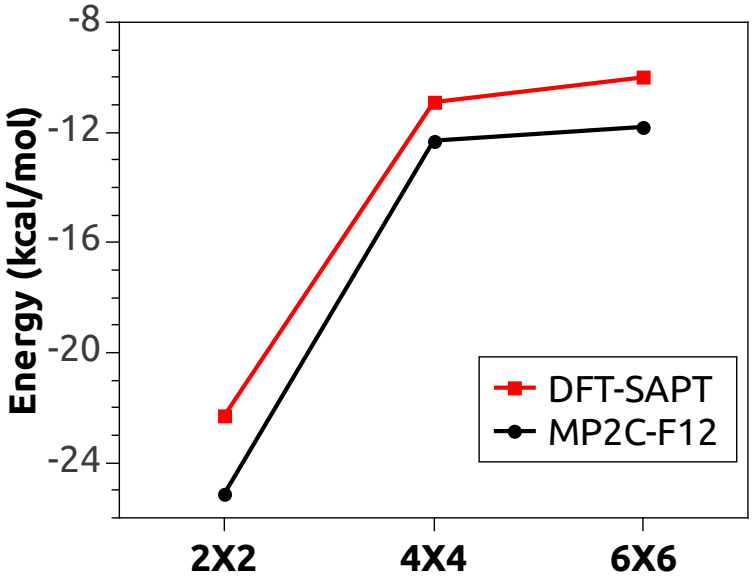

Figure C8: Change in the interaction energy with MgO cluster size.

Table C4: MP2C–F12 binding energies (kcal/mol) for water interacting with MgO(100) clusters.[a]

Geometry	$E_{MP2C-F12}$
2X2 1–Layer (VQZ-F12)	−25.1
2X2 2–Layer (VQZ-F12)	−24.7
2X2 3–Layer (VQZ-F12)	−24.5
4X4 1–Layer (VQZ-F12)	−12.5
4X4 2–Layer (VQZ-F12/VDZ-F12)	−11.1
6X6 1–Layer (VQZ-F12/VDZ-F12)	−11.8
6X6 2–Layer (VQZ-F12)	$(-10.6)^b$
DMC 2–Layer slab model	−11.1

[a] For a water O–Mg separation of 2.31 $\AA$, which is close to the minima of the scanned potentials for the one–layer and two–layer 4X4 models. O–Mg separation of 2.14 $\AA$ is used for 2X2 cluster models.
[b] Estimated as described in the text.

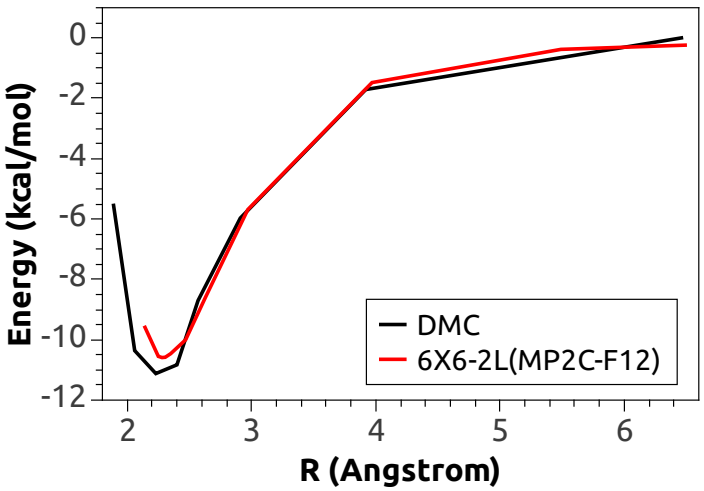

Figure C9: Potential energy curves for DMC compared with MP2C-F12

Table C5: Multipole moments (in au) for the Mg and O atoms in the cluster models.[a]

Atom	q				$\|\mu\|$				$\|Q_2\|$			
Type	2X2 1L	4X4 1L	4X4 2L	6X6 1L	2X2 1L	4X4 1L	4X4 2L	6X6 1L	2X2 1L	4X4 1L	4X4 2L	6X6 1L
Mg1	0.99	0.98	0.97	1.03	0.32	0.05	0.06	0.00	0.59	0.09	0.04	0.05
O1	-0.99	-1.07	-1.03	-1.04	0.05	0.03	0.26	0.00	0.95	1.48	0.75	1.40
Mg2		1.02	1.03	1.00		0.17	0.11	0.07		0.32	0.20	0.10
O2		-1.04	-1.04	-1.04		0.29	0.39	0.04		1.19	0.74	1.38
Mg3		1.13	1.11	0.98		0.31	0.27	0.05		0.68	0.62	0.05
O3		-1.01	-1.03	-1.07		0.14	0.38	0.02		0.93	0.01	1.50
Mg4				1.09				0.09				0.19
O4				-1.05				0.26				1.26
Mg5				1.15				0.33				0.68
O5				-1.02				0.16				0.91

[a] The atom numbering scheme is defined in Fig. 1.

Table C6: Electrostatic interaction energies (kcal/mol) for water/MgO(100) clusters

Cluster size	SAPT–Elst	GDMA–Elst	Charge–penetration
2X2 1 Layer	−52.6	−20.4	−32.3
4X4 1 Layer	−36.7	−14.6	−22.1
4X4 2 Layers	−35.0	−12.7	−22.3
6X6 1 Layer	−36.2	−13.7	−22.5

C.4 CONCLUSIONS

In this study, we have used the MP2, MP2C, and DFT–SAPT methods to calculate the interaction energy of a water molecule with a sequence of cluster models of the MgO(100) surface as well as DMC calculations of a water monomer interacting with a 2–layer model of the surface. Our calculations show that even a basis set as large as aug-cc-pVQZ does not give well converged interaction energies of a water molecule with cluster models of the surface, and the F12 approach was adopted to circumvent this problem. Based on the comparison with the results of CCSD(T)–F12 and DMC calculations using the small $2X2$ cluster model, it is concluded that the MP2C–F12 approach accurately describes the interaction of a water molecule with the cluster models of the surface. Compared to MP2C–F12, the MP2–F12 method underbinds by about 1 kcal/mol and the DFT–SAPT method underbinds by about 2.5 kcal/mol with about half the error in this latter case being to limitations in the basis set employed. Going from a single–layer $4X4$ model to a double–layer $4X4$ model, leads to about a 10% reduction of the magnitude of the binding energy. This can be understood in terms of the unfavorable electrostatic interaction of the water molecule with the second layer Mg and O atoms. Our best estimate of binding energy of a water molecule to the MgO(100) surface obtained from the cluster model calculations is -10.6 kcal/mol which is in good agreement with the DMC slab model result of -11.1 kcal/mol. At the equilibrium structure of a water molecule on the (100) MgO surface charge–penetration contributes about -22 kcal/mol to the interaction energy. As a result, the development of an accurate force field for describing the adsorption of a water on metal oxide surfaces will require inclusion of explicit charge–penetration terms.

C.5 ACKNOWLEDGEMENTS

This research was carried out with the support of NSF grant CHE–1111235. The SAPT, MP2–F12, MP2C–F12, and CCSD(T)–F12 calculations were carried out on computers in the Pittsburgh University's Center for Simulation and Modeling. We thank Dr. G. R. Jenness for valuable discussions on SAPT calculations. The DMC calculations were perfomed on JaguarPF at the Oak Ridge Leadership Computing Facility, located in the National Center for Computational Sciences at Oak Ridge National Laboratory, which is supported by the Office of Science of the Department of Energy under Contract No. DE–AC05–00OR22725. We are grateful to Dr. Ching-Ming Wei for sharing his Mg pseudopotential.

BIBLIOGRAPHY

[1] P. Hohenberg and W. Kohn. Inhomogeneous Electron Gas. *Phys. Rev.*, 136(3B):B864–B871, Nov 1964.

[2] W. Kohn and L. J. Sham. Self-Consistent Equations Including Exchange and Correlation Effects. *Phys. Rev.*, 140(4A):A1133–A1138, Nov 1965.

[3] Anthony J. Stone. *The Theory of Intermolecular Forces*. Oxford University Press, Oxford, U. K., 2002 edition, 1996.

[4] I. G. Kaplan. *Intermolecular Interactions: Physical Picture, Computational Methods and Model Potentials*. Wiley, New York, 2006.

[5] V. A. Parsegian. *Van der Waals Forces. A Handbook for Biologists, Chemists, Engineers, and Physicists*. Cambridge University Press, Cambridge, 2006.

[6] J. N. Israelachvili. *Intermolecular and Surface Forces*. Academic, New York, 1985.

[7] Mel Levy. Universal variational functionals of electron densities, first-order density matrices, and natural spin-orbitals and solution of the v-representability problem. *PNAS*, 76:6062, 1979.

[8] R. G. Parr and W. Yang. *Density-Functional Theory of Atoms and Molecules*. Oxford University Press, New York, 1989.

[9] John P. Perdew, Kieron Burke, and Matthias Ernzerhof. Generalized Gradient Approximation Made Simple. *Phys. Rev. Lett.*, 77(18):3865–3868, Oct 1996.

[10] José M. Pérez-Jordá and A. D. Becke. A density-functional study of van der Waals forces: rare gas diatomics. *Chem. Phys. Lett.*, 233(1-2):134 – 137, 1995.

[11] Sándor Kristyán and Peter Pulay. Can (semi)local density functional theory account for the London dispersion forces? *Chem. Phys. Lett.*, 229(3):175 – 180, 1994.

[12] O. Anatole von Lilienfeld, Ivano Tavernelli, Ursula Rothlisberger, and Daniel Sebastiani. Optimization of Effective Atom Centered Potentials for London Dispersion Forces in Density Functional Theory. *Phys. Rev. Lett.*, 93(15):153004, Oct 2004.

[13] I-Chun Lin, Maurício D. Coutinho-Neto, Camille Felsenheimer, O. Anatole von Lilienfeld, Ivano Tavernelli, and Ursula Rothlisberger. Library of dispersion-corrected atom-centered potentials for generalized gradient approximation functionals: Elements H, C, N, O, He, Ne, Ar, and Kr. *Phys. Rev. B*, 75(20):205131, May 2007.

[14] Pier Luigi Silvestrelli. Van der Waals interactions in density functional theory by combining the quantum harmonic oscillator-model with localized Wannier functions. *J. Chem. Phys.*, 139(5):054106, 2013.

[15] Robert A. DiStasio, O. Anatole von Lilienfeld, and Alexandre Tkatchenko. Collective many-body van der Waals interactions in molecular systems. *Proc. Natl. Acad. Sci.*, 109(37):14791–14795, 2012.

[16] Andreas Heßelmann. Long-range correlation energies from frequency-dependent weighted exchange-hole dipole polarisabilities. *The Journal of Chemical Physics*, 136(1):014104, 2012.

[17] Andreas Heßelmann. Assessment of a Nonlocal Correction Scheme to Semilocal Density Functional Theory Methods. *J. Chem. Theory Comput.*, 9(1):273–283, 2013.

[18] Qin Wu and Weitao Yang. Empirical correction to density functional theory for van der Waals interactions. *J. Chem. Phys.*, 116(2):515–524, 2002.

[19] Lampros Andrinopoulos, Nicholas D. M. Hine, and Arash A. Mostofi. Calculating dispersion interactions using maximally localized Wannier functions. *J. Chem. Phys.*, 135(15):154105, 2011.

[20] Stefan Grimme. Accurate description of van der waals complexes by density functional theory including empirical corrections. *J. Comp. Chem.*, 25(12):1463–1473, 2004.

[21] Stefan Grimme. Semiempirical GGA-type density functional constructed with a long-range dispersion correction. *J. Comp. Chem.*, 27(15):1787–1799, 2006.

[22] Stefan Grimme, Jens Antony, Stephan Ehrlich, and Helge Krieg. A consistent and accurate ab initio parametrization of density functional dispersion correction (DFT-D) for the 94 elements H-Pu. *J. Chem. Phys.*, 132(15):154104, 2010.

[23] Erin R. Johnson and Axel D. Becke. A post-Hartree-Fock model of intermolecular interactions: Inclusion of higher-order corrections. *J. Chem. Phys.*, 124(17):174104, 2006.

[24] Alexandre Tkatchenko and Matthias Scheffler. Accurate Molecular Van Der Waals Interactions from Ground-State Electron Density and Free-Atom Reference Data. *Phys. Rev. Lett.*, 102(7):073005, 2009.

[25] Takeshi Sato and Hiromi Nakai. Density functional method including weak interactions: Dispersion coefficients based on the local response approximation. *The Journal of Chemical Physics*, 131(22):224104, 2009.

[26] Yan Zhao and Donald G. Truhlar. The M06 suite of density functionals for main group thermochemistry, thermochemical kinetics, noncovalent interactions, excited states, and transition elements: two new functionals and systematic testing of four M06-class functionals and 12 other functionals. *Theo. Chim. Acta*, 120:215–241, 2008.

[27] M. Dion, H. Rydberg, E. Schröder, D. C. Langreth, and B. I. Lundqvist. Van der Waals Density Functional for General Geometries. *Phys. Rev. Lett.*, 92(24):246401, Jun 2004.

[28] Kyuho Lee, Éamonn D. Murray, Lingzhu Kong, Bengt I. Lundqvist, and David C. Langreth. Higher-accuracy van der Waals density functional. *Phys. Rev. B*, 82(8):081101, Aug 2010.

[29] Oleg A. Vydrov and Troy Van Voorhis. Improving the accuracy of the nonlocal van der Waals density functional with minimal empiricism. *J. Chem. Phys.*, 130(10):104105, 2009.

[30] Petr Jurecka, Jiri Cerny, Pavel Hobza, and Dennis R. Salahub. Density functional theory augmented with an empirical dispersion term. Interaction energies and geometries of 80 noncovalent complexes compared with ab initio quantum mechanics calculations. *J. Comput. Chem.*, 28(2):555–569, 2007.

[31] Felix O. Kannemann and Axel D. Becke. Van der Waals Interactions in Density-Functional Theory: Rare-Gas Diatomics. *Journal of Chemical Theory and Computation*, 5(4):719–727, April 2009.

[32] J. Hepburn, G. Scoles, and R. Penco. A simple but reliable method for the prediction of intermolecular potentials. *Chemical Physics Letters*, 36(4):451 – 456, 1975.

[33] Jeng-Da Chai and Martin Head-Gordon. Long-range corrected hybrid density functionals with damped atom-atom dispersion corrections. *Phys. Chem. Chem. Phys.*, 10:6615–6620, 2008.

[34] Carlo Adamo and Vincenzo Barone. Toward reliable density functional methods without adjustable parameters: The PBE0 model. *J. Chem. Phys.*, 110(13):6158–6170, 1999.

[35] Stefan Grimme, Stephan Ehrlich, and Lars Goerigk. Effect of the damping function in dispersion corrected density functional theory. *Journal of Computational Chemistry*, 32(7):1456–1465, 2011.

[36] Lori A. Burns, Alvaro Vazquez Mayagoitia, Bobby G. Sumpter, and C. David Sherrill. Density-functional approaches to noncovalent interactions: A comparison of dispersion corrections (DFT-D), exchange-hole dipole moment (XDM) theory, and specialized functionals. *The Journal of Chemical Physics*, 134(8):084107, 2011.

[37] X. Chu and A. Dalgarno. Linear response time-dependent density functional theory for van der Waals coefficients. *The Journal of Chemical Physics*, 121(9):4083–4088, 2004.

[38] F. L. Hirshfeld. Bonded-atom fragments for describing molecular charge densities. *Theo. Chim. Acta*, 44:129–138, 1977.

[39] A. Otero-de-la Roza and Erin R. Johnson. Many-body dispersion interactions from the exchange-hole dipole moment model. *The Journal of Chemical Physics*, 138(5):054103, 2013.

[40] O. Anatole von Lilienfeld and Alexandre Tkatchenko. Two- and three-body interatomic dispersion energy contributions to binding in molecules and solids. *The Journal of Chemical Physics*, 132(23):234109, 2010.

[41] Alexandre Tkatchenko, Robert A. DiStasio, Roberto Car, and Matthias Scheffler. Accurate and Efficient Method for Many-Body van der Waals Interactions. *Phys. Rev. Lett.*, 108:236402, Jun 2012.

[42] Tobias Risthaus and Stefan Grimme. Benchmarking of London Dispersion-Accounting Density Functional Theory Methods on Very Large Molecular Complexes. *Journal of Chemical Theory and Computation*, 9(3):1580–1591, 2013.

[43] Anthony M. Reilly and Alexandre Tkatchenko. Seamless and Accurate Modeling of Organic Molecular Materials. *The Journal of Physical Chemistry Letters*, 4(6):1028–1033, 2013.

[44] Leonard Kleinman and D. M. Bylander. Efficacious Form for Model Pseudopotentials. *Phys. Rev. Lett.*, 48(20):1425–1428, May 1982.

[45] S. Goedecker, M. Teter, and J. Hutter. Separable dual-space Gaussian pseudopotentials. *Phys. Rev. B*, 54(3):1703–1710, Jul 1996.

[46] Krishnan Raghavachari, Gary W. Trucks, John A. Pople, and Martin Head-Gordon. A fifth-order perturbation comparison of electron correlation theories. *Chem. Phys. Lett.*, 157(6):479 – 483, 1989.

[47] A. D. Becke. Density-functional exchange-energy approximation with correct asymptotic behavior. *Phys. Rev. A*, 38(6):3098–3100, Sep 1988.

[48] Chengteh Lee, Weitao Yang, and Robert G. Parr. Development of the Colle-Salvetti correlation-energy formula into a functional of the electron density. *Phys. Rev. B*, 37(2):785–789, Jan 1988.

[49] John P. Perdew. Density-functional approximation for the correlation energy of the inhomogeneous electron gas. *Phys. Rev. B*, 33(12):8822–8824, Jun 1986.

[50] I-Chun Lin and Ursula Rothlisberger. Describing weak interactions of biomolecules with dispersion-corrected density functional theory. *Phys. Chem. Chem. Phys.*, 10:2730–2734, 2008.

[51] I-Chun Lin, Ari P. Seitsonen, Mauricio D. Coutinho-Neto, Ivano Tavernelli, and Ursula Rothlisberger. Importance of van der Waals Interactions in Liquid Water. *J. Phys. Chem. B*, 113(4):1127–1131, 2009.

[52] Radhakrishnan Balu, Edward F. C. Byrd, and Betsy M. Rice. Assessment of Dispersion Corrected Atom Centered Pseudopotentials: Application to Energetic Molecular Crystals. *J. Phys. Chem. B*, 115(5):803–810, 2011.

[53] G. Jenness, O. Karalti, and K. D. Jordan. Benchmark calculations of water-acene interaction energies: Extrapolation to the water-graphene limit and assessment of dispersion-corrected DFT methods. *Phys. Chem. Chem. Phys.*, 12:6375–6381, 2010.

[54] Glen R. Jenness, Ozan Karalti, W. A. Al-Saidi, and Kenneth D. Jordan. Evaluation of Theoretical Approaches for Describing the Interaction of Water with Linear Acenes. *J. Phys. Chem. A*, 115(23):5955–5964, 2011.

[55] Ozan Karalti, Glen R. Jenness, Wissam Al-Saidi, and Kenneth D. Jordan. Is the DCACP Method Primarily Correcting for Dispersion? *unpublished results*.

[56] Ivano Tavernelli, I-Chun Lin, and Ursula Rothlisberger. Multicenter-type corrections to standard DFT exchange and correlation functionals. *Phys. Rev. B*, 79(4):045106, 2009.

[57] T. Thonhauser, Valentino R. Cooper, Shen Li, Aaron Puzder, Per Hyldgaard, and David C. Langreth. Van der Waals density functional: Self-consistent potential and the nature of the van der Waals bond. *Phys. Rev. B*, 76(12):125112, September 2007.

[58] Oleg A. Vydrov and Troy Van Voorhis. Dispersion interactions from a local polarizability model. *Phys. Rev. A*, 81(6):062708, June 2010.

[59] John F. Dobson and Tim Gould. Calculation of dispersion energies. *Journal of Physics: Condensed Matter*, 24(7):073201, 2012.

[60] Y. Zhang and W. Yang. Comment on Generalized Gradient Approximation Made Simple. *Phys. Rev. Lett.*, 80:890, 1998.

[61] Aaron Puzder, Maxime Dion, and David C. Langreth. Binding energies in benzene dimers: Nonlocal density functional calculations. *The Journal of Chemical Physics*, 124(16):164105, 2006.

[62] John P. Perdew and Wang Yue. Accurate and simple density functional for the electronic exchange energy: Generalized gradient approximation. *Phys. Rev. B*, 33:8800–8802, Jun 1986.

[63] Guillermo Román-Pérez and José M. Soler. Efficient Implementation of a van der Waals Density Functional: Application to Double-Wall Carbon Nanotubes. *Phys. Rev. Lett.*, 103(9):096102, Aug 2009.

[64] Pier Luigi Silvestrelli, Karima Benyahia, Sonja Grubisiĉ, Francesco Ancilotto, and Flavio Toigo. Van der Waals interactions at surfaces by density functional theory using Wannier functions. *J. Chem. Phys.*, 130(7):074702, 2009.

[65] Filipp Furche. Molecular tests of the random phase approximation to the exchange-correlation energy functional. *Phys. Rev. B*, 64:195120, Oct 2001.

[66] Filipp Furche and Troy Van Voorhis. Fluctuation-dissipation theorem density-functional theory. *The Journal of Chemical Physics*, 122(16):164106, 2005.

[67] Judith Harl and Georg Kresse. Cohesive energy curves for noble gas solids calculated by adiabatic connection fluctuation-dissipation theory. *Phys. Rev. B*, 77:045136, Jan 2008.

[68] Gustavo E. Scuseria, Thomas M. Henderson, and Danny C. Sorensen. The ground state correlation energy of the random phase approximation from a ring coupled cluster doubles approach. *The Journal of Chemical Physics*, 129(23):231101, 2008.

[69] Judith Harl and Georg Kresse. Accurate Bulk Properties from Approximate Many-Body Techniques. *Phys. Rev. Lett.*, 103(5):056401, July 2009.

[70] Xinguo Ren, Patrick Rinke, and Matthias Scheffler. Exploring the random phase approximation: Application to CO adsorbed on Cu(111). *Phys. Rev. B*, 80(4):045402, July 2009.

[71] Wim Klopper, Andrew M. Teale, Sonia Coriani, Thomas Bondo Pedersen, and Trygve Helgaker. Spin flipping in ring-coupled-cluster-doubles theory. *Chemical Physics Letters*, 510(13):147 – 153, 2011.

[72] Janos G. Angyan, Ru-Fen Liu, Julien Toulouse, and Georg Jansen. Correlation Energy Expressions from the Adiabatic-Connection Fluctuation-Dissipation Theorem Approach. *Journal of Chemical Theory and Computation*, 7(10):3116–3130, 2011.

[73] Andreas Heßelmann and Andreas Görling. Correct Description of the Bond Dissociation Limit without Breaking Spin Symmetry by a Random-Phase-Approximation Correlation Functional. *Phys. Rev. Lett.*, 106:093001, Feb 2011.

[74] David Bohm and David Pines. A Collective Description of Electron Interactions: III. Coulomb Interactions in a Degenerate Electron Gas. *Phys. Rev.*, 92(3):609–625, November 1953.

[75] D.C. Langreth and J.P. Perdew. The exchange-correlation energy of a metallic surface. *Solid State Communications*, 17(11):1425 – 1429, 1975.

[76] D. C. Langreth and J. P. Perdew. The Exchange-Correlation Energy of a Metallic Surface: Wavevector Analysis. *Phys. Rev. B*, 15:2884, 1977.

[77] János G. Ángyán, Iann C. Gerber, Andreas Savin, and Julien Toulouse. van der Waals forces in density functional theory: Perturbational long-range electron-interaction corrections. *Phys. Rev. A*, 72:012510, Jul 2005.

[78] Julien Toulouse, Fran çois Colonna, and Andreas Savin. Long-range-short-range separation of the electron-electron interaction in density-functional theory. *Phys. Rev. A*, 70:062505, Dec 2004.

[79] Alexander I. Kolesnikov, Jean-Marc Zanotti, Chun-Keung Loong, Pappannan Thiyagarajan, Alexander P. Moravsky, Raouf O. Loutfy, and Christian J. Burnham. Anomalously Soft Dynamics of Water in a Nanotube: A Revelation of Nanoscale Confinement. *Phys. Rev. Lett.*, 93(3):035503, Jul 2004.

[80] David Feller and Kenneth D. Jordan. Estimating the Strength of the Water/Single-Layer Graphite Interaction. *J. Phys. Chem. A*, 104:9971–9975, 2000.

[81] Tim O. Wehling, Alexander I. Lichtenstein, and Mikhail I. Katsnelson. First-principles studies of water adsorption on graphene: The role of the substrate. *App. Phys. Lett.*, 93(20):202110, 2008.

[82] O. Leenaerts, B. Partoens, and F. M. Peeters. Adsorption of H_2O, NH_3, CO, NO_2, and NO on graphene: A first-principles study. *Phys. Rev. B*, 77(12):125416, 2008.

[83] Miroslav Rubeš, Petr Nachtigall, Jiří Vondrášek, and Ota Bludský. Structure and Stability of the Water-Graphite Complexes. *J. Phys. Chem. C*, 113(19):8412–8419, 2009.

[84] Glen R. Jenness and Kenneth D. Jordan. DF-DFT-SAPT Investigation of the Interaction of a Water Molecule to Coronene and Dodecabenzocoronene: Implications for the Water-Graphite Interaction. *J. Phys. Chem. C*, 113(23):10242–10248, 2009.

[85] Fangfang Wang, Glen Jenness, Wissam A. Al-Saidi, and Kenneth D. Jordan. Assessment of the Performance of Common Density Functional Methods for Describing the Interaction Energies of $(H_2O)_6$ Clusters. *J. Chem. Phys.*, 132:134303, 2010.

[86] S. J. A. van Gisbergen, P. R. T. Schipper, O. V. Gritsenko, E. J. Baerends, J. G. Snijders, B. Champagne, and B. Kirtman. Electric Field Dependence of the Exchange-Correlation Potential in Molecular Chains. *Phys. Rev. Lett.*, 83(4):694–697, Jul 1999.

[87] Slawomir M. Cybulski and Marion L. Lytle. The origin of deficiency of the supermolecule second-order Möller-Plesset approach for evaluating interaction energies. *J. Chem. Phys.*, 127(14):141102, 2007.

[88] Petr Jurecka, Jiří Šponer, Jiří Černý, and Pavel Hobza. Benchmark database of accurate (MP2 and CCSD(T) complete basis set limit) interaction energies of small model complexes, DNA base pairs, and amino acid pairs. *Phys. Chem. Chem. Phys.*, 8:1985–1993, 2006.

[89] Stefan Grimme. Improved second-order Möller–Plesset perturbation theory by separate scaling of parallel- and antiparallel-spin pair correlation energies. *J. Chem. Phys.*, 118(20):9095–9102, 2003.

[90] Jens Antony and Stefan Grimme. Is Spin-Component Scaled Second-Order Möller–Plesset Perturbation Theory an Appropriate Method for the Study of Noncovalent Interactions in Molecules? *J. Phys. Chem. A*, 111(22):4862–4868, June 2007.

[91] Alexandre Tkatchenko, Jr. Robert A. DiStasio, Martin Head-Gordon, and Matthias Scheffler. Dispersion-corrected Möller–Plesset second-order perturbation theory. *J. Chem. Phys.*, 131(9):094106, 2009.

[92] Michal Pitoňák and Andreas Heßelmann. *J. Chem. Theory Comput.*, 6:168–178, 2010.

[93] Andreas Hermann and Peter Schwerdtfeger. Complete basis set limit second-order Möller–Plesset calculations for the fcc lattices of neon, argon, krypton, and xenon. *J. Chem. Phys.*, 131(24):244508, 2009.

[94] A. Heßelmann, G. Jansen, and M. Schütz. Density-functional theory-symmetry-adapted intermolecular perturbation theory with density fitting: A new efficient method to study intermolecular interaction energies. *J. Chem. Phys.*, 122(1):014103, 2005.

[95] H.-J. Werner, P. J. Knowles, R. Lindh, F. R. Manby, M. Schütz, P. Celani, T. Korona, A. Mitrushenkov, G. Rauhut, T. B. Adler, R. D. Amos, A. Bernhardsson, A. Berning, D. L. Cooper, M. J. O. Deegan, A. J. Dobbyn, F. Eckert, E. Goll, C. Hampel, G. Hetzer, T. Hrenar, G. Knizia, C. Köppl, Y. Liu, A. W. Lloyd, R. A. Mata, A. J. May, S. J. McNicholas, W. Meyer, M. E. Mura, A. Nicklass, P. Palmieri, K. Pflüger, R. Pitzer, M. Reiher, U. Schumann, H. Stoll, A. J. Stone, R. Tarroni, T. Thorsteinsson, M. Wang, and A. Wolf. MOLPRO, version 2010.1, a package of ab initio programs, 2010. see www.molpro.net.

[96] Michael W. Schmidt, Kim K. Baldridge, Jerry A. Boatz, Steven T. Elbert, Mark S. Gordon, Jan H. Jensen, Shiro Koseki, Nikita Matsunaga, Kiet A. Nguyen, Shujun Su, Theresa L. Windus, Michel Dupuis, and John A. Montgomery Jr. General atomic and molecular electronic structure system. *J. Comp. Chem.*, 14:1347–1363, 1993.

[97] CPMD V3.13 Copyright IBM Corp 1990-2008, Copyright MPI fuer Festkoerperforschung Stuttgart 1997-2001.

[98] Volker Blum, Ralf Gehrke, Felix Hanke, Paula Havu, Ville Havu, Xinguo Ren, Karsten Reuter, and Matthias Scheffler. Ab initio molecular simulations with numeric atom-centered orbitals. *Comp. Phys. Comm.*, 180:2175–2196, 2009.

[99] H. W. King. *CRC Handbook of Chemistry and Physics*, pages 12.15–12.18. CRC Press, 88 edition, 2007.

[100] W. S. Benedict, N. Gailar, and Earle K. Plyler. Rotation-Vibration Spectra of Deuterated Water Vapor. *J. Chem. Phys.*, 24(6):1139–1165, 1956.

[101] I. Wayan Sudiarta and D. J. Wallace Geldart. Interaction Energy of a Water Molecule with a Single-Layer Graphitic Surface Modeled by Hydrogen- and Fluorine-Terminated Clusters. *J. Phys. Chem. A*, 110(35):10501–10506, September 2006.

[102] Abraham Reyes, Lioudmila Fomina, Lev Rumsh, and Serguei Fomine. Are water-aromatic complexes always stabilized due to π–H interactions? LMP2 study. *Int. J. Quant. Chem.*, 104:335–341, 2007.

[103] Enrique M. Cabaleiro-Lago, Jorge A. Carrazana-García, and Jesús Rodríguez-Otero. Study of the interaction between water and hydrogen sulfide with polycyclic aromatic hydrocarbons. *J. Chem. Phys.*, 130(23):234307, 2009.

[104] Estelle M. Huff and Peter Pulay. A potential surface for the interaction between water and coronene as a model for a hydrophobic surface. *Mol. Phys.*, 107:1197–1207, 2009.

[105] Alston J. Misquitta, Rafal Podeszwa, Bogumil Jeziorski, and Krzysztof Szalewicz. Intermolecular potentials based on symmetry-adapted perturbation theory with dispersion energies from time-dependent density-functional calculations. *J. Chem. Phys.*, 123(21):214103, 2005.

[106] Fabio Della Sala and Andreas Görling. Efficient localized Hartree–Fock methods as effective exact-exchange Kohn–Sham methods for molecules. *J. Chem. Phys.*, 115(13):5718–5732, 2001.

[107] Andreas Heßelmann and Georg Jansen. The helium dimer potential from a combined density functional theory and symmetry–adapted perturbation theory approach using an exact exchange–correlation potential. *Phys. Chem. Chem. Phys.*, 5:5010–5014, 2003.

[108] Adem Tekin and Georg Jansen. How accurate is the density functional theory combined with symmetry–adapted perturbation theory approach for CH-π and π-π interactions? A comparison to supermolecular calculations for the acetylene-benzene dimer. *Phys. Chem. Chem. Phys.*, 9:1680–1687, 2007.

[109] F. Weigend. A fully direct RI-HF algorithm: Implementation, optimised auxiliary basis sets, demonstration of accuracy and efficiency. *Phys. Chem. Chem. Phys.*, 4:4285, 2002.

[110] Florian Weigend, Andreas Köhn, and Christof Hättig. Efficient use of the correlation consistent basis sets in resolution of the identity MP2 calculations. *J. Chem. Phys.*, 116(8):3175–3183, 2002.

[111] Roberto Peverati and Kim K. Baldridge. Implementation and Performance of DFT-D with Respect to Basis Set and Functional for Study of Dispersion Interactions in Nanoscale Aromatic Hydrocarbon. *J. Chem. Theory Comp.*, 4:2030–2048, 2008.

[112] Axel D. Becke. Density-functional thermochemistry. V. Systematic optimization of exchange-correlation functionals. *J. Chem. Phys.*, 107(20):8554–8560, 1997.

[113] V. Havu, V. Blum, P. Havu, and M. Scheffler. Efficient O(N) integration for all–electron electronic structure calculation using numeric basis functions. *J. Comp. Phys.*, 228(22):8367 – 8379, 2009.

[114] Jon Applequist. Atom charge transfer in molecular polarizabilities: application of the Olson-Sundberg model to aliphatic and aromatic hydrocarbons. *J. Phys. Chem.*, 97(22):6016–6023, June 1993.

[115] Francois Dehez, Jean-Christophe Soetens, Christophe Chipot, Janos G. Angyan, and Claude Millot. Determination of Distributed Polarizabilities from a Statistical Analysis of Induction Energies. *J. Phys. Chem. A*, 104(6):1293–1303, February 2000.

[116] Athony J. Stone. Distributed Multipole Analysis: Stability for Large Basis Sets. *J. Chem. Theory Comp.*, 1:1128, 2005.

[117] M. J. Frisch, G. W. Trucks, H. B. Schlegel, G. E. Scuseria, M. A. Robb, J. R. Cheeseman, J. A. Montgomery, Jr., T. Vreven, K. N. Kudin, J. C. Burant, J. M. Millam, S. S. Iyengar, J. Tomasi, V. Barone, B. Mennucci, M. Cossi, G. Scalmani, N. Rega, G. A. Petersson, H. Nakatsuji, M. Hada, M. Ehara, K. Toyota, R. Fukuda, J. Hasegawa, M. Ishida, T. Nakajima, Y. Honda, O. Kitao, H. Nakai, M. Klene, X. Li, J. E. Knox, H. P. Hratchian, J. B. Cross, V. Bakken, C. Adamo, J. Jaramillo, R. Gomperts, R. E. Stratmann, O. Yazyev, A. J. Austin, R. Cammi, C. Pomelli, J. W. Ochterski, P. Y. Ayala, K. Morokuma, G. A. Voth, P. Salvador, J. J. Dannenberg, V. G. Zakrzewski, S. Dapprich, A. D. Daniels, M. C. Strain, O. Farkas, D. K. Malick, A. D. Rabuck, K. Raghavachari, J. B. Foresman, J. V. Ortiz, Q. Cui, A. G.

Baboul, S. Clifford, J. Cioslowski, B. B. Stefanov, G. Liu, A. Liashenko, P. Piskorz, I. Komaromi, R. L. Martin, D. J. Fox, T. Keith, M. A. Al-Laham, C. Y. Peng, A. Nanayakkara, M. Challacombe, P. M. W. Gill, B. Johnson, W. Chen, M. W. Wong, C. Gonzalez, and J. A. Pople. Gaussian 03, Revision C.02. Gaussian, Inc., Wallingford, CT, 2004.

[118] Liem X. Dang and Tsun-Mei Chang. Molecular dynamics study of water clusters, liquid, and liquid–vapor interface of water with many-body potentials. *J. Chem. Phys.*, 106(19):8149–8159, 1997.

[119] D. B. Whitehouse and A. D. Buckingham. Experimental Determination of the Atomic Quadrupole Moment of Graphite. *J. Chem. Soc. Faraday Trans.*, 89:1909–1913, 1993.

[120] Matthew J. Allen, Vincent C. Tung, and Richard B. Kaner. Honeycomb Carbon: A Review of Graphene. *Chem. Rev.*, 110(1):132–145, January 2010.

[121] Miroslav Rubeš, Jiří Kysilka, Petr Nachtigall, and Ota Bludský. DFT/CC investigation of physical adsorption on a graphite (0001) surface. *Phys. Chem. Chem. Phys.*, 12:6438–6444, 2010.

[122] G. Forte, A. Grassi, G. M. Lombardo, G. G. N. Angilella, N. H. March, and R. Pucci. Quantum-chemical modelling of the structural change of water due to its interaction with nanographene. *Phys. Chem. Liq.*, 47:599–606, 2009.

[123] C. S. Lin, R. Q. Zhang, S. T. Lee, M. Elstner, Th. Frauenheim, and L. J. Wan. Simulation of Water Cluster Assembly on a Graphite Surface. *J. Phys. Chem. B*, 109(29):14183–14188, July 2005.

[124] D C Langreth, B I Lundqvist, S D Chakarova-Käck, V R Cooper, M Dion, P Hyldgaard, A Kelkkanen, J Kleis, Lingzhu Kong, Shen Li, P G Moses, E Murray, A Puzder, H Rydberg, E Schrder, and T Thonhauser. A density functional for sparse matter. *Journal of Physics: Condensed Matter*, 21(8):084203, 2009.

[125] Attila Szabo and Neil S. Ostlund. *Modern Quantum Chemistry: Introduction to Advanced Electronic Structure Theory*. Dover Publications, Inc., 1996.

[126] Claudia Hampel, Kirk A. Peterson, and Hans-Joachim Werner. A comparison of the efficiency and accuracy of the quadratic configuration interaction (QCISD), coupled cluster (CCSD), and Brueckner coupled cluster (BCCD) methods. *Chem. Phys. Lett.*, 190(1-2):1 – 12, 1992.

[127] Miles J. O. Deegan and Peter J. Knowles. Perturbative corrections to account for triple excitations in closed and open shell coupled cluster theories. *Chem. Phys. Lett.*, 227(3):321 – 326, 1994.

[128] Stefan Kurth and John P. Perdew. Density-functional correction of random-phase-approximation correlation with results for jellium surface energies. *Phys. Rev. B*, 59(16):10461–10468, Apr 1999.

[129] Zidan Yan, John P. Perdew, and Stefan Kurth. Density functional for short-range correlation: Accuracy of the random-phase approximation for isoelectronic energy changes. *Phys. Rev. B*, 61(24):16430–16439, Jun 2000.

[130] X. Ren and V. Blum. *Private Communication*, 2010.

[131] Miroslav Rubeš, Pavel Soldán, Petr Nachtigall, and Ota Bludský. A Computationally Feasible DFT/CCSD(T) Correction Scheme for the Description of Weakly Interacting Systems. *O. Chem. Phys. J.*, 1:1–11, 2008.

[132] G. Kresse and J. Hafner. Ab initio molecular dynamics for liquid metals. *Phys. Rev. B*, 47(1):558–561, Jan 1993.

[133] G. Kresse and J. Hafner. Ab initio molecular-dynamics simulation of the liquid-metal–amorphous-semiconductor transition in germanium. *Phys. Rev. B*, 49(20):14251–14269, May 1994.

[134] G. Kresse and J. Furthmller. Efficiency of ab-initio total energy calculations for metals and semiconductors using a plane-wave basis set. *Comput. Mat. Sci.*, 6:15, 1996.

[135] G. Kresse and J. Furthmüller. Efficient iterative schemes for ab initio total-energy calculations using a plane-wave basis set. *Phys. Rev. B*, 54(16):11169–11186, Oct 1996.

[136] Thom H. Dunning, Jr. Gaussian basis sets for use in correlated molecular calculations. I. The atoms boron through neon and hydrogen. *J. Chem. Phys.*, 90(2):1007–1023, 1989.

[137] Rick A. Kendall, Thom H. Dunning , Jr., and Robert J. Harrison. Electron affinities of the first-row atoms revisited. Systematic basis sets and wave functions. *J. Chem. Phys.*, 96(9):6796–6806, 1992.

[138] Hans-Joachim Werner, Thomas B. Adler, and Frederick R. Manby. General orbital invariant MP2-F12 theory. *J. Chem. Phys.*, 126(16):164102, 2007.

[139] Thomas B. Adler, Gerald Knizia, and Hans-Joachim Werner. A simple and efficient CCSD(T)-F12 approximation. *J. Chem. Phys.*, 127(22):221106, 2007.

[140] Gerald Knizia, Thomas B. Adler, and Hans-Joachim Werner. Simplified CCSD(T)-F12 methods: Theory and benchmarks. *J. Chem. Phys.*, 130(5):054104, 2009.

[141] Kevin E. Riley, Michal Pitoňák, Petr Jurečka, and Pavel Hobza. Stabilization and Structure Calculations for Noncovalent Interactions in Extended Molecular Systems Based on Wave Function and Density Functional Theories. *Chem. Rev.*, 110:5023–5063, May 2010.

[142] Andreas Heßelmann. Improved supermolecular second order Möller–Plesset intermolecular interaction energies using time-dependent density functional response theory. *J. Chem. Phys.*, 128(14):144112, 2008.

[143] Andreas Heßelmann. *Private Communication*, 2010.

[144] Kirk A. Peterson, Thomas B. Adler, and Hans-Joachim Werner. Systematically convergent basis sets for explicitly correlated wavefunctions: The atoms H, He, B–Ne, and Al–Ar. *J. Chem. Phys.*, 128(8):084102, 2008.

[145] John A. Pople, Martin Head-Gordon, and Krishnan Raghavachari. Quadratic configuration interaction. A general technique for determining electron correlation energies. *The Journal of Chemical Physics*, 87(10):5968–5975, 1987.

[146] S. F. Boys and F. Bernardi. The calculation of small molecular interactions by the differences of separate total energies. Some procedures with reduced errors. *Mol. Phys.*, 19:553–566, 1970.

[147] Andreas Heßelmann and Georg Jansen. First-order intermolecular interaction energies from Kohn-Sham orbitals. *Chem. Phys. Lett.*, 357(5-6):464 – 470, 2002.

[148] Andreas Heßelmann and Georg Jansen. Intermolecular induction and exchange-induction energies from coupled-perturbed Kohn-Sham density functional theory. *Chem. Phys. Lett.*, 362(3-4):319 – 325, 2002.

[149] Andreas Heßelmann and Georg Jansen. Intermolecular dispersion energies from time-dependent density functional theory. *Chem. Phys. Lett.*, 367(5-6):778 – 784, 2003.

[150] S. G. Lias. Ionization Energy Evaluation. NIST Chemistry WebBook, NIST Standard Reference Database No. 69. http://webbook.nist.gov.

[151] T. Koopmans. On the coordination of wave functions and intrinsic values to the single eletrons of an atom. *Physica*, 1(1-6):104 – 113, 1934.

[152] Ota Bludský, Miroslav Rubeš, Pavel Soldán, and Petr Nachtigall. Investigation of the benzene-dimer potential energy surface: DFT/CCSD(T) correction scheme. *J. Chem. Phys.*, 128(11):114102, 2008.

[153] Eamonn D. Murray, Kyuho Lee, and David C. Langreth. Investigation of Exchange Energy Density Functional Accuracy for Interacting Molecules. *J. Chem. Theory Comput.*, 5(10):2754–2762, October 2009.

[154] Murray Gell-Mann and Keith A. Brueckner. Correlation Energy of an Electron Gas at High Density. *Phys. Rev.*, 106:364–368, Apr 1957.

[155] W. J. Hehre, R. Ditchfield, and J. A. Pople. Self-Consistent Molecular Orbital Methods. XII. Further Extensions of Gaussian-Type Basis Sets for Use in Molecular Orbital Studies of Organic Molecules. *J. Chem. Phys.*, 56(5):2257–2261, 1972.

[156] Michelle M. Francl, William J. Pietro, Warren J. Hehre, J. Stephen Binkley, Mark S. Gordon, Douglas J. DeFrees, and John A. Pople. Self consistent molecular orbital methods. XXIII. A polarization type basis set for second row elements. *The Journal of Chemical Physics*, 77(7):3654–3665, 1982.

[157] M. F. Falcetta and Kenneth D. Jordan. Assignments of the temporary anion states of the chloromethanes. *J. Phys. Chem.*, 94(15):5666–5669, July 1990.

[158] K. N. Houk, Patrick S. Lee, and Maja Nendel. Polyacene and Cyclacene Geometries and Electronic Structures: Bond Equalization, Vanishing Band Gaps, and Triplet Ground States Contrast with Polyacetylene. *J. Org. Chem.*, 66(16):5517–5521, August 2001.

[159] B. Hajgató, D. Szieberth, P. Geerlings, F. De Proft, and M. S. Deleuze. A benchmark theoretical study of the electronic ground state and of the singlet-triplet split of benzene and linear acenes. *J. Chem. Phys.*, 131(22):224321, 2009.

[160] A.J. Stone. Distributed multipole analysis, or how to describe a molecular charge distribution. *Chem. Phys. Lett.*, 83(2):233 – 239, 1981.

[161] S. L. Price and A. J. Stone. A distributed multipole analysis of the charge densities of the azabenzene molecules. *Chem. Phys. Lett.*, 98(5):419 – 423, 1983.

[162] S. L. Price, A. J. Stone, and M. Alderton. Explicit formulae for the electrostatic energy, forces and torques between a pair of molecules of arbitrary symmetry. *Mol. Phys.*, 52:987, 1984.

[163] Revati Kumar, Fang-Fang Wang, Glen R. Jenness, and Kenneth D. Jordan. A second generation distributed point polarizable water model. *J. Chem. Phys.*, 132(1):014309, 2010.

[164] R. S. Mulliken. Electronic Population Analysis on LCAO–MO Molecular Wave Functions. I. *J. Chem. Phys.*, 23(10):1833–1840, 1955.

[165] B Jeziorski, R Moszynski, A. Ratkiewicz, S. Rybak, K. Szalewicz, and H. L Williams. In E. Clementi, editor, *Method and Techniques in Computational Chemistry: METECC94*, volume B, pages 79–129. STEF: Cagliari, Italy, 1993.

[166] Bogumil Jeziorski, Robert Moszynski, and Krzysztof Szalewicz. Perturbation Theory Approach to Intermolecular Potential Energy Surfaces of van der Waals Complexes. *Chem. Rev.*, 94(7):1887–1930, November 1994.

[167] Florian Weigend and Reinhart Ahlrichs. Balanced basis sets of split valence, triple zeta valence and quadruple zeta valence quality for H to Rn: Design and assessment of accuracy. *Phys. Chem. Chem. Phys.*, 7:3297–3305, 2005.

[168] Biswajit Santra, Angelos Michaelides, Martin Fuchs, Alexandre Tkatchenko, Claudia Filippi, and Matthias Scheffler. On the accuracy of density-functional theory exchange-correlation functionals for H bonds in small water clusters. II. The water hexamer and van der Waals interactions. *J. Chem. Phys.*, 129(19):194111, 2008.

[169] Erin E. Dahlke, Ryan M. Olson, Hannah R. Leverentz, and Donald G. Truhlar. Assessment of the Accuracy of Density Functionals for Prediction of Relative Energies and Geometries of Low-Lying Isomers of Water Hexamers. *J. Phys. Chem. A*, 112(17):3976–3984, May 2008.

[170] Julius T. Su, Xin Xu, and William A. Goddard. Accurate Energies and Structures for Large Water Clusters Using the X3LYP Hybrid Density Functional. *J. Phys. Chem. A*, 108(47):10518–10526, November 2004.

[171] André K. Kelkkanen, Bengt I. Lundqvist, and Jens K. Nørskov. Density functional for van der Waals forces accounts for hydrogen bond in benchmark set of water hexamers. *J. Chem. Phys.*, 131(4):046102, 2009.

[172] Desiree M. Bates and Gregory S. Tschumper. CCSD(T) Complete Basis Set Limit Relative Energies for Low-Lying Water Hexamer Structures. *J. Phys. Chem. A*, 113(15):3555–3559, April 2009.

[173] Sotiris S. Xantheas, Christian J. Burnham, and Robert J. Harrison. Development of transferable interaction models for water. II. Accurate energetics of the first few water clusters from first principles. *J. Chem. Phys.*, 116(4):1493–1499, 2002.

[174] Peifeng Su and Hui Li. Energy decomposition analysis of covalent bonds and intermolecular interactions. *J. Chem. Phys.*, 131(1):014102, 2009.

[175] Luigi Genovese, Alexey Neelov, Stefan Goedecker, Thierry Deutsch, Seyed Alireza Ghasemi, Alexander Willand, Damien Caliste, Oded Zilberberg, Mark Rayson, Anders Bergman, and Reinhold Schneider. Daubechies wavelets as a basis set for density functional pseudopotential calculations. *J. Chem. Phys.*, 129(1):014109–14, July 2008.

[176] Ingrid Daubechies. *Ten Lectures on Wavelets*. Society for Industrial and Applied Mathematics, 1992.

[177] Luigi Genovese, Thierry Deutsch, Alexey Neelov, Stefan Goedecker, and Gregory Beylkin. Efficient solution of Poisson's equation with free boundary conditions. *J. Chem. Phys.*, 125(7):074105–5, August 2006.

[178] B.M. Adams, W.J. Bohnhoff, K.R. Dalbey, J.P. Eddy, M.S. Eldred, D.M. Gay, K. Haskell, P.D. Hough, and L.P. Swiler. "DAKOTA, A Multilevel Parallel Object-Oriented Framework for Design Optimization, Parameter Estimation, Uncertainty Quantification, and Sensitivity Analysis: Version 5.0 User's Manual,". Technical report, Sandia Technical Report SAND2010-2183, 2010.

[179] Mutasem Omar Sinnokrot and C. David Sherrill. Highly Accurate Coupled Cluster Potential Energy Curves for the Benzene Dimer: Sandwich, T-Shaped, and Parallel-Displaced Configurations. *J. Phys. Chem. A*, 108(46):10200–10207, November 2004.

[180] Lucie Gráfová, Michal Pitoňák, Jan Řezáč, and Pavel Hobza. Comparative Study of Selected Wave Function and Density Functional Methods for Noncovalent Interaction Energy Calculations Using the Extended S22 Data Set. *J. Chem. Theory Comput.*, 6(8):2365–2376, 2010.

[181] O. Anatole von Lilienfeld. Force correcting atom centred potentials for generalised gradient approximated density functional theory: Approaching hybrid functional accuracy for geometries and harmonic frequencies in small chlorofluorocarbons. *Mol. Phys.*, 111(14-15):2147–2153, 2013.

[182] Ashok Kumar and William J. Meath. Dipole oscillator strength properties and dispersion energies for acetylene and benzene. *Mol. Phys.*, 75(2):311–324, 1992.

[183] J. Klimes, D. R. Bowler, and A. Michaelides. Chemical accuracy for the van der Waals density functional. *J. Phys.: Condens Matter*, 22:022201, 2010.

[184] J. Klimes, David R. Bowler, and Angelos Michaelides. Van der Waals density functionals applied to solids. *Phys. Rev. B*, 83:195131, May 2011.

[185] Alston J. Misquitta, Bogumil Jeziorski, and Krzysztof Szalewicz. Dispersion Energy from Density-Functional Theory Description of Monomers. *Phys. Rev. Lett.*, 91(3):033201, Jul 2003.

[186] Alston J. Misquitta and Krzysztof Szalewicz. Symmetry-adapted perturbation-theory calculations of intermolecular forces employing density-functional description of monomers. *J. Chem. Phys.*, 122(21):214109, 2005.

[187] D. Alfè and M. J. Gillan. Ab initio statistical mechanics of surface adsorption and desorption. I. H2O on MgO (001) at low coverage. *J. Chem. Phys.*, 127(11):114709, 2007.

[188] D. Alfè and M. J. Gillan. Ab initio statistical mechanics of surface adsorption and desorption. II. Nuclear quantum effects. *J. Chem. Phys.*, 133(4):044103–9, July 2010.

[189] Jamila Ahdjoudj and Christian Minot. Adsorption of H2O on metal oxides: a periodic ab-initio investigation. *Surf. Sci.*, 402-404(0):104 – 109, 1998.

[190] Yan Wang and Thanh N. Truong. Theoretical Study of Adsorption of Water Dimer on the Perfect MgO(100) Surface: Molecular Adsorption versus Dissociative Chemisorption. *J. Phys. Chem. B*, 108(10):3289–3294, 2004.

[191] Maureen I. McCarthy, Gregory K. Schenter, Carol A. Scamehorn, and John B. Nicholas. Structure and Dynamics of the Water/MgO Interface. *J. Phys. Chem.*, 100(42):16989–16995, 1996.

[192] Michael A. Johnson, Eugene V. Stefanovich, Thanh N. Truong, Jens Gunster, and D. W. Goodman. Dissociation of Water at the MgO(100) Water Interface: Comparison of Theory with Experiment. *J. Phys. Chem. B*, 103(17):3391–3398, 1999.

[193] D Ferry, S Picaud, P.N.M Hoang, C Girardet, L Giordano, B Demirdjian, and J Suzanne. Water monolayers on MgO(100): structural investigations by LEED experiments, tensor LEED dynamical analysis and potential calculations. *Surf. Sci.*, 409(1):101 – 116, 1998.

[194] Viacheslav A. Tikhomirov and Karl Jug. MSINDO Study of Water Adsorption on the Clean MgO(100) Surface. *J. Phys. Chem. B*, 104(32):7619–7622, 2000.

[195] Michael Odelius. Mixed Molecular and Dissociative Water Adsorption on MgO[100]. *Phys. Rev. Lett.*, 82(19):3919–3922, May 1999.

[196] Chr. Möller and M. S. Plesset. Note on an Approximation Treatment for Many-Electron Systems. *Phys. Rev.*, 46(7):618–622, Oct 1934.

[197] Hans-Joachim Werner, Frederick R. Manby, and Peter J. Knowles. Fast linear scaling second-order Moller-Plesset perturbation theory (MP2) using local and density fitting approximations. *J. Chem. Phys.*, 118(18):8149–8160, 2003.

[198] Stanisław Rybak, Bogumił Jeziorski, and Krzysztof Szalewicz. Many-body symmetry-adapted perturbation theory of intermolecular interactions. H_2O and HF dimers. *J. Chem. Phys.*, 95(9):6576–6601, 1991.

[199] M. Grüning, O. V. Gritsenko, S. J. A. van Gisbergen, and E. J. Baerends. Shape corrections to exchange-correlation potentials by gradient-regulated seamless connection of model potentials for inner and outer region. *J. Chem. Phys.*, 114(2):652–660, 2001.

[200] R J Needs, M D Towler, N D Drummond, and P Lpez Ros. Continuum variational and diffusion quantum Monte Carlo calculations. *J. Phys.: Condensed Matter*, 22(2):023201, 2010.

[201] M. D. Towler. The quantum Monte Carlo method. *phys. stat. sol. (b)*, 243(11):2573–2598, 2006.

[202] C. J. Umrigar, J. Toulouse, C. Filippi, S. Sorella, and R. G. Hennig. Alleviation of the Fermion-Sign Problem by Optimization of Many-Body Wave Functions. *Phys. Rev. Lett.*, 98(11):110201, March 2007.

[203] J. Toulouse and C. J. Umrigar. Optimization of quantum Monte Carlo wave functions by energy minimization. *J. Chem. Phys.*, 126(8):084102–16, February 2007.

[204] L. Mitáš, Shirley E. L., and Ceperley D. M. Nonlocal pseudopotentials and diffusion Monte Carlo. *J. Chem. Phys.*, 95(5):3467–3475, 1991.

[205] J. R. Trail and R. J. Needs. Smooth relativistic Hartree–Fock pseudopotentials for H to Ba and Lu to Hg. *J. Chem. Phys.*, 122(17):174109, 2005.

[206] Ching-Ming Wei. private communication. private communication.

[207] D. Alfè and M. J. Gillan. Efficient localized basis set for quantum Monte Carlo calculations on condensed matter. *Phys. Rev. B*, 70(16):161101, October 2004.

[208] S. de Gironcoli S. Baroni, A. Dal Corso and P. Giannozzi. http://www.pwscf.org.

[209] P. P. Ewald. The calculation of optical and electrostatic lattice potentials. *Ann. Phys.*, 369:253, 1921.